Injection Methods and Instrumentation

for

Serial X-ray Free Electron Laser Experiments

by

Daniel James

A Dissertation Presented in Partial Fulfillment
of the Requirements for the Degree
Doctor of Philosophy

Approved April 2015 by the
Graduate Supervisory Committee:

John Spence, Chair
Uwe Weierstall
Richard Kirian
Kevin Schmidt

ARIZONA STATE UNIVERSTIY

May 2015

ABSTRACT

Scientists have used X-rays to study biological molecules for nearly a century. Now with the X-ray free electron laser (XFEL), new methods have been developed to advance structural biology. These new methods include serial femtosecond crystallography, single particle imaging, solution scattering, and time resolved techniques.

The XFEL is characterized by high intensity pulses, which are only about 50 femtoseconds in duration. The intensity allows for scattering from microscopic particles, while the short pulses offer a way to outrun radiation damage. XFELs are powerful enough to obliterate most samples in a single pulse. While this allows for a "diffract and destroy" methodology, it also requires instrumentation that can position microscopic particles into the X-ray beam (which may also be microscopic), continuously renew the sample after each pulse, and maintain sample viability during data collection.

Typically these experiments have used liquid microjets to continuously renew sample. The high flow rate associated with liquid microjets requires large amounts of sample, most of which runs to waste between pulses. An injector designed to stream a viscous gel-like material called lipidic cubic phase (LCP) was developed to address this problem. LCP, commonly used as a growth medium for membrane protein crystals, lends itself to low flow rate jetting and so reduces the amount of sample wasted significantly.

This work discusses sample delivery and injection for XFEL experiments. It reviews the liquid microjet method extensively, and presents the LCP injector as a novel device for serial crystallography, including detailed protocols for the LCP injector and anti-settler operation.

ACKNOWLEDGMENTS

First, I would like to thank my advisor John Spence, who has a bottomless well of great ideas, and is one of the best teachers I've had the privilege to learn from. I appreciate the work that has gone into his research, and hope that I have done my part well. It is by strange fortune that I came to work in his lab, and I want to thank him for keeping me there.

Thanks to my mentor Uwe Weierstall, who has taught me much of the practicalities of experimental physics, and who always seems to be able to find the lynchpin of any problem.

Thanks to the students and postdocs who were there early on during my PhD, Rick Kirian, Nadia Zatzepin, and Mark Hunter, for the advice… it was sorely needed.

To my fellow PhD students Chris Kupitz, Garrett Nelson, Yun Zhao, Jesse Coe, Chelsie Conrad and Chufeng Li, thanks for your work, willingness, and company down in the hole. To Dingjie Wang who was my closest colleague for almost four years, thank you for your hard work, and fearlessness.

Lastly, thanks to my family, Heidi, Peter and Penny. Your love and support has sustained me through this whole process, and I am grateful in the extreme.

TABLE OF CONTENTS

Page

LIST OF TABLES viii

LIST OF FIGURES ix

CHAPTER

1 INTRODUCTION 1

1.1.1 Why XFELs? 1

1.1.2 Radiation Damage 2

1.1.3 Serialization 3

1.2 The Four Types of XFEL Experiments 5

1.2.1 Serial Femtosecond Crystallography 6

1.2.2 Single Particle Imaging 7

1.2.3 Solution Scattering 7

1.2.4 Pump Probe 8

1.3 The Three Experimental Stages 9

1.3.1 Sample Preparation 9

1.3.2 Data Collection 10

1.3.3 Data Analysis 11

1.4 The Scope of This Thesis 12

2 INJECTION AND SAMPLE HANDLING IN XFEL EXPERIMENTS 13

CHAPTER Page

2.1 Sample Delivery 13

2.1.1 Aerosol Injectors 14

2.1.2 Scanned Fixed Target 14

2.1.3 Continuous Stream Injectors 14

2.1.4 Drop on Demand Systems 15

2.1.5 The GDVN Nozzle 18

2.2 Sample Handling and Environments 25

2.2.1 Sample Delivery 26

2.2.2 Settling and the Anti-Settler 26

2.3 Sample Delivery for the Four Experimental Types 28

2.3.1 Serial Crystallography 28

2.3.2 Solution Scattering 29

2.3.3 Single Particle Imaging 29

2.3.4 Time Resolved Experiments 29

2.3.5 Data Analysis 31

2.4 Results from SFX 31

2.4.1 TR-SFX of Photosystem II 31

2.4.2 TR-SFX of Photoactive Yellow Protein 32

3 SFX WITH LIPIDIC CUBIC PHASE 34

CHAPTER Page

3.1.1 Liquid Microjet Sample Waste Problem 34

3.1.2 LCP as a Delivery Medium 35

3.2 Properties of LCP 36

3.3 LCP Injector Development 38

3.3.1 The LCP Nozzle 39

3.3.2 Pressure Amplification 41

3.4 Fabrication of Consumables 42

3.4.1 Capillary Tip Fabrication 42

3.4.2 Gas Apertures 43

3.4.3 Assembly and Adjustment 44

3.5 LCP Injector Control 44

3.5.1 Liquid Pressure Control 44

3.5.2 Gas Pressure Control 45

3.5.3 Injector Control Calculations 46

3.5.4 Jet Phase Change 47

3.6 LCP-SFX Results 50

3.6.1 Biomolecules 52

3.6.2 SFX of GPCR 5-HT_{2B} 52

3.6.3 Smoothened/Cyclopamine 53

CHAPTER Page

3.6.4 Bacteriorhodopsin SMX 54

3.7 Further Research 56

3.7.1 Alternative Delivery Media 56

3.7.2 Pump Probe Experiments in LCP 56

4 LCP INJECTOR PROTOCOL 58

4.1 List of Parts 58

4.2 Initial Setup 61

4.3 Installation with the In Vacuum Injector 63

4.4 Inline Syringe Assembly 66

4.5 Purging the Hydraulic Stage 67

4.6 Installation for Standalone or In Air Operation 68

4.7 Loading the Reservoir 71

4.8 Building the Nozzle 76

4.8.1 Grinding the Tips 76

4.8.2 Melting the Apertures 77

4.8.3 Assembling the Nozzle 79

4.8.4 A Note about Preparation 84

4.9 Putting the Loaded Reservoir/Nozzle in the Injector 84

4.10 Operating the Injector 86

CHAPTER Page

4.10.1 Nozzle Removal for the In Vacuum Injector 88

4.10.2 Nozzle Removal for In Air/Standalone Operation 88

4.10.3 Nozzle/Reservoir Disassembly 89

4.11 Troubleshooting 89

5 ARIZONA STATE ANTI-SETTLER OPERATIONS PROTOCOL 92

5.1 Anti-Settler Device Setup 93

5.2 Anti-Settler Device Pretest 95

5.3 Sample Delivery System Setup 96

5.4 Reservoir Preparation and Loading 99

5.5 Loading the Syringe into the Anti-Settler 103

5.6 Operating the Injector System 105

5.7 Removing the Reservoir 107

REFERENCES 108

LIST OF TABLES

Table Page

3.1: Sample Consumption Comparison 51

4.1: List of Custom Injector Parts and Consumables..... 59

4.2: List of Equipment and Custom Tools..... 60

4.3: List of Tubing, Fittings, and Seals..... 61

4.4: LCP Injector Troubleshooting Guide 90

5.1: Anti-Settler Parts List 92

LIST OF FIGURES

Figure Page

1.1: XFEL Serial Scattering Experiment. 4

1.2: Four Types of XFEL Experiment 5

2.1: Shrouded Injector System 16

2.2: GDVN Schematic 17

2.3: GDVN Construction 19

2.4: Gas Aperture Melting 20

2.5: Capillary Tip Grinding 21

2.6: Ice Events 25

2.7: ASU Anti-Settler 27

2.8: Pump-Probe Experiment Schematic 30

2.9: Light and Dark PSII Electron Density Map 32

3.1 Phase Behavior of Lipids 37

3.2: Early LCP Extrusion 38

3.3: LCP Injector With Improved Nozzle 40

3.4: Latest Model of LCP Injector 41

3.5: Lamellar Phase Transition 49

3.6: 5-HT_{2B} Structure Comparison 53

3.7: Serial Millisecond Crystallography 55

4.1: Injector Parts. 59

4.2: Custom Tools 60

4.3: Schematic Diagram of LCP Injector Setup 63

Figure Page

4.4: Injector Rod Setup 65

4.5: Syringe Assembly 66

4.6: Hydraulic Stage Purge 68

4.7: Examples of Injector Setup for In Air Operation 69

4.8: Example Camera Setup 71

4.9: Reservoir Preparation 73

4.10: Loading Needle Assembly and Use 75

4.11: Tip Grinding 77

4.12: Gas Aperture Construction 78

4.13: Nozzle Assembly 1 80

4.14: Nozzle Assembly 2 81

4.15: Gas Aperture Adjustment 82

4.16: Compression Fitting Nozzle Body Assembly 83

4.17: Reservoir/Nozzle Installation 85

4.18: LCP Steam Stability 87

5.1: Anti-Settler Components 93

5.2: Rotor Installation 94

5.3: Attach Cooler Wiring 94

5.4: Wiring and Tubing Support Loop 95

5.5: Setting the Temperature Controller 96

5.6: Single Valve Tubing Schematic 98

5.7: Two Multi-position Valve Tubing Schematic 99

Figure Page

5.8: Inserting Plunger 100

5.9: Syringe Assembly 101

5.10: Sample Loading and Sample Line Purging 102

5.11: Syringe Loading 104

1 INTRODUCTION

Life is shaped by biological macromolecules such as cell membrane proteins. Determining the correct structures of these molecules is key to understanding their function, yet the nature and size of these crucial biological macromolecules has made them historically difficult, and in many cases impossible, to image. The advent of the X-ray free electron laser (XFEL) within the last decade is changing the outlook of this difficult problem. XFELs provide access to unprecedented X-ray power at unexplored time scales in the X-ray sciences and have already paved the way to major breakthroughs in structural biology.

The free electron laser was conceived by John Madey (1971). Later the first one was built by Madey and colleagues in his lab at Stanford University. Free electron lasers were later built to operate at X-ray wavelengths using highly relativistic electrons from linear accelerators, the first of which was FLASH built at the Deutsches Elektronen-Synchrotron in Hamburg Germany (Ayvazyan et al. 2006). Since then many more XFELs have been built, are under construction, or are in planning. The Linac Coherent Light Source (LCLS) at SLAC National Accelerator Laboratory was the first XFEL to operate in the hard X-ray regime, and came online in 2009 (Emma et al. 2010). The LCLS is significant for this thesis as the majority of the experimental work was done at that facility.

1.1.1 Why XFELs?

Scientists have used X-rays to study materials for over a century, and in the early 1920's turned the power of these techniques to discovering the structures of biological molecules. XFELs now offer an X-ray source over a billion times brighter than the

previous generation. It is the XFEL's unique attributes that allow new techniques for structural studies of biological molecules.

XFELs are characterized by their high brightness and ultra-short pulses. LCLS has a peak brightness of 20×10^{32} photons s^{-1} mm^{-2} $mrad^{-2}$ per 0.1% spectral bandwidth, and pulses ranging from 10-500 femtoseconds in duration (Emma et al. 2010). The high intensity allows for an experimentally significant number of elastically scattered photons from a single pulse, even on small targets, and the short pulses allow for fine resolution in time while offering a way to outrun radiation damage.

1.1.2 Radiation Damage

Radiation damage refers to the destruction of a molecule by X-rays, and the degradation of diffraction data as a result. The processes involved are the photoelectric effect and Compton scattering. An atom ionized by the ejection of a photoelectron will very likely eject another lower energy electron through Auger decay. These free electrons shoot through the molecule causing a photoelectron cascade before exiting the sample (Barty et al. 2012).

Radiation damage is a constraint in all X-ray diffraction experiments, as any illuminant photon of sufficient energy to resolve a molecule at "atomic resolution" will more likely destroy the molecule, through inelastic processes, than scatter elastically (Breedlove and Trammell 1970). Radiation damage is a fundamental limitation when the X-ray exposure is longer than the characteristic time of the photoelectron damage. Normally the radiation damage problem is avoided by limiting the dose (absorbed energy per unit mass). Practically this means using low intensity X-ray beams, and/or large

sample volumes. Additionally, samples may be cooled to cryogenic temperatures (100K) to reduce the rate of radiation damage (Garman 2013).

The ultra-short X-ray pulses from an XFEL provide a way to bypass the radiation damage problem. If all scattering events (elastic or inelastic) occur simultaneously, then the diffraction data would correspond to damage free structure (Neutze et al. 2000). XFEL methods have advantages with radiation damage because pulse lengths are orders of magnitude shorter than at other sources, allowing for a "diffraction before destruction" approach that yields reduced damage structures (Chapman et al. 2011).

1.1.3 Serialization

Because the XFEL beam is so intense, any target, be it single molecule or microcrystal, is completely obliterated in a single pulse. This requires that the experiment be serialized, meaning that data is taken from a series of many identical particles or similar crystals. Serialization presents new challenges in all aspects of experimental design from sample preparation, to data collection, and data analysis.

As serial X-ray scattering experiments require a new sample for every pulse, new sample injection methods were developed. Sample injection is the process of placing target samples into the X-ray beam, and is constrained by both the XFEL experimental design requirements and the needs of the biological sample itself. The injectors discussed in this thesis are designed to place a moving stream of fully hydrated biological particles into the X-ray beam at room temperature (Weierstall, Spence, and Doak 2012; Weierstall et al. 2014). A liquid sample stream is most often produced with a gas dynamic virtual nozzle (GDVN), a gas flow focused nozzle that produces micron sized liquid jets (DePonte et al. 2008).

The XFEL beam probes the sample stream at a given repetition rate (i.e. 120Hz at LCLS). If the beam intercepts a particle (or crystal as the case may be) a diffraction pattern is recorded at the detector (Figure 1.1). The experimental setup allows for the sample stream to run for many hours collecting data. This leads to a massive number of captured frames (most of which contain little to no useful information) representing terabytes of data.

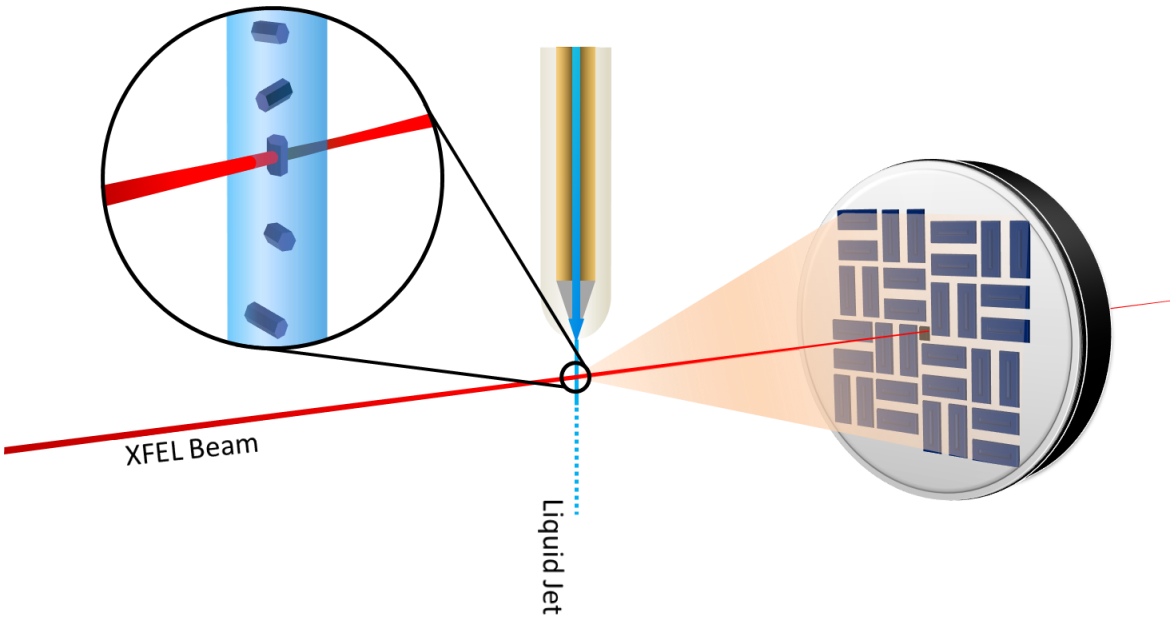

Figure 1.1: XFEL Serial Scattering Experiment.
In a typical XFEL scattering experiment, a nozzle, or other apparatus, provides sample in such a way that it is continuously renewed. Sample molecules that pass through the interaction region may be hit by the X-ray beam. Diffraction patterns are recorded at the detector.

The data must be reduced, via hit finding algorithms (Barty et al. 2014), and particle orientation determined (indexing solves this problem for crystallographic experiments). Because the data comes from particles/crystals in random orientation, many diffraction patterns (>10,000) must be collected to complete molecular structure.

1.2 The Four Types of XFEL Experiments

There are three types of structural experiments discussed in this thesis: serial femtosecond crystallography (SFX), single particle diffractive imaging, and solution scattering (e.g. wide angle X-ray scattering or WAXS, and small angle X-ray scattering or SAXS). Additionally, any experiment of these types could be time resolved or "pump-probe".

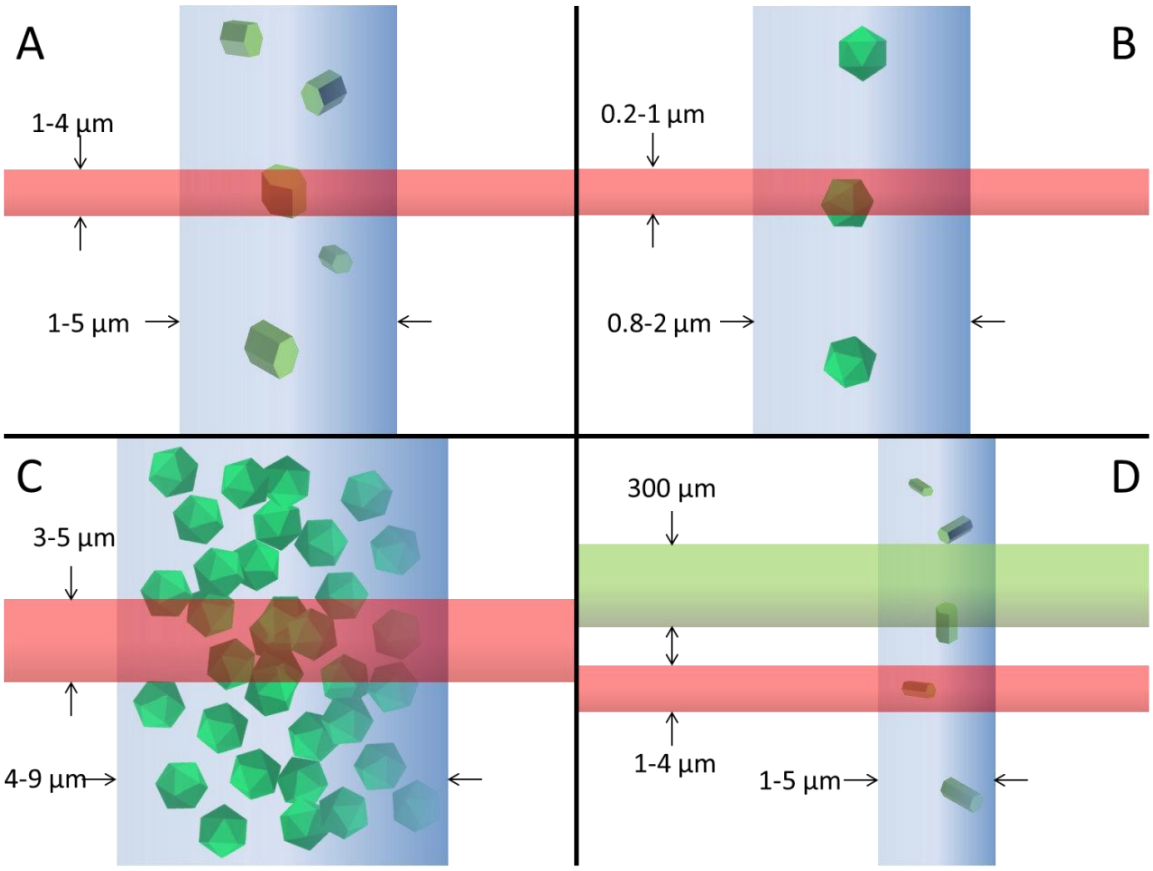

Figure 1.2: Four Types of XFEL Experiment
This thesis discusses four types of serial X-ray scattering experiments. Typical values for beam and jet diameter are given. Serial femtosecond crystallography (A) is the collection of single shot diffraction patterns from a stream of microcrystals. Single particle diffractive imaging (B) is the collection of X-ray diffraction from single particles like viruses. Solution scattering (C) is diffraction from many identical, randomly oriented particles. Any of these three experiment types can be time resolved or pump-probe (D). Pump-probe experiments excite the sample with a laser pulse prior to collecting X-ray diffraction.

1.2.1 Serial Femtosecond Crystallography

The most successful method for structural determination of biological molecules to date is X-ray crystallography. Despite the success of this method many proteins of interest are not available for crystallographic experiments because they are difficult, if not impossible, to crystallize. Typical microcrystallography beamlines require highly ordered crystals of appropriate size (>10 microns) to yield high resolution diffraction data (Smith, Fischetti, and Yamamoto 2012). Additionally these experiments are usually performed at cryogenic temperatures to protect the crystal from radiation damage.

SFX is a crystallographic technique that uses XFEL pulses to collect single shot diffraction patterns from a series of small crystals. The XFEL mitigates the need for growing single large crystals, as diffraction data can be collected on crystals less than one micron in diameter. This provides benefits to the crystal grower, as clusters of microcrystals are more readily obtained. A crystal suspension with a high concentration of nanocrystals is an ideal candidate sample for SFX.

In SFX a series of microcrystals is introduced into the X-ray beam at room temperature, by either a continuous fluid stream (DePonte et al. 2008; Sierra et al. 2012), a viscous extrusion (Weierstall et al. 2014), or a scanned membrane (Hunter et al. 2014). Crystals are randomly oriented, and (aside from some fixed target cases) no effort is made to target individual crystals. The number of crystal hits per second, i.e. the hit rate (H), therefore, is given by: $H = nVR$, where n is the number density of crystals in the sample, V is the interaction volume, and R is the FEL repetition rate. The hit rate is often defined as the percentage of shots that contain a diffraction pattern $H' = nV$. Crystal concentration is adjusted to maximize the number of single hits (Chapman et al. 2011).

If an XFEL pulse hits a crystal, a diffraction snapshot is collected at the detector. After a large number of shots are taken, computer software (T. a. White et al. 2012; Barty et al. 2014) searches for hits, indexes, merges, phases, and transforms the data to recover the electron density of the crystal molecule.

1.2.2 Single Particle Imaging

In the case where the molecule of interest cannot be crystallized, data could potentially still be collected from single particles (e.g. whole viruses, metal nanoparticles). By eliminating crystallization as a requirement for data collection, single particle diffractive imaging (SPI) provides opportunities to examine biomolecules that have heretofore been excluded from crystallographic experiments.

An SPI experiment consists of the sample particles being shot through the interaction region via liquid microjet (DePonte et al. 2008) or gas phase injector (Bogan, Boutet, et al. 2010). Like the SFX method, when a particle is hit, the diffraction pattern is recorded at the detector. However, diffraction from single particles is often, and easily, lost in background scattering. For this reason, SPI experiments done with a liquid microjet require strong scatterers to overcome the background scattering from the jet. Aerosol type injectors will isolate the particles in vacuum (ideally with a water jacket of minimal thickness), reducing overall background scattering, but may suffer from low hit rates (~10%) (Spence, Weierstall, and Chapman 2012).

1.2.3 Solution Scattering

Solution scattering (e.g. SAXS, WAXS) is an X-ray scattering technique that looks at particles in solution, rather than crystals or single isolated particles. The X-ray diffraction from many randomly oriented particles is spherically averaged. Typically for

an XFEL WAXS experiment, a liquid jet produced by a nozzle introduces a solution of proteins (or other molecules of interest) into the XFEL beam. The concentration of molecules in solution is high, to ensure that many molecules are in the beam for each shot (often the nozzle liquid flowrate is increased to produce a thicker jet and place even more scatterers in the interaction volume). The hit rate for a SAXS/WAXS experiment is effectively 100%.

1.2.4 Pump Probe

In a "pump-probe" experiment, sample molecules are triggered to change states just before being hit by the X-rays. In this way, the changes in the molecular structure can be recorded like a movie camera captures frames in a film. Pump-probe experiments have mostly used proteins with photo-activated cycles as samples. This allows for a simple setup where a short laser pulse hits the sample just upstream of the interaction region. Micrometer precision is required in aligning the jet, pump laser, and XFEL beam, and is provided by the injector described in Weierstall, Spence, and Doak (2012). Time delays are constrained by the XFEL repetition rate, and the speed of the sample stream through the interaction region.

Microfluidic mixing may provide an alternative method for time resolved measurements. Fast mixing of an enzyme and substrate, for example, would allow for the study of the reaction kinetics of the molecule (Schmidt 2013). A microfluidic mixing GDVN has been developed, but as of this writing has yet to be implemented in an XFEL experiment (Wang et al. 2014).

1.3 The Three Experimental Stages

The XFEL experiments described above have three distinct stages: sample preparation, data collection, and data analysis.

1.3.1 Sample Preparation

Experiments start with sample preparation. Samples are selected based on many factors, but ultimately the molecule of interest must be responsive to expression, purification, and possibly crystallization. These requirements are perhaps the largest bottleneck in macromolecular structural experiments. Crystallization is especially difficult as it can take many years to discover the appropriate conditions for growing large well-ordered crystals.

For SPI experiments, a purified monodisperse sample is aerosolized in a volatile buffer solution with either an electrospray nozzle, or GDVN (Bogan, Starodub, et al. 2010). High salt buffers should be avoided, as salt crystals may grow as aerosol droplets evaporate in vacuum.

The deliberate growth of nano-scale crystals has historically been ignored in favor of macro-scale crystallization, despite crystallization trials often showing "showers of microcrystals". Since the development of SFX, new techniques have been advanced to produce nano to micro-scale crystals. These techniques include: the batch method, free interface diffusion, free interface diffusion centrifugation, and growth quenching, which are detailed in Kupitz et al. (2014). Microcrystals have also been grown in living cells (Redecke et al. 2013), in lipidic cubic phase (Liu, Ishchenko, and Cherezov 2014),and also produced by mechanically breaking up larger crystals via sonication or centrifugation with glass beads.

Sample characterization is done by ultraviolet microscopy, dynamic light scattering (DLS), nanoparticle tracking analysis, and second order nonlinear optical imaging of chiral crystals (SONICC) (Gualtieri et al. 2011). DLS and nanoparticle tracking show particle size distributions, and SONICC is the only technique that explicitly shows crystallinity, however not all proteins are responsive to this method.

One difficulty with sample preparation is that SFX using the GDVN may require more protein than can feasibly be produced. Additionally, most of the microcrystals used in SFX are never hit by the X-ray beam, and flow into waste. The sample waste problem is addressed in more detail in chapter 3 of this thesis. As injection and data analysis methods improve the total protein required to yield a structure should decrease dramatically.

1.3.2 Data Collection

Data collection refers to the recording and storing of X-ray diffraction patterns. This experimental stage encompasses X-ray beamline setup and operation (this includes beam alignment, detector setup, and data handling, which will not be discussed in this thesis), and sample delivery and injection.

Sample delivery includes any process that brings sample to the injection device. This includes sample loading, sample pumping, and the sample environment. For continuous stream injection, samples are loaded into pressurized reservoirs to drive the sample to the nozzle. Samples may stay in the reservoir for several hours, therefore, consideration is given to temperature sensitivity, light sensitivity, and settling (Lomb et al. 2012). Chapter 5 gives a description of the ASU designed temperature controlled anti-

settler. Additionally, tubing, valves, and in-line filters are selected to minimize dead volume, and protect the nozzle from clogging.

Injection refers to the process of placing a sample into the X-ray beam. The different injector types are selected based on the type of experiment (as described above), and have different advantages with respect to hit rate, sample consumption, and background scattering. For effective data collection the injection must be stable, and free from problems like icing and clogging.

With a stable injector the beamline operator is free to align the X-ray beam and initiate data collection. Often the initial alignment of the XFEL beam is laborious and takes several hours. The injector should therefore be running stably with a sample substitute when feasible (e.g. water or empty LCP).

1.3.3 Data Analysis

The data collected during an XFEL beamtime can result in 10-100 terabytes of data (transfer of data offsite may take many days). The first step in the analysis process, therefore, is data reduction. Data reduction is accomplished by software that finds frames where there are likely particle hits. The hit finding program Cheetah is available freely under the GNU public license, and also provides useful online monitoring tools, that allow rapid feedback on data quality during the beamtime (Barty et al. 2014).

After data reduction (hit finding), particle orientation must be determined. Crystallographic indexing solves this problem for the SFX case (for a review touching on SFX and SPI data analysis methods see Spence, Weierstall, and Chapman (2012)). The data is then merged, phased (via known solutions to the crystallographic phase problem), and transformed to recover the electron density of the target molecule. Several software

packages are now available for automating SFX data analysis (T. a. White et al. 2012; Sauter et al. 2013). While data analysis methods are out of the scope of this thesis, more detail can be found in the Spence et al. review mentioned above, and in Kirian et al. (2010; 2011).

1.4 The Scope of This Thesis

This thesis is primarily concerned with sample injection methods for serial X-ray scattering experiments at XFEL sources. Emphasis is given to sample delivery and injection with the GDVN and viscous jet injectors. Chapter 2 describes SFX instrumentation in detail while chapter 3 covers the same technique done with the viscous jet injector. Chapter 4 gives a detailed protocol for LCP injector operation, and can be used "stand-alone" as a manual for that device. Chapter 5 contains a similar manual of operation of the ASU designed anti-settler.

2 INJECTION AND SAMPLE HANDLING IN XFEL EXPERIMENTS

As discussed in the introduction, the XFEL has provided new methods for structural biology. The XFEL's ultra-short pulses can outrun radiation damage allowing for pulse intensities much higher than those used at other facilities. These conditions can provide significant elastic scattering from nanocrystals and even single particles. There remain many experimental problems however. How does one isolate a single microscopic particle in a microscopic beam spot? The XFEL beam is destructive to all samples both crystalline and single particle. If the beam destroys the sample how does one replace it quickly, collect expended sample material, or even collect complete data sets?

Most X-ray diffraction experiments today are conducted on cryo-cooled macroscopic crystals, and at comparatively low doses. Sample alignment and rotation are accomplished by a goniometer, a device that supports and moves a single crystal (simple in theory, not necessarily simple in practice). The problems of sample replenishment, and placement are not trivial in the XFEL case where both precision alignment and continuous renewal are required.

In this chapter the different sample injection techniques will be discussed in detail. Also, emphasis will be placed on sample delivery in the four types of XFEL experiments outlined in the previous chapter.

2.1 Sample Delivery

There are at least four different ways of introducing sample material into the XFEL beam: as an aerosol, embedded in a continuous liquid stream, embedded in droplets ejected from drop on demand injector, or on a scanned fixed target holder.

2.1.1 Aerosol Injectors

Aerosol injectors are designed to collect data from free floating particles. Having a free floating particle enables data collection with minimal background scattering, which is essential for data collection on weak scattering single particles (i.e. single protein molecules). Aerodynamic lenses are often employed to collimate the aerosol in order to increase hit rate (Bogan, Starodub, et al. 2010).

Ideally, if the aerosolized particles are biological, the particle will be surrounded by a water jacket of minimal thickness. This would allow the sample to be probed while still hydrated, and also minimize background scattering.

2.1.2 Scanned Fixed Target

Fixed target injectors are an adaptation of existing X-ray sample mounting technologies to XFEL experiments. Sample particles are fixed in place on a solid support (i.e. capillary, mesh, thin film etc.) which is scanned in front of the beam (Cohen et al. 2014; Lyubimov et al. 2015; Hunter et al. 2014). There is additional background scattering from the sample support structure, but this may be negligible in certain cases. The fixed target scheme has potential for high hit rate, as particles can be individually targeted and hit; however, there is a high cost requirement in data collection time.

2.1.3 Continuous Stream Injectors

Continuous stream injectors are designed to stream sample particles suspended in a carrier medium across the focus of the X-ray beam. This simplifies the alignment problems, as the stream directs all sample particles into the interaction region. Having the

sample particles surrounded by a carrier medium increases background scattering which may bury the signal from weakly scattering single particles.

There are also experimental benefits in the choice of carrier medium. For example microcrystals are often streamed in their mother liquor, which keeps the crystals fully hydrated, stable, and at room temperature. The following chapter will discuss lipidic cubic phase (LCP) as a carrier medium for serial crystallography. LCP offers advantages in that it can be used for both injection, and as a growth medium for membrane protein crystals (e.g. G-protein coupled receptors (GPCR))(Liu et al. 2013).

Continuous stream injection is normally accomplished by one of three injector types: gas flow focused liquid jet, electrospinning, and viscous extrusion. The majority of this chapter will focus on gas focused liquid jets, as the author has had extensive experience with this injector type.

2.1.4 Drop on Demand Systems

Drop on demand systems describe a class of injector that, rather than introducing a continuous jet of liquid into the X-ray beam, are triggered to produce a single droplet. Drop on demand systems can produce droplets by acoustic levitation (Soares et al. 2011), by piezo triggered droplet ejection (similar to inkjet printing technology), and potentially by a fast switching GDVN.

As an alternative to continuous stream injectors, which can consume excessive amounts of sample, drop on demand systems have the potential to reduce the total amount of sample needed to collect a complete set of data, by hitting every drop with an XFEL pulse. They are limited, however, in that they are not suitable for use in vacuum.

2.1.4.1 Shrouded Micro Positioning Injector

The specific serial X-ray scattering experiments discussed in this thesis were done at the Linac Coherent Light Source (LCLS), located at SLAC National Accelerator Laboratory (SLAC). The experiments were done at the CXI end station (Boutet and J Williams 2010), in vacuum, using the bioparticle injector described in Weierstall et al. (2012) (Figure 2.1). The injector shroud provides a differentially pumped space that allows continuous stream injectors (especially those that use a co-flowing sheath gas) to operate without compromising the instrument chamber vacuum. The injector also provides the precision alignment of both the shroud, and the nozzle within the shroud.

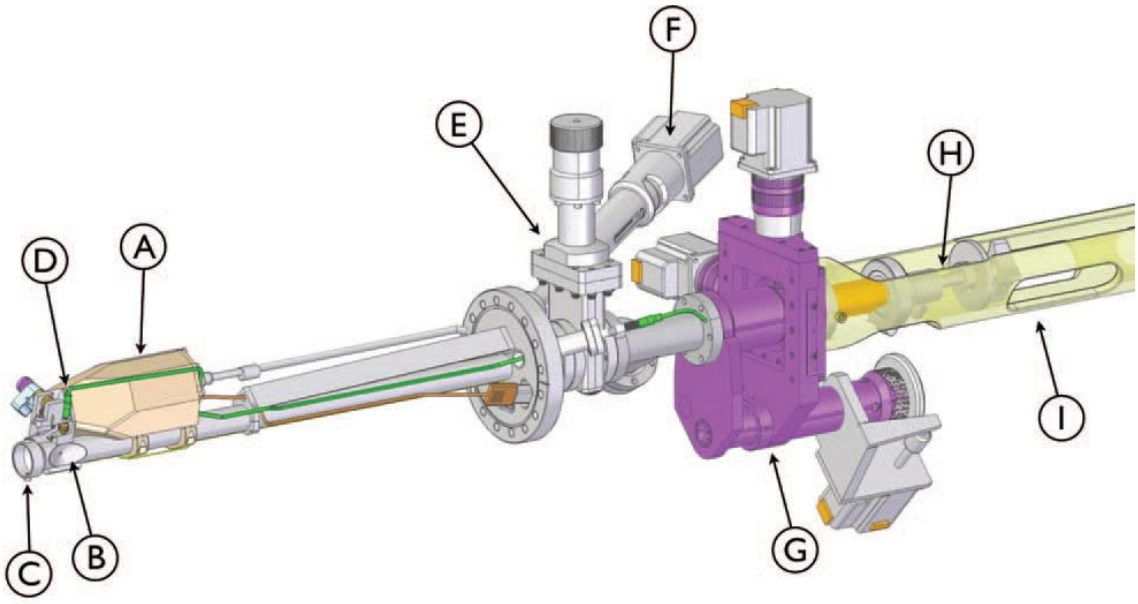

Figure 2.1: Shrouded Injector System
The injector system pictured above is mounted to an instrument vacuum chamber. A sample catcher and pump (not pictured) are attached at C, to accommodate the differential pumping. The nozzle is attached to a long rod (H), which is inserted into the shroud via load lock (E), and positioned via a three axis stage (G). The nozzle is observed with an in-vacuum microscope (A), which is focused by an external motor (F). X-rays pass through the shroud and exit via the cone (B). Reproduced with permission from Weierstall et al. (2012)

2.1.4.2 Flow Focused Liquid Microjet

The primary method for injection is a flow focused liquid microjet , called here the gas dynamic virtual nozzle (GDVN) (DePonte et al. 2008). The GDVN produces narrow streams of liquid for probing by the X-ray beam. The nozzles are resistant to clogging because the diameter of the nozzle outlet is much larger than the stream produced. This allows for the injection of crystal suspensions where the mean crystal size is larger than the output stream.

The flow speed of a GDVN produced microjet is about 10m/s. Sample waste is a primary concern as typical flow rates range from 8-15µl/min.

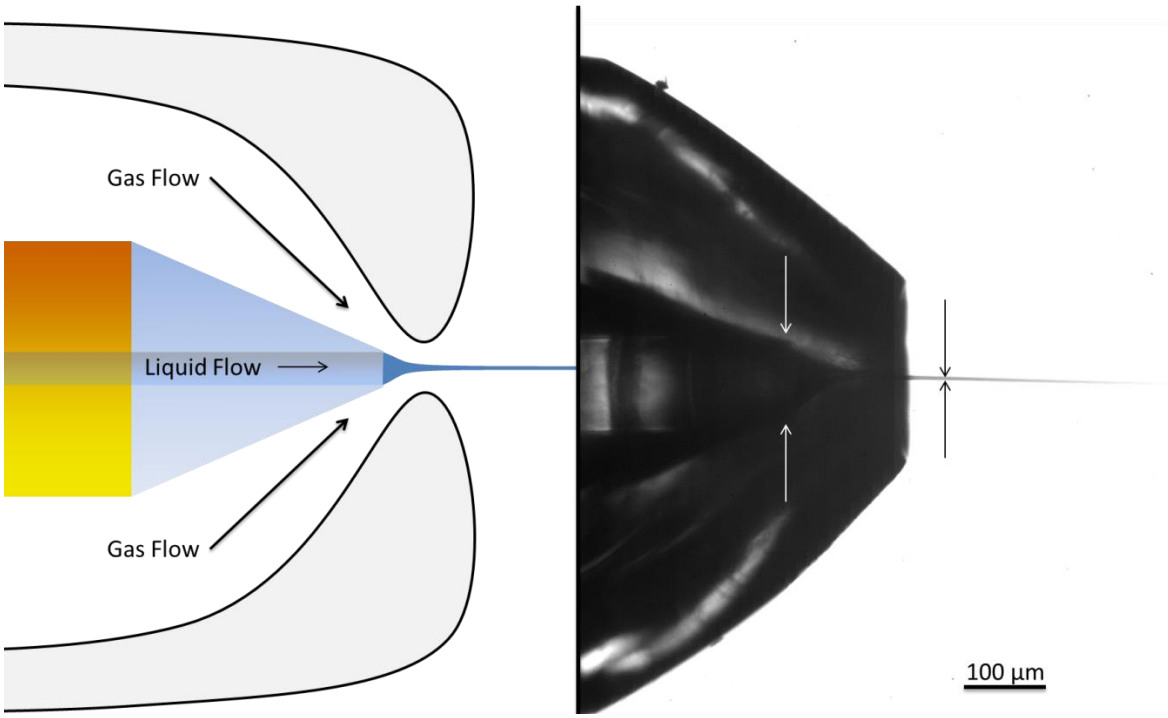

Figure 2.2: GDVN Schematic
A GDVN produces a thin jet of liquid by flow focusing a larger stream from the inner capillary tube. The liquid is flow focused by the sheath gas pressure and shear forces.

2.1.4.3 Electrospinning

The electrospinning microjet and the GDVN operate on similar principles, except that the focusing for the electrospinning microjet is provided by electrostatic forces, not a sheath gas (Gañán-Calvo and Montanero 2009). This allows for jet operation inside the instrument chamber without compromising the vacuum. Having the shroud removed also provides an easy path to simultaneous X-ray scattering, and spectroscopic experiments.

The electrospinning method requires that the liquid sample contain a polymer solution (usually glycerol, or polyethylene glycol (PEG)) (Sierra et al. 2012). These molecules facilitate the electro spinning, but limit the use of this injector to samples that can accommodate the polymer solution. Because the polymer solutions tend to have higher viscosities, the flowrates achievable by this injector vary from 0.14-3.1 µl/min.

2.1.4.4 Viscous Extrusion

An injector was designed to facilitate the injection of highly viscous fluids, specifically LCP. Design elements from the GDVN were adapted to allow stable jetting of LCP at extremely low flowrates. Viscous extrusion injector development comprises the original work done for this thesis, and will be discussed in chapter 3.

2.1.5 The GDVN Nozzle

The GDVN's use in serial X-ray scattering experiments is prevalent because of its effectiveness and its success in the early serial femtosecond crystallography (SFX) experiments (Chapman et al. 2011; Boutet et al. 2012). The GDVN has been used to inject: crystals in sponge phase (Johansson et al. 2012), solutions for wide angle scattering (Arnlund et al. 2014), and crystal suspensions for pump probe or time resolved crystallography (Aquila et al. 2012; Kupitz, Basu, et al. 2014).

2.1.5.1 Nozzle Construction

The GDVN consists of two capillary tubes, a gas aperture, a few miscellaneous small parts, and a stainless steel “nozzle holder” that allows for disassembly and adjustment of the GDVN (Figure 2.3).

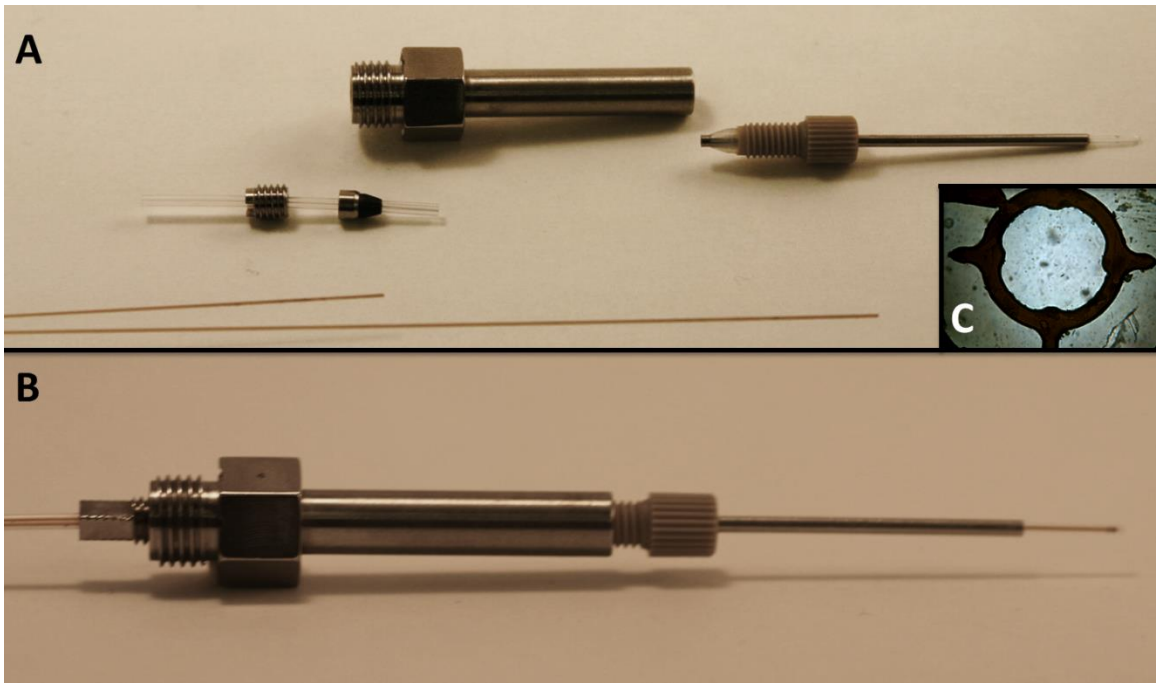

Figure 2.3: GDVN Construction
GDVN parts are shown disassembled in A: nozzle holder, gas aperture with fitting and ferrule, dual lumen sleeve with fitting and ferrule, the gas line capillary, liquid line capillary, and the centering spacer (C). The nozzle is shown fully assembled in B.

The liquid line capillary is conically ground at the outlet, and passed through a dual lumen sleeve, the nozzle holder and into the gas aperture. The gas line capillary (should be clearly marked) is passed through the dual lumen sleeve, and terminates shortly after it exits the sleeve. The dual lumen sleeve is secured in the back of the nozzle holder by a fitting and ferrule (IDEX). The liquid line is centered in the gas aperture by a custom laser-cut Kapton spacer (Figure 2.3). The liquid line should be adjusted so that the tip of the cone is centered just before the exit of the gas aperture.

Gas apertures are 1mm OD borosilicate glass tubes glued into1/16” stainless steel tubing. Then the glass is flame polished until the tip melts to form a converging-diverging nozzle (Figure 2.4). To ensure a symmetric gas aperture a specialized melting rig was built to spin the outer glass as it is melted in a propane flame. Measurements of the gas apertures melted in this way show deviations from concentricity of less than 1%. After melting, the gas aperture tip may be ground away to prevent the nozzle from shadowing the detector.

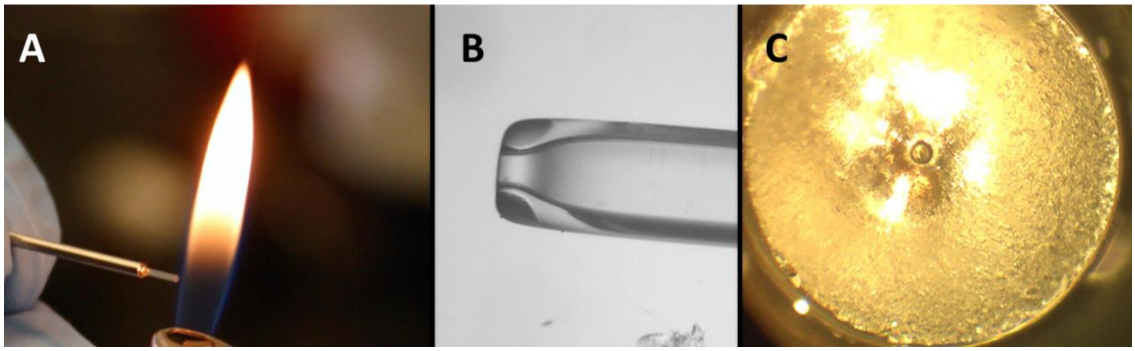

Figure 2.4: Gas Aperture Melting
Gas apertures are borosilicate capillaries melted in a propane flame (A). Melting causes the end of the glass capillary to narrow, forming a converging nozzle shape (B). The size of the aperture can be changed to optimize jetting for any particular sample liquid. Typically the gas aperture is melted to closely match the ID of the inner capillary tube (~50 microns). C shows an end-on microscope image of a melted gas aperture.

Capillary cones are ground on a sample preparation polisher (Allied), with 9-30 micron grit polishing films. The capillary is axially rotated in an angle adjustable stage (Figure 2.5). The grinding angle should be between 15-20 degrees, and the tip should be free from large chips and cracks.

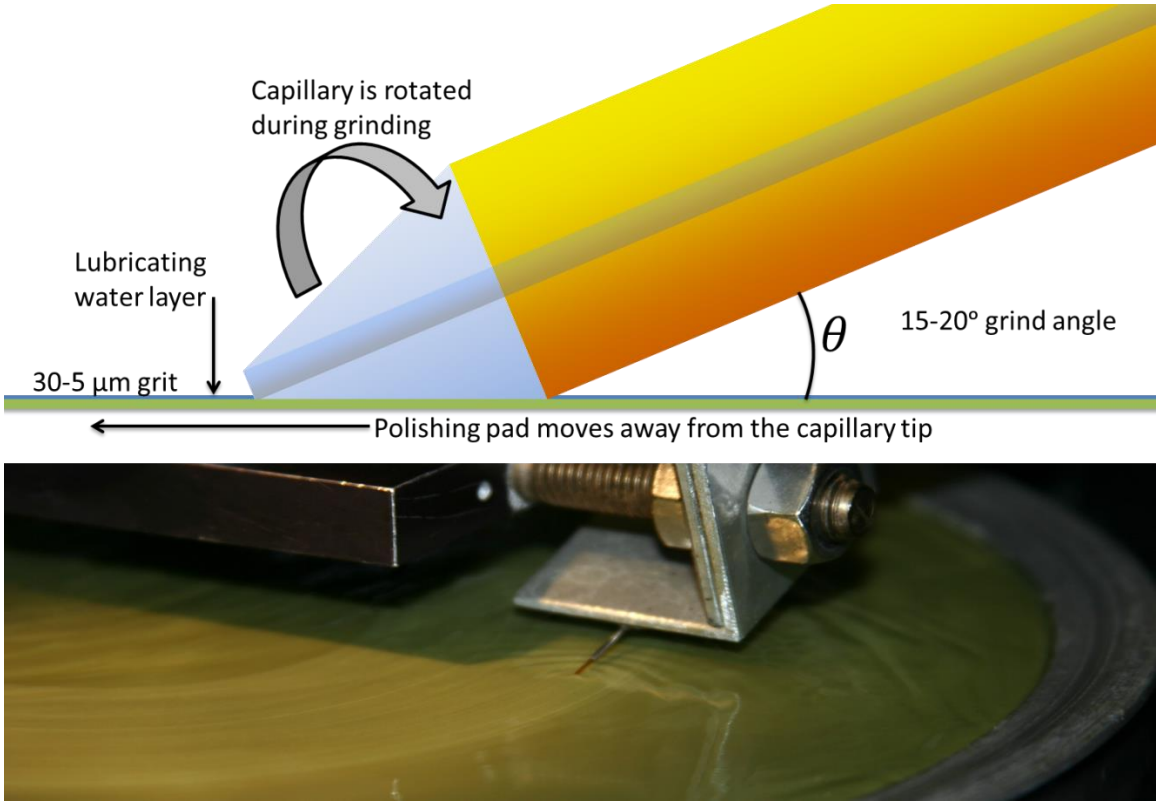

Figure 2.5: Capillary Tip Grinding
Capillary tips are conically ground by being rotated while lowered onto the polishing pad. An angled rotation stage is needed to facilitate the grinding (not shown).

2.1.5.2 Nozzle Improvements

The GDVN nozzle has evolved since its original conception in DePonte et al. (2008). The improvements in fabrication allow the nozzle to be disassembled, where originally it was glued together. Disassembly allows for the replacement of broken or malfunctioning parts. More importantly, the assembled nozzle can be adjusted, post-manufacture to accommodate the wide variety of sample liquids.

There are a few design changes described in Weierstall et al. (2012) namely the use of a square glass outer tube to make the gas aperture, and the asymmetrical inner bored capillary. The square glass size is selected such that the inner walls act to center the

liquid capillary in the gas aperture, and the asymmetrical inner bore provides a point for the jet to form off of. These changes, while effective for certain applications, have been phased out in favor of round gas apertures with Kapton spacers for centering, and a standard symmetric capillary cone.

As mentioned above, gas apertures are melted while being axially rotated to keep the aperture as symmetric as possible. In addition, the inner capillary is centered with the aid of custom laser-cut Kapton spacers (Figure 2.3). The centering of the capillary cone relative to the gas aperture is critical to the stable operation of the GDVN. Off center capillaries may still produce a microjet, however the jet will emerge from the nozzle crooked, which may be a severe problem under experimental conditions.

2.1.5.3 Nozzle Adjustment and Operation

After assembly the GDVN is ready for initial testing and adjustment. The liquid line is attached to a pressurized water-filled reservoir, or a constant flow-rate pump. The gas line should be attached to a regulated helium gas tank (the gas regulator should allow for precise control between 50-100 psi). After the lines are attached and the nozzle is placed in a vacuum test cell (for offline laboratory tests), the gas is turned on (~400psi should suffice for most nozzle tests). The test cell is evacuated, and then the liquid line is pressurized.

A GDVN has three normal operating modes: no flow, dripping, and jetting. The no flow mode occurs when the liquid pressure cannot overcome the resistance of the fluid in the capillary and the back pressure from the focusing gas (the liquid does not leave the nozzle tip). The dripping mode occurs when the liquid pressure is sufficient to create a stream of droplets from the nozzle, but insufficient to create a continuous jet. Finally, the

jetting mode occurs when the pressure has reached a critical value, and the liquid forms a jet, characterized by a contiguous column of liquid that breaks into droplets due to the Plateau-Rayleigh instability.

The onset and cessation of jetting is a hysteretic process, with the onset occurring at a higher pressure than the cessation. When a nozzle is characterized with a particular sample, the gas and liquid line pressures should be recorded at the onset of jetting to provide a reference point during the experiment.

Adjustments to the nozzle are required when: the nozzle does not jet, the jet is severely crooked, the nozzle produces ice, or the jet is too thick. The single most important parameter in nozzle adjustment is the location of the capillary cone relative to the gas aperture. The capillary should be centered (hence the spacers), and positioned just behind the narrowest constriction of the gas aperture. Adjustments to the capillary tip along the axis of the nozzle are made to maximize stability, or to minimize flowrate or jet size.

As a general guideline pulling the capillary back produces a straighter jet, but also may limit the minimum jet diameter that can be obtained with the nozzle. Pushing the capillary toward the gas aperture can produce a thinner jet, but usually results in a crooked jet. There is the possibility that when the capillary is pushed forward that it will: completely plug the gas aperture, break off the tip of the capillary cone, or that the liquid meniscus will make contact with the aperture wall (wetting the surface and disrupting nozzle operation). If the nozzle tip can protrude from the gas aperture a jet may still be formed in the free expansion region (Gañán-Calvo et al. 2010).

Once the nozzle is optimized the capillary should be secured in place by tightening the fitting at the back of the nozzle holder. Since the capillary is forced forward when the fitting is tightened, the capillary should first be pulled back (about 50-150 microns) before tightening. The nozzle is then retested to determine if the capillary has returned to the desired position.

After assembly, testing, and the recording of operating parameters, the nozzle is ready to be loaded into the instrument chamber. The nozzle is attached to the nozzle rod, the rod is inserted into the injector, and the gas and liquid lines are connected. The nozzle is positioned by the micromanipulation stage on the injector until it is visible on the injector microscope described in Weierstall et al. (2012). The nozzle is then operated just as in the test cell, by pressurizing the gas and liquid lines as described above.

2.1.5.4 Common Nozzle Problems

Once the jet begins operation, there are commonplace problems that occur frequently enough to address here. First, it should be noted that while a GDVN resists clogging by design, they can still clog easily enough. An inline filter should always be placed in the sample line to prevent large crystals, amorphous aggregates, or other large particles from clogging the capillary. Gradual clogging comes about as sample material forms a constriction somewhere in the sample line, and is manifested by an increasing pressure during sample jetting. Best practice is to run water through the nozzle before the gradual clog stops the flow completely.

Nozzle operation in vacuum creates a stream of rapidly cooling liquid. The droplets of super-cooled water will instantly form ice if they hit a surface, such as the inside of the shroud or catcher. Strong diffraction from water ice can be catastrophic for

sensitive detectors. Long towers of ice can build up and follow the jet back to the nozzle, causing a clog. As ice blocks the jet at the gas aperture, the nozzle can continue to fill with liquid, which will freeze in the vacuum (possibly damaging the nozzle in the process). In many cases a severe ice event requires the nozzle be removed, and replaced.

In case of ice, shut off the liquid pressure, and turn the gas pressure to maximum. The ice should sublimate away in the vacuum, and normal operation can resume after a few minutes. Often, ice events can occur from irregular jet flow caused by debris build up on the gas aperture (the XFEL beam blows sample material back toward the nozzle). If the glass surface of the gas aperture is wetted by the inner nozzle or debris blowback, then an ice event is almost inevitable.

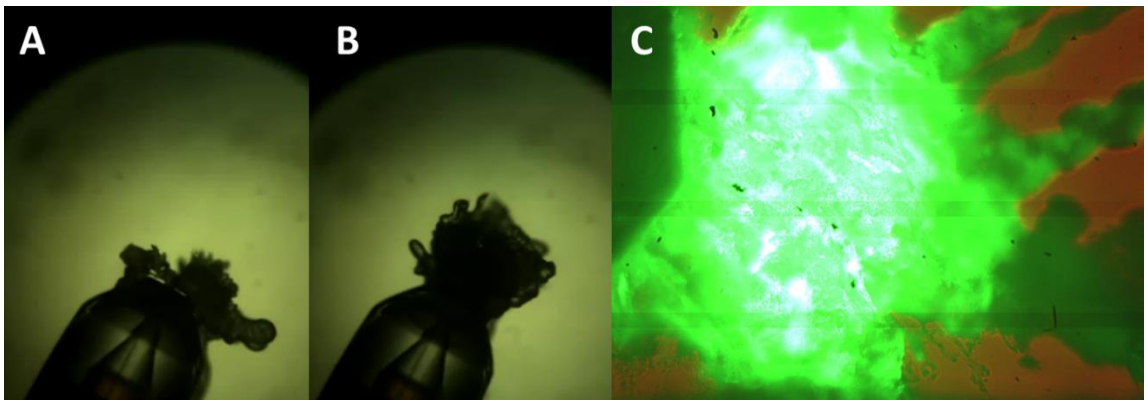

Figure 2.6: Ice Events
A and B show ice events from internal wetting caused by the inner capillary being off center. C shows an ice event from an experiment where an ice tower formed from the wall of the shroud and clogged the nozzle (the green light is pump laser illumination).

2.2 Sample Handling and Environments

For effective data collection the sample must be kept viable until it is probed by the X-ray beam. Some samples require special conditions to maintain viability while they await injection. Special sample reservoirs, light conditions, anti-settlers, and temperature controllers are often required. All of these sample delivery systems must be either

controlled remotely or operate independently to keep samples viable while they are stored in the X-ray hutch.

2.2.1 Sample Delivery

Sample delivery is accomplished by systems of pumps, lines, and valves that send the liquid sample to the nozzle. The most basic sample delivery system consists of a single column or loop of sample that is gas pressurized, and attached directly to the nozzle. The more complicated systems may contain one or more pumps, multi-position valves, multiple temperature controlled sample reservoirs, and an anti-settler.

2.2.2 Settling and the Anti-Settler

It has been observed that, when left undisturbed, certain crystals will settle out of suspension. When a sample reservoir sits in the hutch during several hours of data collection the settling of crystals will negatively affect the experiment (Lomb et al. 2012). The primary concern is sample hit rate. As sample begins to settle out, an initial spike in concentration (and therefore hit rate) is followed by a sharp drop in hits. The rotating anti-settler described in Lomb et al. (2012) was developed to counter the settling, and provide a more consistent hit rate throughout the experiment.

A smaller version of the rotating anti-settler was developed in the Arizona State injector lab. The ASU anti-settler was developed to provide all the benefits of the previous version, including temperature control, as well as maintaining a smaller form factor. The operation procedure for the ASU anti-settler system is provided in chapter 5 of this thesis.

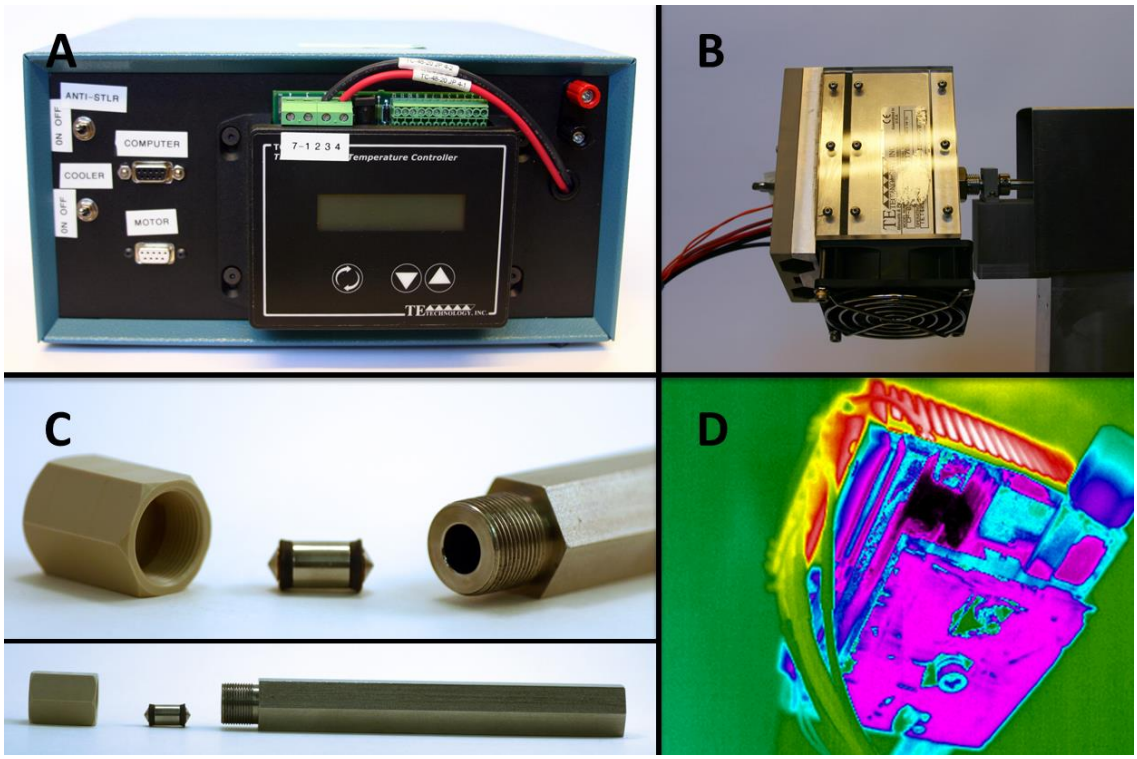

Figure 2.7: ASU Anti-Settler
The ASU anti-settler control box (A), and stand/rotor (B). C shows the stainless steel syringe reservoir. D shows a false color thermal image of the rotor with the thermoelectric cooler activated (red and yellow regions are hot, blue purple and black regions are cold).

2.2.2.1 Reservoirs

The reservoirs used with the anti-settler are similar to the ones described in Lomb et al. (2012). The reservoirs are essentially hydraulically driven syringes. They are designed to hold large amounts of sample, and can be agitated without introducing air into the system. The body is made of stainless steel, and is sealed at one end by a PEEK cap. The plunger is also stainless steel, and is sealed with hydraulic gaskets (Trelleborg). The reservoir loading procedure is given in chapter 5.

2.2.2.2 Sample switching

A sample delivery system that uses the ASU designed anti-settler/reservoirs requires at least one valve. The valve(s) (IDEX) allows switching between reservoirs or water.

2.2.2.3 Temperature

The rotor on the anti-settler has a built in thermoelectric cooler (TE technology) that allows cooling of the sample reservoirs down to 4ºC (Figure 2.7). The reservoirs should be precooled prior to loading to minimize cooling time. The anti-settler has been stress tested to maintain temperature for over 12 hours. Measures should be taken to contain condensation if the cooler will be operated below the dew point.

2.2.2.4 Lighting Conditions

Samples molecules are often photosensitive, and must be kept in the dark until probed by the X-ray beam (or possibly exposed to a pump laser pulse). When the reservoirs are sealed they are light tight, however sample delivery tubing may not be. If the experiment involves photosensitive samples, the tubing should be opaque. Also consider the capillary tubing used in nozzle construction, as it is nearly transparent. A piece of PEEK tubing should be used as a capillary sleeve to keep the sample in the nozzle lines from being exposed.

2.3 Sample Delivery for the Four Experimental Types

Injection methods for the four experimental types are presented below.

2.3.1 Serial Crystallography

For SFX experiments the primary methods of sample delivery are the continuous stream injectors. Results from liquid jet experiments are presented below, while those

from the viscous jet are given in chapter 3. The continuous stream injectors are preferred for SFX because of the high hit rate (compared to aerosol), and sample hydration offered by the technique. The higher background scattering from the carrier medium is not considered a problem for SFX because the Bragg diffraction is often much stronger than the background scattering. Crystallization is optimized to offer maximum resolution, and crystal concentration is optimized to maximize the number of single hits (Chapman et al. 2011).

2.3.2 Solution Scattering

The solution scattering experiments (SAXS and WAXS) have typically used a GDVN liquid jet for sample injection. Samples consist of many single molecules suspended in solution, and the data produced represents the spherically averaged molecular transform (hit rate is effectively 100%). In order to provide enough scatterers to the interaction volume, sometimes the GDVN must be pushed to operate at a high flow rate (20-30µl/min); this increases the interaction volume by providing a thicker jet.

2.3.3 Single Particle Imaging

Single particle experiments are typically conducted with aerosol injection (Seibert et al. 2011). This is because the weak scattering from single particles can easily be lost in the background scattering from a liquid jet. Continuous jet injection may be appropriate if the single particles are strong scatterers (i.e. metal nanoparticles).

2.3.4 Time Resolved Experiments

Time resolved experiments at the LCLS have used the liquid jet injector almost exclusively (Aquila et al. 2012; Kupitz, Basu, et al. 2014; Tenboer et al. 2014). The flow

speed of the liquid jet (~10m/s) is fast enough to completely clear pumped material between XFEL pulses, and allows for an easy "pump-probe" scheme.

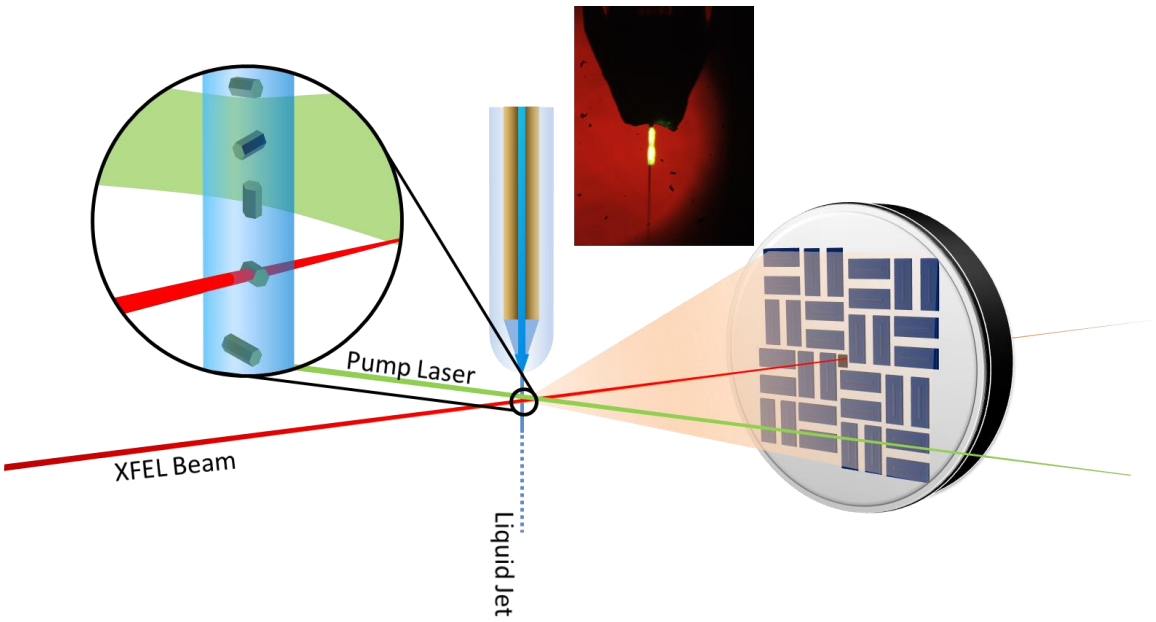

Figure 2.8: Pump-Probe Experiment Schematic
The pump-probe experiment described by the schematic above shows the addition of a pulsed "pump" laser. The inset photograph shows the illuminated region of the jet during an experiment.

Not all biological processes are photo-activated. This limits the number of molecules available for the pump-probe scheme described above. A different class of time resolved experiment may be done by observing the chemical kinetics from mixing solutions (i.e. enzyme-substrate interaction) (Schmidt 2013). A new type of liquid jet injector was developed to initiate fast mixing, with variable delay times between mixing and X-ray probing (Wang et al. 2014). The mixing nozzle has not yet been proven to work in an XFEL experiment, and there are problems with excessive dilution by the substrate solution. However, microfluidic "nozzle-on-a-chip" designs have shown a solution to the dilution problem in a double-focused liquid jet system by constricting the

channel at the mixing point (Trebbin et al. 2014). The problems associated with the mixing jet time-resolved experiments (i.e. adapting soft lithography devices to the shrouded in-vacuum injector) have yet to be resolved, and remain an active area of research.

2.3.5 Data Analysis

The final area of work in serial X-ray scattering experiments is data analysis. Once data is collected researchers are left with terabytes of data, the bulk of which contains no relevant information. Each experimental type requires data analysis methods unique to that type with little overlap. For serial crystallography, software packages have been developed and are now available for use (T. a. White et al. 2012; Sauter et al. 2013). Analysis methods for crystallography, and single particle diffractive imaging are described in the review by Spence et al. (2012).

2.4 Results from SFX

Results from selected SFX experiments are presented below with emphasis on injection and sample delivery.

2.4.1 TR-SFX of Photosystem II

Photosystem II (PSII) is the membrane protein complex that splits water in oxygenic photosynthesis. As PSII functions it evolves through a multi-state (S_0 to S_4) photo-driven process. In this experiment, time resolved SFX was done with PSII nanocrystals. During injection, but prior to probing, the PSII nanocrystals were excited to the S_3 state by two saturating laser pulses (Kupitz, Basu, et al. 2014).

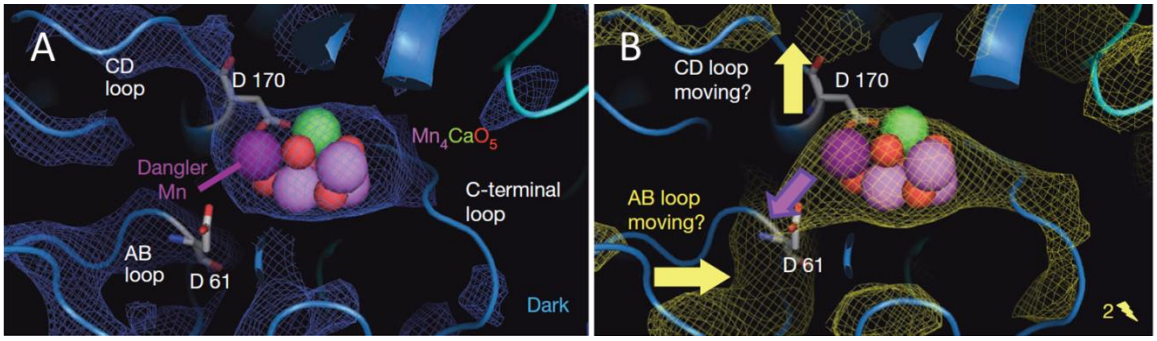

Figure 2.9: Light and Dark PSII Electron Density Map
The light (B) and dark (A) electron density maps from the PSII experiment are shown. Although resolution is limited, the density maps suggest conformational changes in the manganese cluster and may offer clues to the mechanism responsible for photosynthetic water splitting. Reproduced from Kupitz, Basu, et al. (2014)

Results from the PSII time resolved SFX (TR-SFX) show conformational states in the oxygen evolving cluster as the molecule is excited into the S_3 state. These results, while limited in resolution, show possible molecular mechanisms for photosynthetic water splitting.

Experiments were done at LCLS in the CXI end station. Sample delivery was done with the large anti-settler, stainless steel hydraulic syringe reservoirs (with temperature control), and GDVN. Syringe loading was done in a dark room (or with low intensity green light) to ensure that the PSII remains in the ground (S_1) state.

2.4.2 TR-SFX of Photoactive Yellow Protein

Photoactive yellow protein (PYP) is a bacterial blue light receptor. PYP begins a multi-state photo cycle when it absorbs a blue photon. It has been used extensively in other time resolved crystallography experiments using the Laue method at synchrotrons. Time resolution is limited by X-ray pulse time. With XFEL pulses on the order of 100fs there is an opportunity to get high resolution in time. New resolutions offered by the

XFEL, and the extensive work already done make PYP an ideal model system for TR-SFX.

TR-SFX data was collected at LCLS CXI end station. The pump laser illuminated the sample stream in an interleaved manner (2 dark frames then 1 light frame). This ensures that both light and dark frames were collected for every sample preparation. TR-SFX's advantages over the Laue method include: short pulses (high temporal resolution), and more effective laser pumping due to the small crystals. Sample delivery was done with SLAC designed hydraulic syringes with no temperature control, no anti-settling, and the GDVN (Tenboer et al. 2014).

3 SFX WITH LIPIDIC CUBIC PHASE

As described previously, serial femtosecond crystallography (SFX) had its beginning after the construction of the first X-ray free electron laser (XFEL). SFX uses the high intensity ultra-short pulses from the XFEL to collect diffraction data from a series of similar crystals. The data is then merged, phased, and transformed to recover the electron density of the crystal molecule.

XFELs are so intense that molecules in the path of the beam are obliterated in a single pulse. For this reason technology was developed to continuously renew sample for SFX experiments. Primarily these technologies have implemented the flow-focused liquid microjet produced by a gas dynamic virtual nozzle (GDVN) as the sample delivery source (DePonte et al. 2008). The GDVN successfully fulfills its role in an SFX experiment, but suffers from excessive sample consumption.

3.1.1 Liquid Microjet Sample Waste Problem

Typical SFX experiments that use a GDVN as the sample delivery device run a liquid microjet at a flow rate of 10µl/min. Operating a GDVN at average flow rates (i.e. 10µl/min) for a full beamtime (i.e. 62 hours) requires many milliliters (i.e. 37ml) of sample. A complete data set may be obtained in as little as six hours of beamtime, but may consume as much as 10-100 milligrams of pure protein.

Unfortunately due to the nature of continuous jet SFX experiments most of the sample volume is wasted (meaning never probed by X-rays). For an SFX experiment at Linac Coherent Light Source (LCLS), it is estimated that on average only 1 in 10,000 crystals are hit with the XFEL beam (Uwe Weierstall et al. 2014). For many samples, amassing the amounts of protein needed to run a GDVN render SFX impractical.

To address the sample waste problem a new injector was developed to slow the sample flow rate, which would reduce sample waste, and therefore reduce total protein required for SFX structure determination. The new injector achieves low flow rate operation by replacing the low viscosity samples typically used with the GDVN with high viscosity media. The high viscosity media chosen should maintain crystal quality, have a reasonable X-ray scattering background, and form a continuous column at low flow rates. Lipidic cubic phase (LCP) was selected as the primary sample delivery media for the injector, because it meets these criteria.

3.1.2 LCP as a Delivery Medium

LCP was selected as the primary high viscosity crystal delivery material because of its use as a growth medium for membrane protein crystals. Beginning with the foundational work in Landau & Rosenbusch (1996), a new method for the crystallization of proteins was developed using lipidic mesophases. Crystallographic studies on protein crystals grown in LCP have yielded structures of membrane proteins from disparate families: ion channels, transporters, and enzymes (Pebay-Peyroula et al. 1997; Cherezov et al. 2007; Santos et al. 2012; Liao et al. 2012; Li et al. 2013).

Protein crystals grown in LCP tend to be well ordered, but optimization for growing large crystals can be a lengthy process. A sample with a high density of micron sized crystals is more readily obtained than one that would produce crystals large enough for data collection at a synchrotron source. These “showers of microcrystals” are ideal for trial in serial crystallography experiments.

Proteins in LCP are embedded in a lipid bilayer similar to the cell membrane, and have been shown to remain active (Rayan et al. 2014). Additionally LCP-SFX diffraction

data is recorded from membrane proteins at room temperature. These experimental conditions are closer to those that that exist within the cell, and may produce more biologically relevant results. Electron density data between SFX and more conventional synchrotron microcrystallography experiments show differences that could be attributed to these environmental dissimilarities (Liu et al. 2013).

While LCP has proven successful at membrane protein crystallization, these methods have not seen wide adoption because of the difficulty in working with the material. Specialized tools and procedures have been developed to aid in crystallization, and sample preparation (Cherezov 2011; Liu, Ishchenko, and Cherezov 2014).

3.2 Properties of LCP

LCP forms spontaneously when the lipid and water are mixed in the proper proportions (lipid to water ratios are specific to the lipid used). LCP is thick and gel-like, and maintains its shape when under no stress. As a fluid, LCP exhibits non-Newtonian properties that the best fit Maxwell fluid models still fail to describe accurately (Mezzenga et al. 2005).

LCP is just one of the phases of liquid crystal that can form from the mixture of lipid and water. The sponge phase can also be used to grow protein microcrystals, and has been used in SFX with a GDVN nozzle (Johansson et al. 2012).

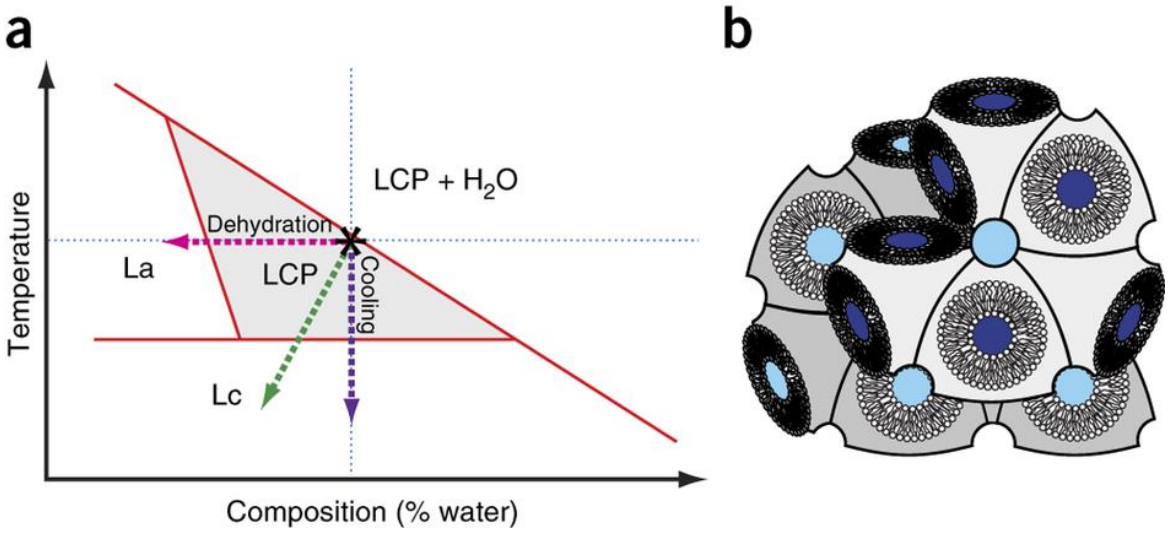

Figure 3.1 Phase Behavior of Lipids
A Simplified temperature water concentration phase diagram is shown in (a). Here lipid phase is shown to shift toward the lamellar crystalline phase (L_c) when the LCP is cooled and dehydrated (as it is in vacuum). A representation of the cubic phase is also shown (b), where the dark and light blue circles represent non-intersecting water channels. Reproduced with permission from Liu, Ishchenko, and Cherezov (2014)

The phase diagram for lipid water system in Figure 3.1 reveals a problem for LCP injection into vacuum. Because of the rapid evaporative cooling effects of vacuum, the lipid matrix may undergo a phase change from the cubic to the lamellar crystalline phase. The phase change is easily seen by both X-ray diffraction (Qiu and Caffrey 2000), and polarized light microscopy (see Figure 3.5). A more detailed description of how to avoid phase change during injection will be given in section 3.5.4.

For the purposes of continuous column extrusion, the fluid properties of injection media are a major concern. Experiments conducted by Mezzenga et al. (2005) show that LCP exhibits viscoelasticity and shear thinning. Shear thinning fluids decrease in viscosity with higher rates of shear strain. In a tube, as the boundary layers decrease in viscosity, the inner annuli can flow with the same velocity (plug flow). The shear

thinning exhibited by LCP ultimately proves beneficial by lessening the pressure required for extrusion.

The fluid properties of the LCP will vary as different protein, buffers, and precipitants are used in sample preparation. Therefore the exact properties of any particular sample need not be known. Ultimately a test of the injection media in the lab will show whether the microextrusion injector is appropriate for sample delivery.

3.3 LCP Injector Development

The original LCP extrusion apparatus was a tube backfilled with LCP, and connected to a short piece of capillary tubing (Figure 3.2). Experiments showed that although the LCP could be extruded from the capillary, the sticky gel-like LCP would curl back, and foul the stream. While there were brief periods of time where the injector produced a constant stream, the curling would inevitably cause problems. These occurrences were also exacerbated by the XFEL beam.

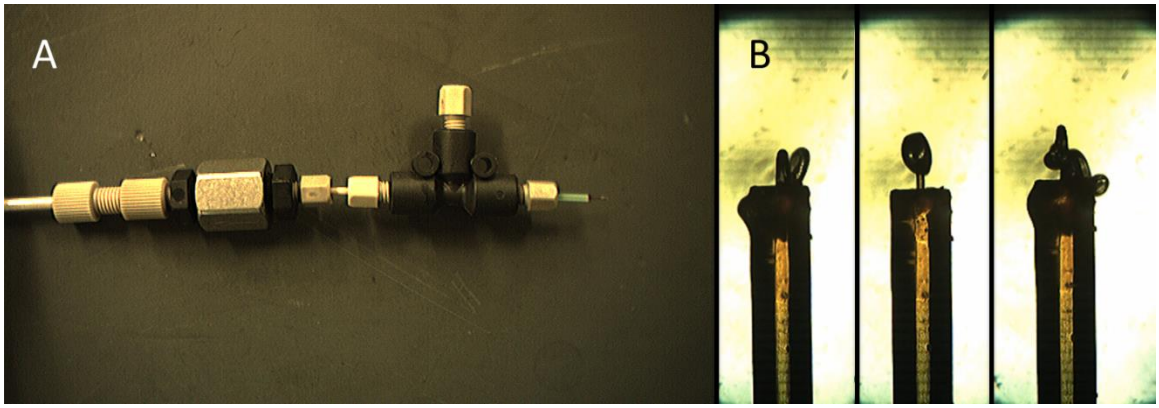

Figure 3.2: Early LCP Extrusion
The first attempt to extrude LCP for SFX was done with this injector (A). It consists of a gas pressurized reservoir pushing the LCP through a capillary tube. LCP extrusion is possible, but highly unstable with the LCP stream curling and sticking to the capillary tip (B).

3.3.1 The LCP Nozzle

To solve the problems of the LCP curling, a sheath gas system similar to the one used in a GDVN was developed. Like the GDVN, the capillary is conically ground, and passes through a glass tube with a melted aperture. While the construction and use are similar, the LCP nozzle does not flow-focus the stream like in the GDVN. The sheath gas is used only to keep the LCP stream on axis, stable, and as straight as possible. Stream breakup occurs when the shear forces from the sheath gas overpower the internal viscous forces of the LCP stream. Further improvements produced a nozzle where the tip of the capillary tubing protrudes from the opening of the gas aperture. The protrusion places the nozzle exit in a lower shear region of the sheath gas jet.

To apply the sheath gas a new generation of LCP injector was developed. Custom parts were machined to introduce the sheath gas via a capillary feed through (Figure 3.3). The rest of the injector used technology adapted from a standard GDVN nozzle. The reservoir remained a short length tubing which was backfilled with LCP. Pressure was applied to the sample with compressed gas.

It was found that compressed gas did not fully use the available sample but rather pushed a “path of least resistance” through the sample until the gas could escape through the nozzle. Later, an attempt was made to use water to push the LCP through the nozzle. However, water contamination of LCP causes a transition to the sponge phase, and ruins the sample. To solve the sample contamination problem, polyethylene microspheres (Cospheric) were placed in the tubing reservoir to act as a barrier between the water, and the LCP (Figure 3.3).

While the improved injector worked, there was a high failure rate due to: leakage around the spheres, crushed spheres from high pressure, clogging due to particulate from crushed spheres, and fitting failures and leaking due to high pressure.

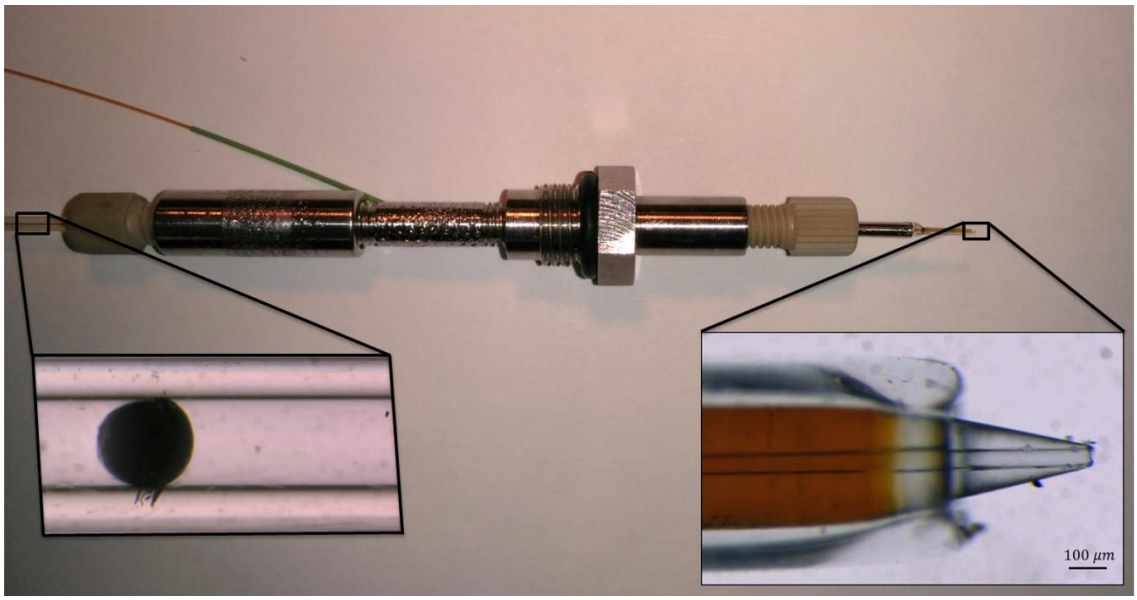

Figure 3.3: LCP Injector With Improved Nozzle
The second generation of LCP injector is shown. The major improvement in this iteration is the sheath gas nozzle. The co-flowing gas keeps the LCP on-axis and stable. Also visible is the microsphere used to separate the LCP reservoir from the pressurizing water. Due to a high failure rate the microsphere reservoir was abandoned in favor of the latest design in Figure 3.4.

To address the sample contamination and other problems associated with tubing reservoirs, a new injector design was built that uses an isolated reservoir. The reservoir is sealed at the back with compressed Teflon spheres, and at the front with a 10-32 coned port, to which the LCP nozzle is attached. The nozzle is contained in a new nozzle body with a built in gas port, alleviating the need for an inline feedthrough like in the previous generation, and providing a much simpler assembly. The sample is extruded from the reservoir and through the nozzle by pressure applied from a hydraulic piston.

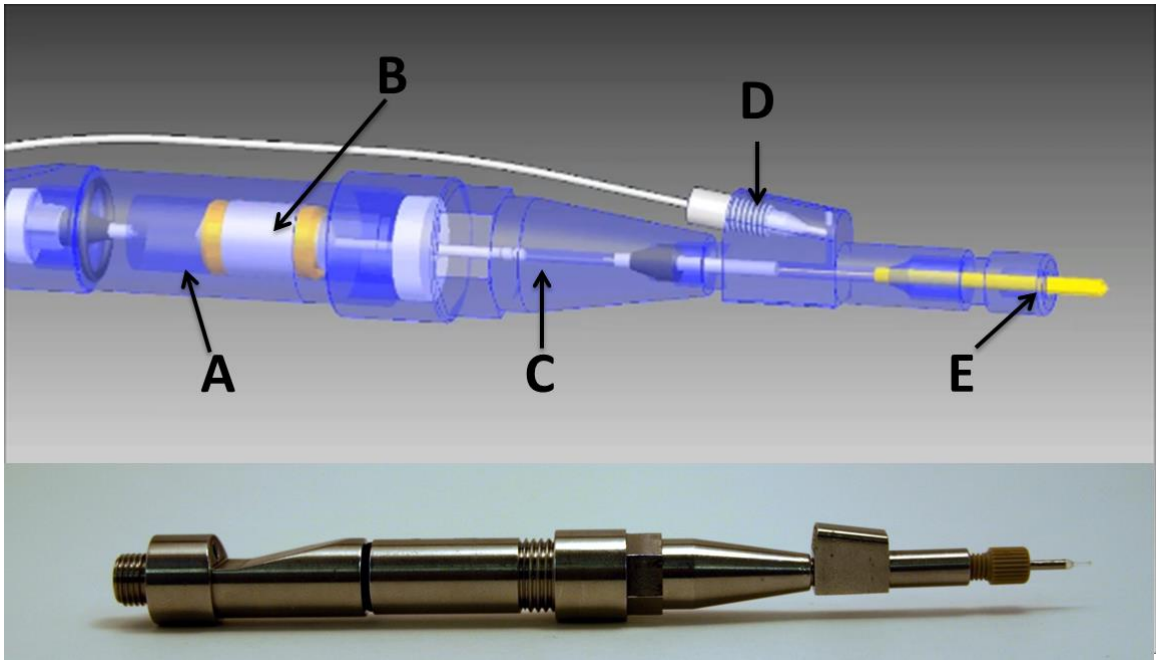

Figure 3.4: Latest Model of LCP injector
This, the latest model of LCP injector, consists of three main parts: the hydraulic stage (A), sample reservoir (C), and the nozzle (E). Pressure amplification is provided by the piston (B) and sheath gas is routed in the nozzle port (D).

The injector was designed to adapt the in vacuum liquid jet injector described in Weierstall et al. (2012). The whole LCP injector assembly can be put at the end of the nozzle rod in the place of the GDVN nozzle. The LCP injector can also be operated at atmospheric pressures in a stand-alone configuration.

3.3.2 Pressure Amplification

The LCP injector requires a source of pressure to drive the sample through the nozzle. Typically the pressure is sourced by a constant flow rate pump of the kind used in HPLC systems (Shimadzu). Pressure from the pump is amplified by the injector's hydraulic stage. The piston in the hydraulic stage has two radii, a larger bored input, and a smaller bored output. The asymmetric design of the piston provides amplification to the applied pressure given by:

$$\chi = \frac{A_i}{A_o}$$

Where A_i and A_o are the bore cross sectional areas of the input and output respectively, and χ is the amplification factor. The pressure amplifier also works as a flow rate divider; as volumetric flow rate is reduced by the same factor.

Pressure amplification at the last stage in the injector also removes the high pressure constraint from the rest of the system. The only high pressure fitting in the entire system is located between the reservoir and the nozzle.

Under adequate pressure the LCP in the reservoir is extruded through the nozzle, and, directed by the sheath gas, flows into the interaction region where it is probed by the X-ray beam.

3.4 Fabrication of Consumables

While most of the injector parts are machined from stainless steel and are reusable, some pieces of the injector are considered consumables namely: the capillary tubing through which the sample is extruded, the gas aperture, the ferrules, and seals. The gas aperture can be reused, but breakages are common enough that it should be considered a consumable.

The capillary and gas aperture are fabricated in the lab, as they are not available off the shelf, and are expended frequently. In this section a detailed fabrication procedure and guide will be given.

3.4.1 Capillary Tip Fabrication

The LCP is extruded through a short section of fused silica capillary tubing (Molex/Polymicro). The tip of the capillary is conically ground at one end. To accomplish the grinding, a machine like the Allied Tech MultiPrep, or the Ultrapol fiber

lensing machine is used. The grinding surface of the machine is covered in 30-12 micron grit film (Allied).

A section of capillary (capillary tubing is cleaved easily by scratching the surface of the glass through the protective polyimide coating) is secured to a stage where it can be rotated axially, and supported laterally (to keep it from flexing during grinding). The stage should hold the capillary at an angle to the polishing surface (typically between 15 and 20 degrees). The polishing stage should be rotating away from the capillary tip (see Figure 2.5) and water lubricated.

The rotating capillary tip is lowered onto the rotating abrasive until it just makes contact, then lowered an additional 50-100 microns (microscope observation is critical to grinding accurate capillary tips). If it is available on the grinder, oscillate the capillary position on the grinding surface. Checking progress periodically with the microscope, make adjustments to the capillary height as needed. After a few minutes (depending on the grit chosen) the capillary tip should be conically ground.

After removal from the grinder, check the tip under a microscope to ensure the tip is concentric, and free of cracks. Rinse the capillary tube with clean water (high pressure is required to rinse small diameter capillaries) to remove any grinding debris, and blow dry with clean compressed air. With the tip ground, inspected, and cleaned, trim the length to about 10cm for storage, and transport.

3.4.2 Gas Apertures

The gas aperture is assembled from a one inch section of stainless steel tubing (IDEX), and a 15mm length of square profiled glass tubing (Friedrich & Drummond). The stainless steel tubing must be cut to length before use with a saw or other tool that

will not pinch the tubing closed. After it is cut the tube should be de-burred (a piece of the square glass should slide in easily).

A 15mm section of glass tubing is prepared by cleaving the appropriate length, and ensuring the ends are flat (after cleaving, the ends may be ground on abrasive film to achieve flatness). Insert the glass into the stainless steel tubing and glue in place with quick set epoxy (Hardman).

After the epoxy has cured, flame polish the tip of the glass until a conically ground capillary tip just protrudes from the opening. The shape of the melted gas aperture is not quite round in cross section, allowing for gas flow even when the capillary tip is protruding. Note that the glass of the gas aperture is extremely fragile, and forcing a conically ground tip through the opening will cause breakages. After construction the gas aperture is normally seated in a 10-32 coned port (IDEX) for use in an LCP nozzle.

3.4.3 Assembly and Adjustment

Nozzle assembly and adjustment are discussed in detail in the next chapter.

3.5 LCP Injector Control

The LCP injector is usually controlled remotely as experiments are usually located in areas with X-rays. Once the injector is installed there are only two parameters that can be controlled by the operator: sheath gas pressure, and liquid line pressure.

3.5.1 Liquid Pressure Control

The liquid line can be pressurized by any method available to the user. The injector was developed to use an HPLC pump (Shimadzu) as the primary provider of liquid pressure, but the injector has also been operated with a gas pressurized water reservoir. The HPLC pump is the preferred system because of the automatic pressure

adjustment when operated in constant flow rate mode. The constant pressure provided by compressed gas does not offer the accurate flow rate control, and, because of the complex non-Newtonian fluid properties of LCP, can cause a "slippage" event where all of the LCP in the reservoir is pushed through the nozzle in a matter of seconds.

The HPLC pumps used with the LCP injector have a slow pressure response when trying to increase flow rate; especially at the low flow rates commonly used. When an event occurs that would cause an increase in pressure (i.e. a clog), the pump will slowly build pressure until the clog is cleared or the maximum set pressure is reached. The wait time for pressure buildup can be unnecessarily long (especially when first starting the injector), and can be bypassed by manually ramping the pressure. To manually ramp the pressure enter a flow rate an order of magnitude (or more) higher than the desired flow rate, and wait until the pressure reaches a predetermined point, then reset the flow rate to the desired level.

3.5.2 Gas Pressure Control

Sheath gas is delivered by compressed gas cylinders (usually helium, sometimes nitrogen). Pressure regulators should be accurate to ±5 psi, and provide accurate control at low pressures (Matheson, Parker, or Proportion Air). It should be noted that while the gas pressure at the regulator and the gas pressure in the nozzle are related they are not the same. Pressure drops across long lengths of small diameter tubing like the kind used in the LCP injector. The reading at the regulator should only be used as a guide when characterizing LCP nozzles.

Sheath gas pressure is adjusted to maximize LCP stream stability. Stability relies on a stable interaction between the LCP and a supersonic expansion gas jet. This

interaction is difficult to predict based on: variability in the nozzle construction (different gas aperture sizes, capillary protrusion etc.), variability in sample composition, and inaccuracy of gas pressure control.

There are a few consistent observations that may help when trying to achieve stream stability. When the shear forces of the gas jet are stronger than the internal viscous forces of the LCP, the stream will break. For this reason lower gas pressure usually allows for longer LCP streams. Stream whipping is usually improved by lowering the gas pressure. Without gas flow, LCP will often form a droplet at the tip of the capillary. Low gas flow may allow for LCP extrusion, but still permit jet curling. Ideally the sheath gas should allow a straight, stable, and long running jet.

3.5.3 Injector Control Calculations

When LCP injection starts the sheath gas should be on, and the plunger of the hydraulic stage advanced so that it makes contact with the seal at the back of the reservoir. The maximum pressure, P_{max}, should be calculated and entered as the maximum pressure cutoff if that feature is available on the pump.

$$P_{max} = P_{rated}\,\chi$$

Where P_{rated} is the rated pressure for the ferrule used in the nozzle/reservoir (usually 10000 psi). The flow rate entered at the pump is F_{pump} calculated by dividing the sample flow rate (F_{sample}) by the amplification factor (χ):

$$F_{pump} = \frac{F_{sample}}{\chi} = \frac{\pi\, n\, \delta}{\chi}\left(\frac{d}{2}\right)^2$$

Where n is the X-ray pulse repetition rate, δ is the desired distance between shots, and d is the inner diameter of the capillary tubing. The desired distance between shots (δ)

represents the distance that the LCP travels in the time between X-ray pulses and should be determined based on the beam spot dimensions, and size of the area on the LCP stream affected by radiation damage.

From the calculated flow rate, other useful quantities can be estimated. The sample run time (T) is given by:

$$T = F_{sample}/V$$

Where V is the total volume of sample loaded. The calculated run time (T) can be made more accurate by estimating the dead volume in the sample reservoir.

Once the desired flow rate is calculated and entered into the pump, a baseline operating pressure should be measured. Baseline pressure represents the amount of pressure at the pump needed to extrude the sample at the desired flow rate. The HPLC pump's constant flow rate mode of operation will adjust pressure until the entered flow rate is reached. The baseline pressure is shown at the pump when the pump has reached steady state operation. Baseline pressure is used to identify problems during sample injection like: capillary clogs, empty reservoirs, and leaks.

A more detailed procedure for installing, and operating the LCP injector is given in the next chapter.

3.5.4 Jet Phase Change

As mentioned above, LCP has a complex phase diagram, and under certain experimental conditions may undergo a phase change. Specifically, LCP made with monoolein has a phase transition from a cubic to a lamellar phase at 18ºC. The lamellar phase transition can occur because of sample dehydration or cooling. When sample is injected into vacuum the initial change in temperature, due to evaporative cooling, can be

as fast as 10^6K/s. During data collection lamellar phase formation manifests as sharp rings at high angle (Figure 3.5). The transition to lamellar phase can disrupt data collection by obscuring Bragg peaks in the background, potentially damaging sensitive detectors, or even disrupting the operation of the injector.

The lamellar phase transition can be observed by polarized light microscopy (PLM). With PLM the birefringent lamellar phase can be seen to glow while the cubic phase remains dark. PLM is useful for diagnosing potential phase transition problems while at a home lab. Adequate time should be given to testing the injection properties of each sample prior to a beamtime. If problems are discovered time will be needed to adapt sample preparations to the injection environment.

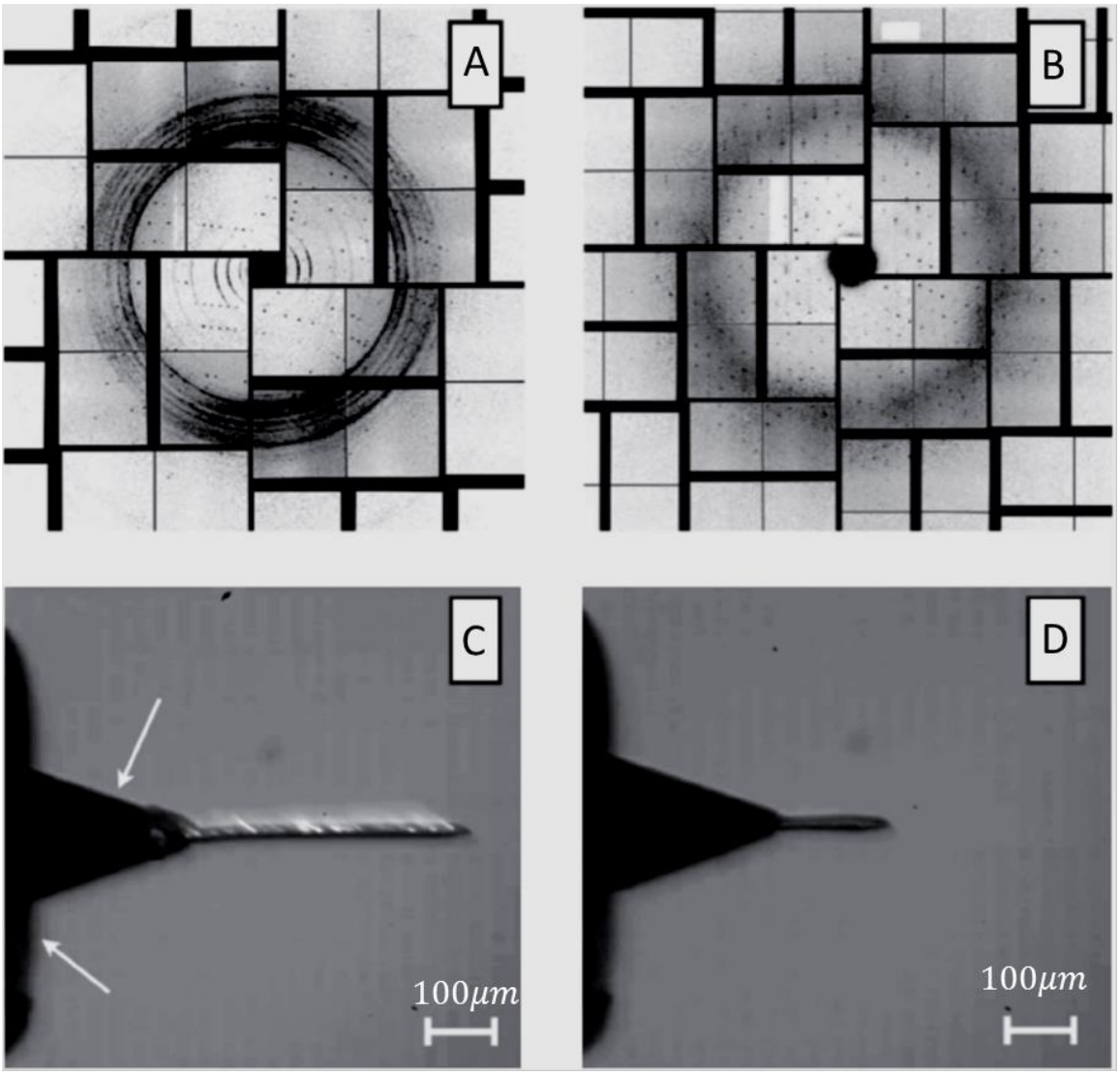

Figure 3.5: Lamellar Phase Transition
Diffraction patterns from micro crystals in LCP are shown. In (A) the LCP has transitioned to the lamellar crystalline phase. In (B) the phase change has been suppressed. In the lab lamellar phase can be seen with polarized light microscopy. (C) shows PLM image of LCP extrusion with helium sheath gas. (D) shows PLM image of the same jet with nitrogen as the sheath gas. Reproduced from Weierstall et al. (2014).

The transition to lamellar phase has been avoided using two methods: by a change in sheath gas from helium to nitrogen, and using a lipid with a different transition temperature. The sheath gas change can be done easily if the nitrogen is available. Often the need for a second sheath gas can be anticipated, and a second gas installed with a

remote controlled switching valve. The more effective method involves doping the crystal laden LCP with the low transition lipid (Liu et al. 2013). The LCP is doped with the lipid just before injection, rather than having to adapt crystallization for an entirely new lipid. This allows for the lipid best suited for crystallization to be used in growing the crystals, while still avoiding lamellar phase transition.

3.6 LCP-SFX Results

The injector effectively extrudes streams of LCP in vacuum or at ambient pressure. Flow rates are quite variable based on pump setting and sample composition (i.e. 1-800nl/min). Data is collected from crystal laden LCP at room temperature, in vacuum or ambient pressure.

Because of the low flow rates, protein consumption is dramatically reduced when compared to GDVN experiments. Table 3.1 shows a comparison between a few data sets collected with the GDVN versus LCP injector.

Table 3.1: Sample Consumption Comparison
Table comparing sample consumption and hit rates for data sets collected with different SFX injectors. For the PS I and lysozyme datasets, hits were registered for diffraction patterns with >10 Bragg spots, for the 5-HT2B, SMO and DgKA datasets, diffraction patterns with >15 Bragg spots were registered as hits. Reproduced from Weierstall et al. (2014) supplementary materials.

Protein	**PS I**	**Lysozyme**	**5-HT_{2b}**	**SMO**	**DgkA**
Crystal growth medium	Liquid	Liquid	LCP	LCP	LCP
Injector	GDVN	GDVN	LCP	LCP	LCP
Total frames recorded	1,850,000	1,471,615	4,217,508	3,510,525	1,987,632
Crystal hits	112,725	66,442	152,615	274,214	263,435
Indexed Hits	15,445	12,247	32,819	61,964	66,165
Hit rate, %	6	4.5	3.6	7.8	13
Indexing rate, %	17.7	18.4	21.5	22.6	25
Sample consumption (liquid and protein mass)	10,000µL 10 mg	10,800µL 15 mg	100 µL 0.3 mg	83 µL 0.5 mg	4.6 µL 0.3 mg
Flow rate in µL/min	10	30	0.17	0.17	0.17
Consumed protein per 10,000 indexed patterns	6.5 mg	12.2 mg	0.091 mg	0.081 mg	0.045 mg

3.6.1 Biomolecules

The injector was designed for streaming LCP specifically because of the advantage gained when collecting data on crystals grown in the LCP itself. This includes membrane proteins, and to a lesser extent soluble proteins (Aherne, Lyons, and Caffrey 2012). Membrane proteins are of particular interest as they make up a large portion of the proteome of most organisms, and a majority of current drug targets.

Having three dimensional high resolution structures of membrane proteins offers insight into their cellular and physiological function. Further, these structures are crucial for designing drugs with high degrees of selectivity and potency. Despite the potential medical application, structural discovery of membrane proteins has trailed behind soluble proteins; highlighting the need for developing new methods (S. H. White 2005).

Reported in this section are the several membrane proteins where the structure was determined from LCP SFX using the LCP injector to deliver sample to an X-ray beam. The three cases highlighted here are presented because they demonstrate a "proof of principle", or show a unique feature of serial crystallography with the LCP injector.

3.6.2 SFX of GPCR 5-HT_{2B}

G-protein coupled receptors (GPCR) are eukaryotic membrane proteins that facilitate cellular communication. In humans, the GPCR superfamily represents about 800 proteins that mediate extracellular signaling. The central role of GPCRs in physiological and sensory processes makes them important drug targets. Figure 3.6 shows overlapping models of the GPRC 5-HT_{2B}. The two models represent data collected

from 5-HT_{2B} crystals using two different techniques; LCP-SFX, and synchrotron microcrystallography (Liu et al. 2013).

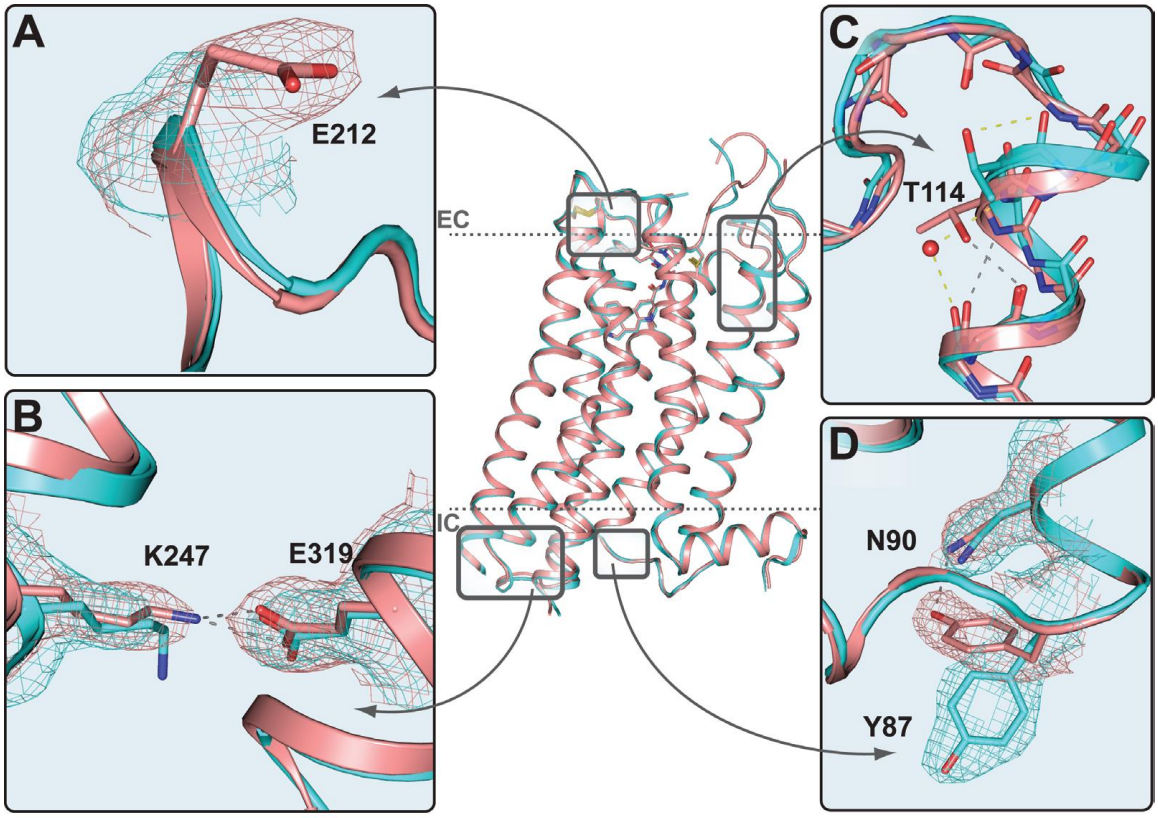

Figure 3.6: 5-HT_{2B} Structure Comparison
This figure shows overlapping structures of 5-HT_{2B}. The light red structure was obtained using LCP-SFX, while the light blue structure was obtained using synchrotron microcrystallography (at cryogenic temperatures). While the structures show good agreement there are differences (A, B, C, D) that might be attributed to the temperature difference, cryocooling, and radiation damage during data collection. Reproduced with permission from Liu et al. (2013).

3.6.3 Smoothened/Cyclopamine

Another data set was collected for the human GPCR smoothened (SMO) receptor in complex with cyclopamine (a naturally occurring teratogen). The data was collected using LCP-SFX, and structure was solved to 3.2 angstroms. This case is unique because, even though the SMO structure had been solved previously, attempts to collect data on

the SMO-cyclopamine complex using synchrotron microcrystallography had failed. Synchrotron data collection failure was due to poor diffraction from larger SMO crystals grown in LCP (Uwe Weierstall et al. 2014). This suggests that the crystals accumulated many defects during growth.

3.6.4 Bacteriorhodopsin SMX

Microbial rhodopsin was the first structure solved from crystals grown in LCP (Pebay-Peyroula et al. 1997). Recently (also using bacteriorhodopsin) LCP serial millisecond crystallography (SMX) was attempted using the microfocus beamline ID13 at the European Synchrotron Radiation Facility (ESRF). Bacteriorhodopsin microcrystals (<50 microns) grown in LCP were streamed across the X-ray beam, in air, using the LCP injector. While the data set may lack the features acquired from using the high intensity ultra-short pulses from an XFEL, a structure was solved. This opens up more opportunities for serial crystallography as synchrotrons are more abundant than the newer XFEL sources.

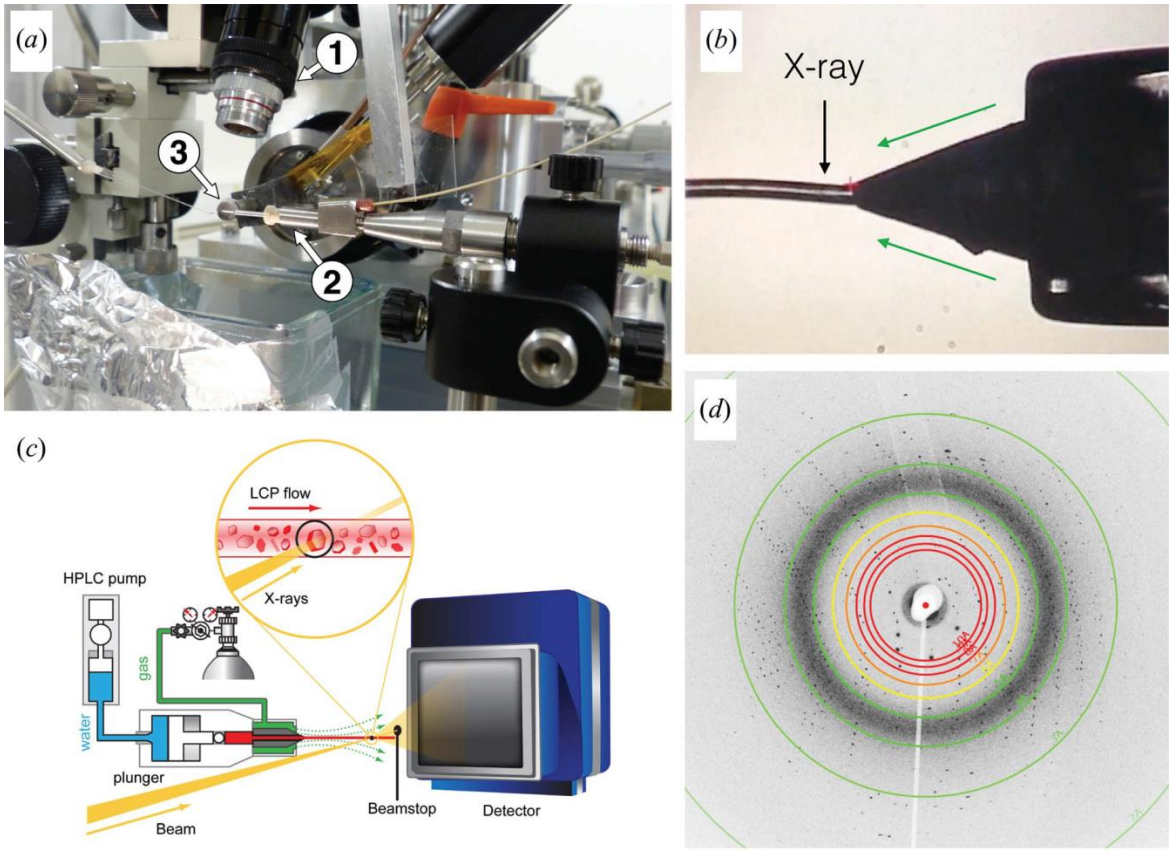

Figure 3.7: Serial Millisecond Crystallography
The serial millisecond crystallography experiment used the LCP injector in air (a) with the injector mounted horizontally (2) just in front of the beam collimator (3), and the microscope mounted above (1). LCP was extruded at low flow rates with X-rays hitting the LCP stream just 40 microns away from the nozzle tip (b). The experimental setup is similar to SFX, but in air operation reduces complexity significantly (c). A diffraction pattern from a bacteriorhodopsin microcrystal is also shown (d). Reproduced from Nogly et al.(2015).

While synchrotron microcrystallography is better suited to the brightness of the source, SMX holds a few advantages over the cryogenic technique normally used at synchrotrons. First, the data collection is done at room temperature. Second, the crystals need not be harvested from the LCP, a painstaking process, which can result in ruined crystals. Of course, as with all serial crystallography, many snapshots must be taken and merged to complete a dataset using many hours of beamtime.

3.7 Further Research

Although the LCP injector itself is well developed, there are areas where improvements can be made. Some improvements with the injector design are still needed (i.e. the gas aperture adjustment), but most of the future research will involve using the detector with new material or to develop new methods.

3.7.1 Alternative Delivery Media

The defining characteristic of the injector is that it will extrude highly viscous media. Here we have focused on LCP, but the injector need not be limited to extruding only membrane crystals grown in the LCP. Gels, greases, and high viscosity oils are all potential candidates for viscous extrusion in the LCP injector (it would perhaps be more appropriate to call it a micro extrusion injector). The only condition for operation is that the material can be extruded stably. Other viscous crystal laden media can be used if they either support crystal growth, or can keep crystals stable post mixing. Another consideration would be to use LCP as a carrier only, and mix in protein post crystallization.

3.7.2 Pump Probe Experiments in LCP

Because of the extreme savings in total used protein versus the GDVN, there is some interest in using the LCP injector in a pump-probe configuration. The pump would be provided by a laser pulse of appropriate wavelength, and illuminate the flowing extruded portion of the LCP stream before being probed by the X-ray beam. The delay time between pump and probe could be very long with the LCP injector because the stream speed is so slow (2mm/sec).

There are difficulties present in the LCP pump-probe setup because of instabilities in the stream speed. There are often small feedback loops in the operation of the HPLC pump. This happens when the HPLC increases pressure until a slippage threshold is surpassed, and the LCP is extruded at a speed much higher than the desired maximum. The HPLC pump's automatic feedback system then responds by dropping the pressure until the jet slows; usually well below the desired minimum. This process repeats itself indefinitely. This does not allow for the accurate timing needed for pump-probe SFX.

4 LCP INJECTOR PROTOCOL

The lipidic cubic phase (LCP) injector is a device designed to extrude a continuous column of LCP for use in a serial crystallography experiment. LCP is a membrane mimetic, and is commonly used as a growth medium for membrane protein crystals. As such it is an excellent choice for a crystal delivery medium for serial crystallography, but its high viscosity makes it a challenging medium to use. The injector can be used with other high viscosity fluids or gels, but its primary purpose and operation remain the same.

The injector was designed to be used with the in-vacuum injector body described in Weierstall, Spence, and Doak (2012), but can also be used in a standalone configuration. The injector can operate in air at or near ambient pressures (Nogly et al. 2015), as well as in vacuum. This chapter will cover the installation of the LCP injector for both cases, the loading of the LCP reservoir, the assembly of the LCP nozzle, and the operation of the LCP jet. Also included is a brief guide to nozzle component fabrication (for a more detailed description see chapter 3 of this thesis). This chapter also includes a list of equipment, tools, and parts used as well as a troubleshooting guide.

4.1 List of Parts

The installation and operation of the LCP injector requires special equipment, custom tools, and consumables. All of the pieces needed for operation of the LCP injector as described in this chapter are listed in this section. The primary piece of equipment is the LCP injector itself. A more detailed description of the injector, and its function are described elsewhere in this thesis and in Weierstall et al. (2014).

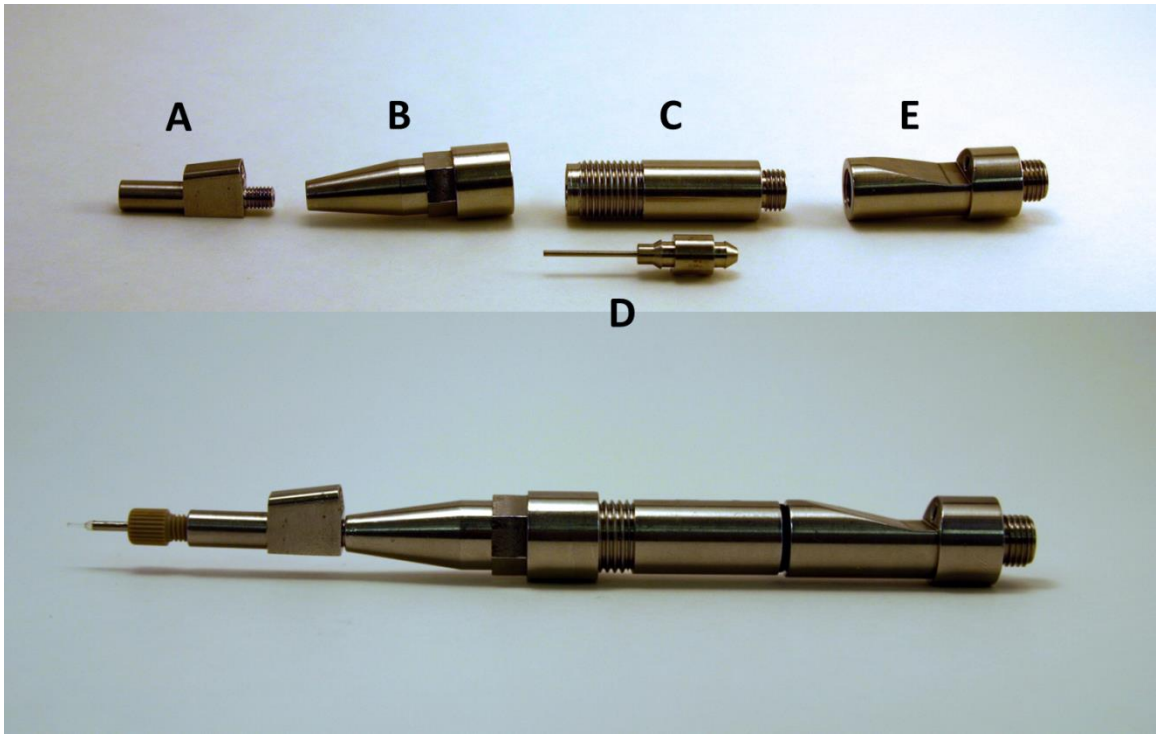

Figure 4.1: Injector Parts.
Photographs of the LCP injector. Top photo shows parts disassembled. Parts are labeled: A) nozzle body, B) reservoir, C) hydraulic stage body, D) piston (without seals installed), E) gas line feedthrough. Bottom photo shows the injector pieces assembled with a nozzle in place.

Table 4.1: List of Custom Injector Parts and Consumables

Injector Parts	Supplier	Injector Consumables	Supplier: Part Number
Nozzle body	ASU	Capillary tubing 360 micron OD, 20 – 50 micron ID	Molex/Polymicro: TSP050375, TSP040375, TSP030375, TSP020375
LCP Reservoir	ASU	Square Glass Tubing	Friedrich & Dimmock Inc.: BST-040-10
Hydraulic Stage Body	ASU	Stainless Steel Tubing (For gas apertures)	IDEX: U-115
Hydraulic Stage Plunger	ASU	5 min Epoxy	Hardman: Double/Bubble Red
Gas Line Feedthrough	ASU	Teflon Spheres 1/16 inch diameter 3/32 inch diameter	BalTec: 92818, 97341

In addition to common tools (i.e. wrenches, hex keys, pliers, cutters) LCP injector installation and operation requires a few custom tools. These are listed below, and shown in Figure 4.2.

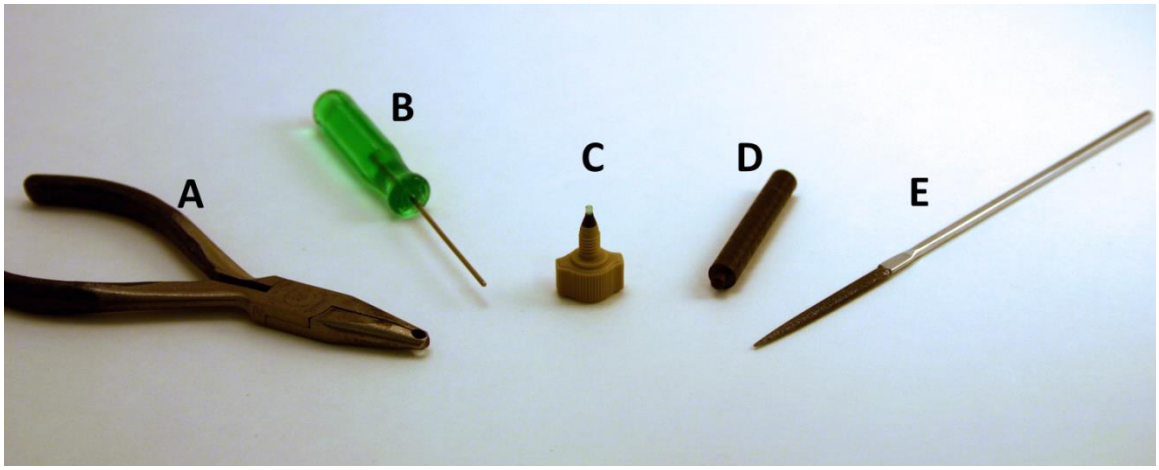

Figure 4.2: Custom Tools
Photograph of custom tools for LCP injector operation. Tools pictured include: A) Knurled pliers, b) sphere insertion rod, C) gapping tool, D) sphere seating rod, E) diamond file.

Table 4.2: List of Equipment and Custom Tools

Equipment	Supplier: Model number	Tools	Supplier
HPLC Pump	Shimadzu: LC-20AD	Knurled pliers	ASU
Mounting hardware (optional)	Edmunds	Teflon ball seating tool	ASU
Camera 1	Motic: Moticam 2300	Teflon ball insertion tool	ASU
Camera 2	Photron: Fastcam SA4	Gapping tool	IDEX*
Microscope (Tube, Objective, Eyepiece)	Edmunds: #54-869, #36-131, #37-660	Diamond file	DBH: DBH-3-D46
Gas regulator(s)	Proportion air: GP1	Loading Needle	Hamilton/IDEX*
Gas Valve (optional)	IDEX: MXP7900-000	Headless nut driver	IDEX: F-345
Fiber light	Dolan-Jenner:	Hamilton syringe needle 22 gauge 1.25” end style 3	Hamilton: 7804-01
*assembled from parts listed in this document.			

Table 4.3: List of Tubing, Fittings, and Seals

Equipment	Supplier: Part Number	Equipment	supplier/part number
Stainless Steel Tubing (Supply line)	IDEX: U-163, U-162	1/16” PEEK tubing (Liquid line)	IDEX: 1533
10-32 coned port fittings	IDEX: F-333N	1/32” PEEK Tubing (Gas Line)	IDEX: 1568XL
Tezfel ferrules	IDEX: F-142N	10-32 stainless steel flush nut	IDEX: F-354
LiteTouch ferrules	IDEX: LT-135, LT-100	6-32 coned port fittings	IDEX: F-126-H
10-32 coned port plugs	IDEX:U-467R	Unions	IDEX: P-704
Tees	IDEX:P-727	Manual Shutoff Valve	IDEX: P-732
Luer lock to 10-32 coned port adapter	IDEX:P-629	Viton O-rings	McMaster-Carr: 9263K169
10-32 to 6-32 union	IDEX:P-881	Hydraulic Seals	Trelleborg: Variseal M/Radial Seal PVA000080 – T40SD
Teflon adapter sleeves	IDEX: F-242x, F-246x	5ml syringe (w/ female Leur-Lok)	BD: 301027

4.2 Initial Setup

The LCP injector is a hydraulic device and as such requires a pump or other source of pressure. Typically pressure is supplied by a constant flow rate pump, of the kind commonly used in HPLC systems (Shimadzu). Unless the pump can be controlled remotely it should be installed outside the X-ray hutch where the controls can be accessed while the X-rays are on. This may require routing tubing through a chicane or other hutch feedthrough. This tubing should have a small inner diameter to minimize purging time, but large enough to flow water at low pressures. Tubing material should also be inelastic as elasticity in the liquid lines creates significant lag in the response time of the pump. Tubing is typically made of stainless steel or PEEK (IDEX).

The supply line should terminate as near to the injector as is feasible. For the in vacuum injector this means near the nozzle rod insertion point. For in air installation the supply line should not terminate more than one meter away from the injector. Once the

pump is installed (with a large reserve of pure water), and the supply line is routed, purge the supply line. Plug the end of the supply line and continue with injector installation (IDEX U-467R and P-704).

The LCP injector uses a sheath gas to keep the extruded stream stable. The gas normally used is helium, but nitrogen has been used because it may prevent the phase transition of monoolein LCP to lamellar phase during in vacuum experiments (Weierstall et al. 2014). Gas supply normally comes from compressed gas cylinders, and installation of the gas supply will vary widely. Gas cylinders located in the hutch mandate the use of remotely controlled regulators. Gas cylinders outside the hutch require routing gas lines through a chicane or other hutch feedthrough. It is best to consult with the beamline scientists with regard to what will be most appropriate. Remote controllable electronic regulators (Proportion air, GP1) are typically used as they interface easily with most beamlines, and offer precise control even at low pressures.

Like the liquid line, the gas line should terminate near the injector. If the gas line is very short or has a large inner diameter there is often not enough resistance to gas flow, and the required gas pressure for reliable LCP flow is too low to be dialed in with the regulator. Resistance can be added by installing a short piece of small inner diameter tubing, (i.e. 30 cm of 100 micron ID capillary tubing). If multiple gasses are being used they should be regulated separately, and routed to a remote controllable valve (IDEX) for switching during the experiment.

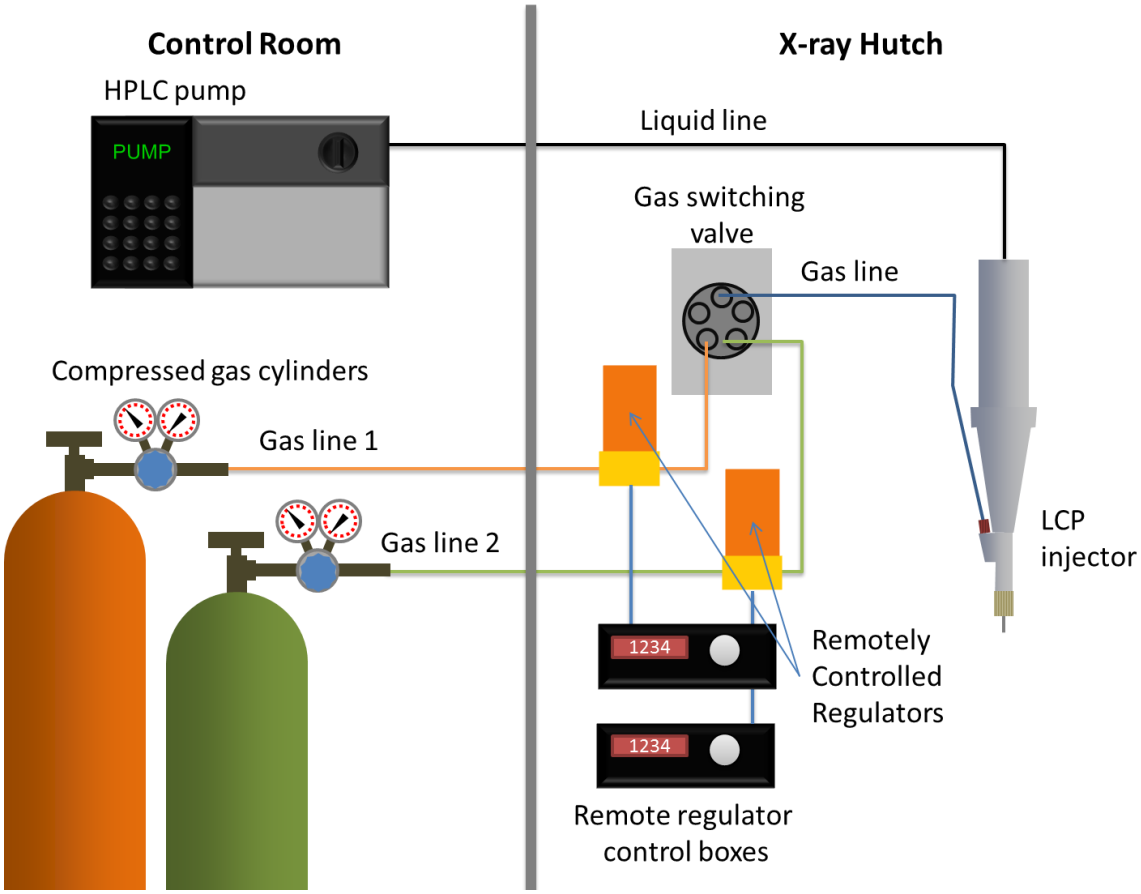

Figure 4.3: Schematic Diagram of LCP Injector Setup
Here, an example of the general setup for injector operation is shown. The second gas cylinder, gas switching valve, and remote control regulators are optional.

4.3 Installation with the In Vacuum Injector

The installation of the LCP injector must be preceded by the installation of the in vacuum injector (U Weierstall, Spence, and Doak 2012) which will not be covered here. LCP injector installation begins with the assembly of the nozzle rod. Any nozzle rod threaded with standard M9x1.0 threads can be used. Ideally the rod will be slightly shorter than the one used with Gas Dynamic Virtual Nozzles (GDVN), as the LCP injector adds about 15cm to the rod length, and nozzle insertion is made easier with a rod

of appropriate length. The rod should have the handle, guide disk, KF feed through, and O-ring preinstalled.

Begin by cutting appropriate lengths of tubing for the gas and liquid lines. Suggested gas and liquid lines are listed in Table 4.3. There must be enough slack in the lines to allow easy extraction of the nozzle rod from the vacuum chamber. The length depends on where the supply line terminates in relation to the injector, but a good guideline is roughly two and a half times the length of the nozzle rod.

With the nozzle rod supported on a bench top, feed the lines through the rod leaving about 20cm exposed on the threaded side. Install an 8mm O-ring (McMaster Carr) over the threads of the gas line feedthrough. Push the gas line through the back of the 6-32 coned port in the gas line feedthrough and secure in place with a fitting (IDEX F-126-H). Pass the liquid line through the center of the gas line feedthrough. Thread the gas line feedthrough onto the nozzle rod until the O-ring forms an adequate seal.

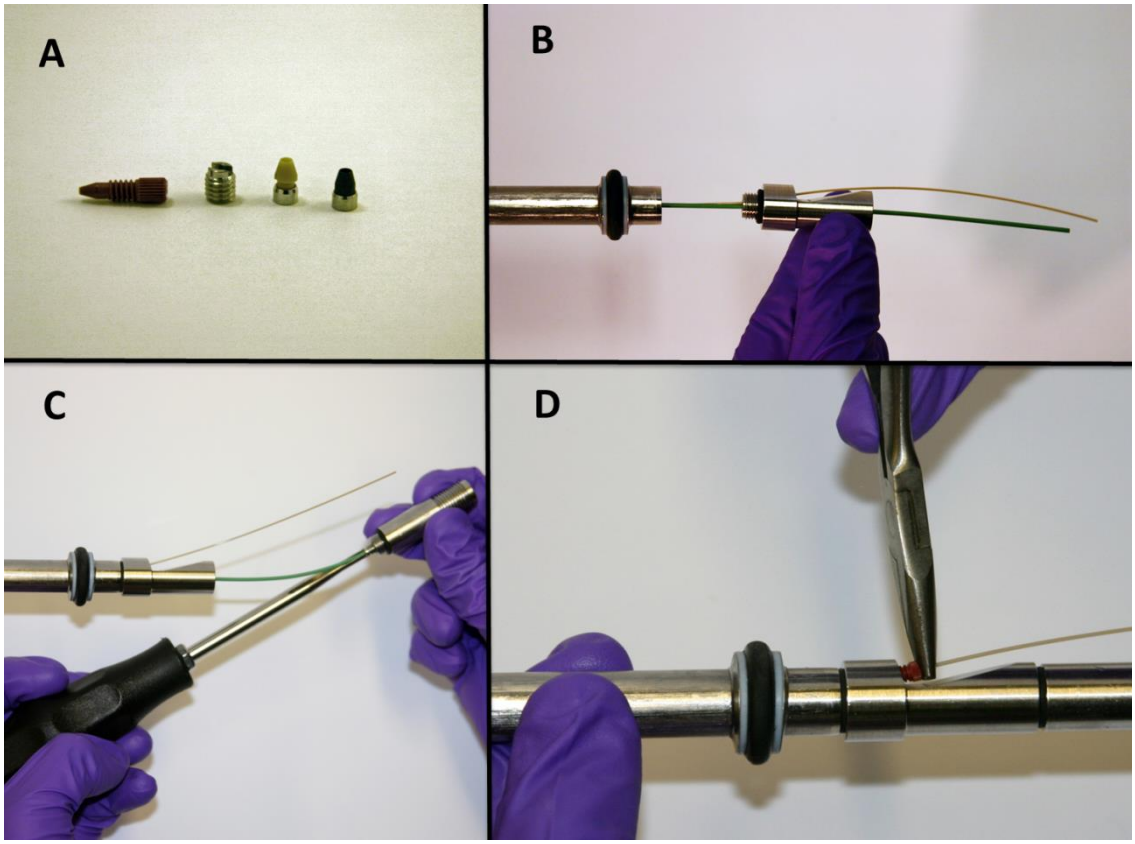

Figure 4.4: Injector Rod Setup
(A) Fittings and ferrules needed for rod setup are shown (only one ferrule is required in this setup). (B) Gas line feed through installation is shown. Note the gas line is passing through the 6-32 coned port on the feedthrough, and the liquid line (green) passes through the center. (C) The liquid line is secured to the hydraulic stage with one of the ferrules and the headless flush nut pictured in A. The headless nut tool pictured is required. (D) The gas line is secured in the feedthrough, with the 6-32 fitting shown in A, using the knurled pliers. This fitting forms a vacuum seal, since the inside of the nozzle rod is at atmospheric pressure.

Place an O-ring over the threads on the hydraulic stage. Attach the liquid line to the hydraulic stage with a ferrule, and headless nut (IDEX LT-100 or LT-135, and F-354) using the FlushNut wrench (IDEX F-345). Thread the hydraulic stage into the gas line feedthrough until the O-ring forms an adequate seal. Temporarily thread an LCP reservoir with a nozzle body attached to adjust gas line length. The gas line should be long enough to reach the gas inlet port on the nozzle body. It may be advisable to attach

the gas line to the hydraulic stage with Kapton tape. Tighten the 6-32 fitting on the gas line feedthrough with knurled pliers to secure gas line.

4.4 Inline Syringe Assembly

Attach a Tee (IDEX P-727) to the other end of the liquid line. With a short length of tubing, attach a manual shut-off valve (IDEX P-732) to the Tee. With another short length of tubing attach a 5ml plastic syringe filled with pure water to the other side of the shut-off valve with a male Luer lock to female 10-32 coned port adapter (IDEX P-629) (see Figure 4.5). Thread a plug (IDEX U-467R) into the remaining port of the tee. The Tee and syringe are needed to move the plunger by hand after reloading the LCP reservoir.

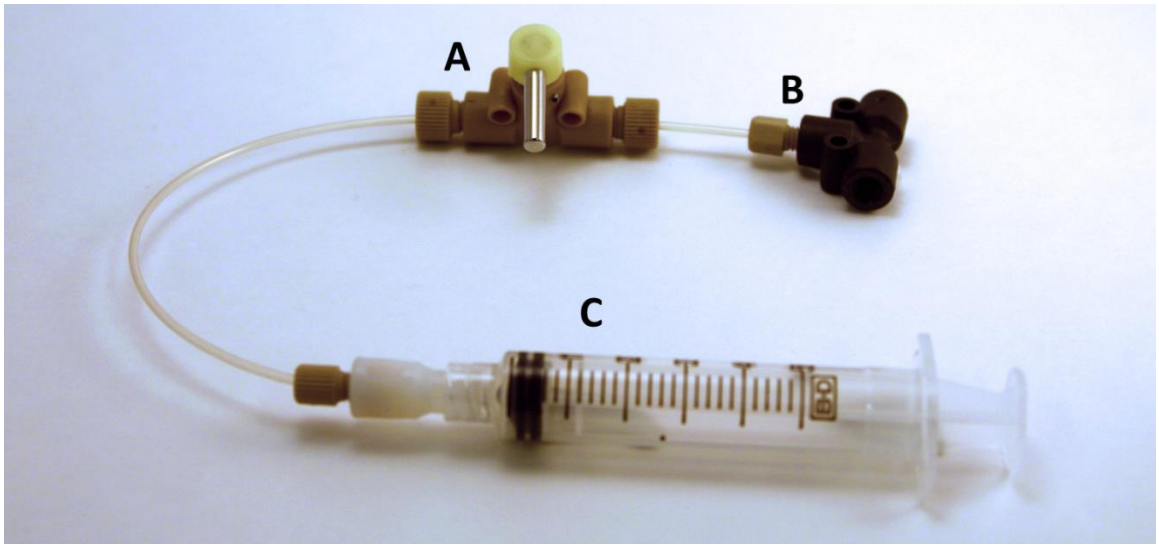

Figure 4.5: Syringe Assembly
The syringe assembly provides manual injector control (i.e. advancing the plunger after a new reservoir is loaded). The assembly is made with standard 1/16" tubing with appropriate fittings, and three major components: A) Shut-off valve, B) Tee union, C) 5ml syringe with female Luer lock to female 10-32 coned adapter.

4.5 Purging the Hydraulic Stage

If the piston is already installed in the hydraulic stage remove it. Open the shut-off valve and press on the syringe plunger to purge the liquid line. Continue to press on the plunger until all of the air is removed from the line and the hydraulic stage body is over-filled with water. Insert the piston, with hydraulic seals installed (Trelleborg), being careful to not introduce any air into the system, and avoid bending the rod extending from the piston (Figure 4.6). As the piston is pressed into the hydraulic stage body, the syringe will fill with water; ensure that there is enough available volume in the syringe to accommodate this. Once the piston is completely inserted into the hydraulic stage body, close the shut-off valve.

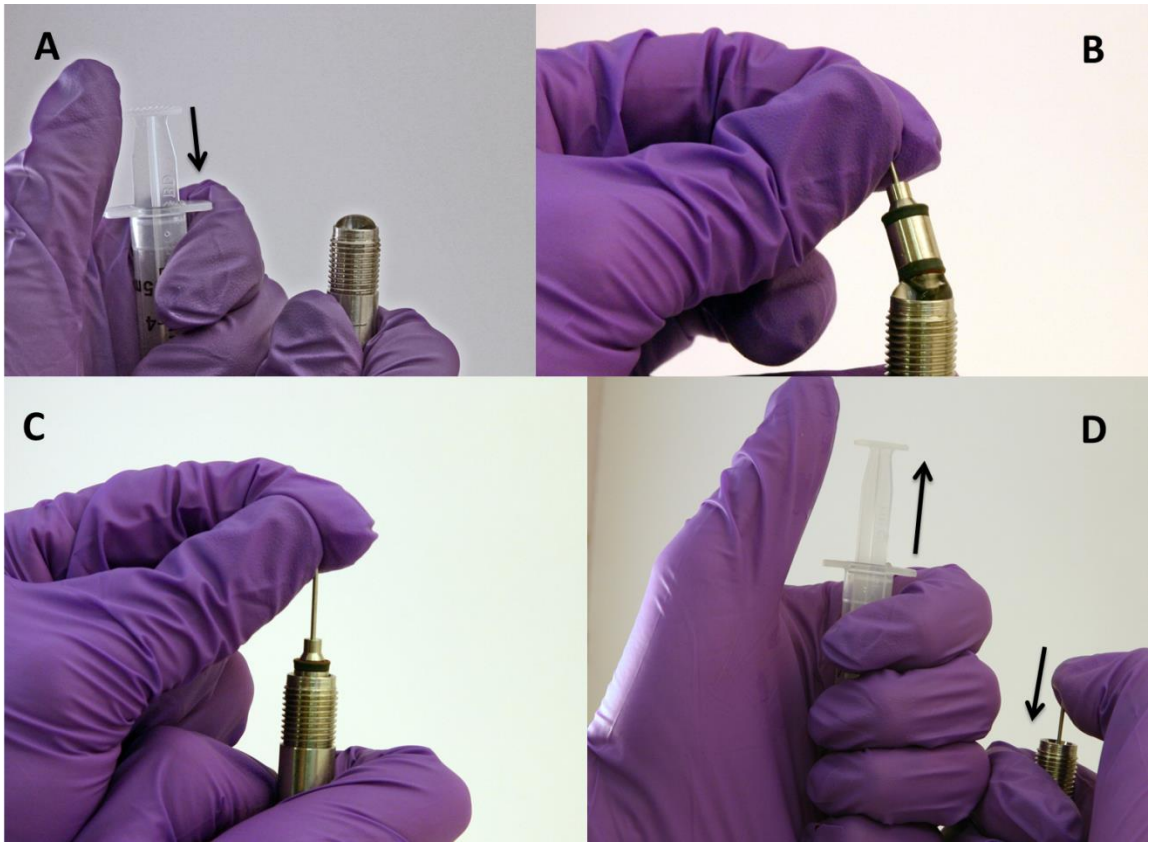

Figure 4.6: Hydraulic Stage Purge
The procedure for purging the hydraulic stage is demonstrated. A) Press the plunger on the syringe to overfill the hydraulic stage body with water. B) Insert the piston (with seals installed) into the bore of the hydraulic stage body. C) Press the piston in, seating both seals. D) Continue pressing in the piston until it hits the bottom of the hydraulic stage body. Note that the syringe fills with the volume of water displaced by the piston.

Take the fully assembled nozzle rod to the experimental chamber and set it down in a secure place (i.e. supported on a table, or clamped upright near the injector). Find the tee at the end of the liquid line, remove the plug and attach the supply line from the HPLC pump without introducing air into the system. Locate the gas supply line, and attach it to the gas line with a 10-32 to 6-32 coned port union (IDEX P-881)

4.6 Installation for Standalone or In Air Operation

If the LCP injector is to be used in a standalone configuration, support hardware must be obtained and assembled on a case by case basis. To facilitate this, the body of the hydraulic stage has the same diameter as a standard ½" optical post. With the hydraulic stage body mounted in any ½" optical post clamp, injector placement becomes trivial. The injector can be mounted horizontally or vertically, and can be made to swing away or retract from the interaction region for easy reloading (see Figure 4.7).

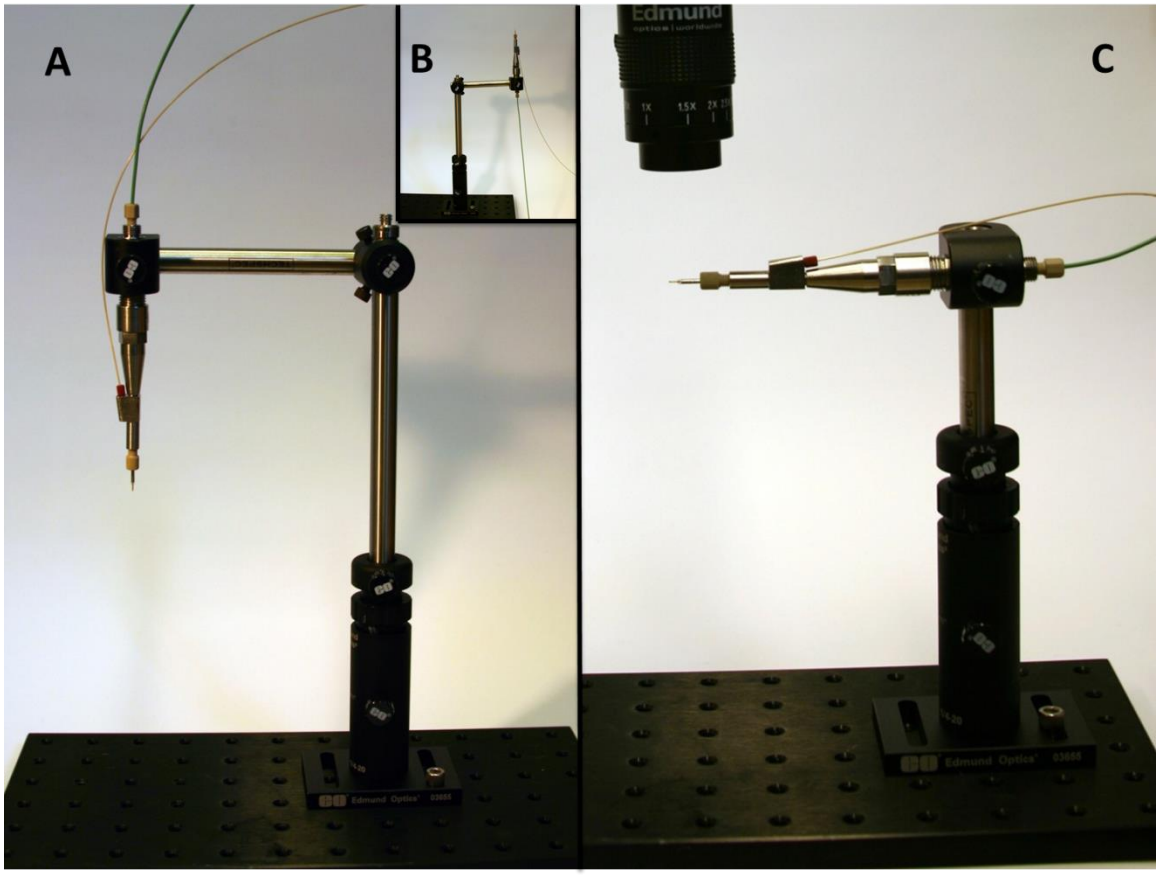

Figure 4.7: Examples of Injector Setup for In Air Operation
Vertical mounting configuration shown with injector inserted (A) and withdrawn (B).
Horizontal injector mounting shown with the microscope visible (C).

Alignment of the injector relative to the X-ray beam is done with a remotely controlled three-axis stage. While usually provided by the beamline, the stage size, location, and range of motion should be known in advance.

One piece of hardware that is essential for LCP jet operation is a microscope with a camera. Camera monitoring is the only reliable way to ensure the injector is working properly. The camera must be able to provide a real-time image of the LCP nozzle during operation. A high-speed camera is advantageous because X-ray hits can be directly observed, and the distance between hits along the LCP stream can be estimated. Two examples of cameras used are the Photron Fastcam SA-4 high-speed camera with a 12x Navatar lens, or a Moticam 4000 mounted to a single tube DIN microscope (Edmunds). See

Figure 4.8 for camera setup examples. Camera setup and installation usually require a computer directly connected to the camera. Computers left in the hutch should have remote access setup to enable injector monitoring from the control room. Note that a microscope camera requires illumination, this cannot be neglected. Fiber lights or LED backlights are adequate in most cases.

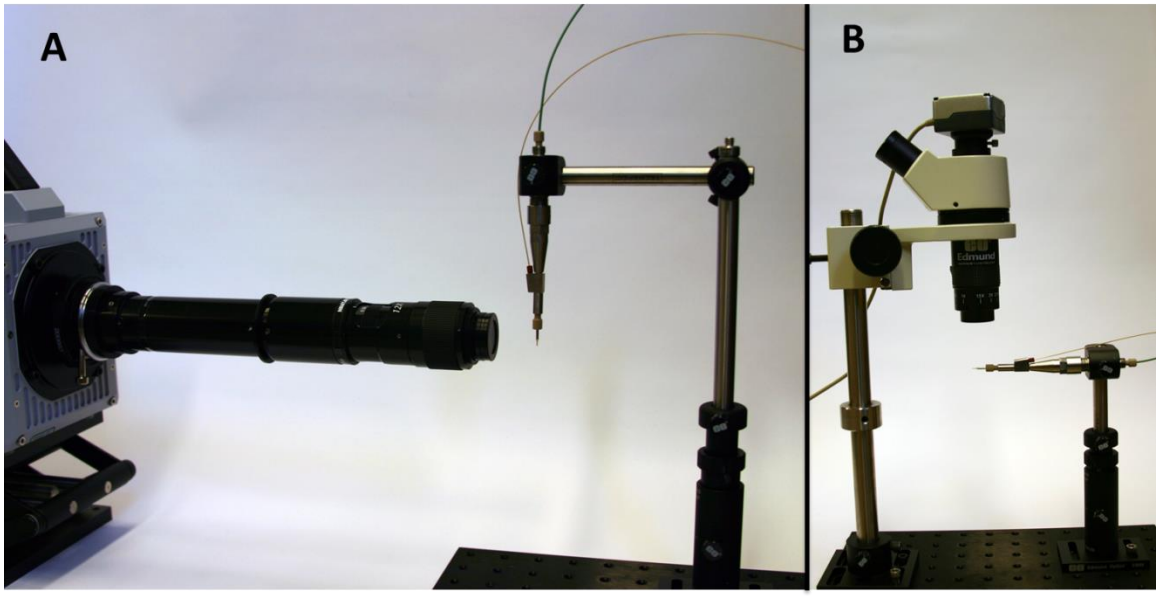

Figure 4.8: Example Camera Setup
(A) High speed camera and (B) USB microscope camera setup for monitoring injection.

To continue installation purge the hydraulic stage and install the piston as described above.

Route the gas line along the injector supports leaving enough line near the injector to reach the gas port on the LCP nozzle. With the injector mounted to a three axis stage, a camera installed and focused onto the interaction region with adequate illumination, and gas supply lines routed, you are ready to load a reservoir and assemble the LCP nozzle.

4.7 Loading the Reservoir

The LCP reservoir is a small stainless steel cone with a smooth internal bore, and a 10-32 coned port at the end. Internal bores have a diameter of 0.054” or 0.084” inch. Note that the reservoirs may come in different sizes, and therefore have different pressure amplification factors. The volume of the internal bore determines the maximum amount of sample that can be loaded into the reservoir. Maximum sample volume for the small bore reservoirs is 20 microliters, and 40 microliters for the large bore.

To load sample into the reservoir, first ensure the reservoir is clean. Insert the appropriate number and size of Teflon spheres (Baltec) into the back of the reservoir. For the small bore reservoirs insert two 1/16” diameter spheres, or one 3/32” diameter sphere for the large bore reservoir. Insertion of the sphere(s) is done with special tools. Spheres are first partially seated into the bore with a large flat ended rod, and then pressed into the bore with a small diameter rod (see Figure 4.9). Note that since the bore is slightly smaller than the diameter of the Teflon spheres, when the spheres are inserted they will deform into cylinders, and that when inserting two spheres, the gap between spheres should be minimized.

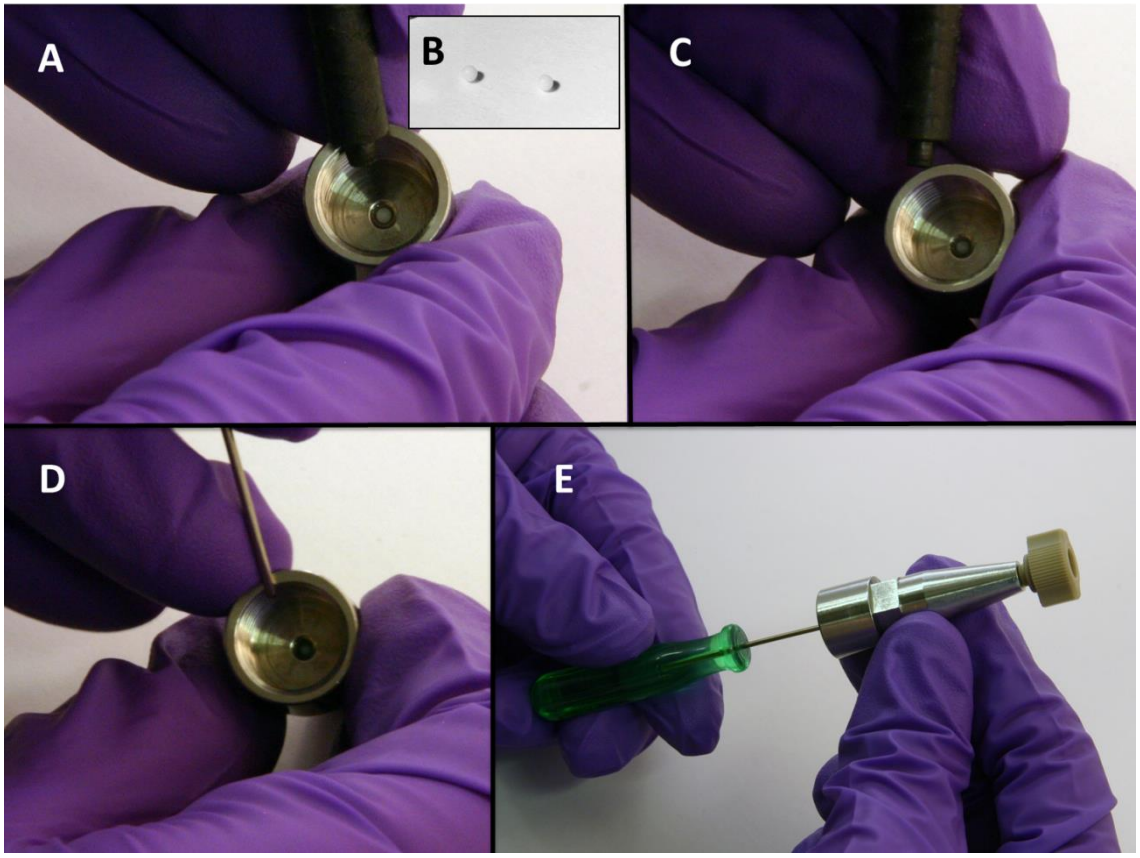

Figure 4.9: Reservoir Preparation
Place one Teflon sphere (B) of appropriate size into reservoir (A). With the sphere seating tool firmly press the sphere into the bore of the reservoir (C). Press the sphere into the bore with a small diameter rod (D). Repeat previous steps if inserting more than one sphere then attach the gapping tool and press sphere(s) forward until contact is made with the tool (E).

With the sphere(s) inserted thread the gapping tool into the 10-32 coned port on the front of the reservoir. The gapping tool is assembled from a single 10-32 fitting, a ferrule, and a short piece of 1/16" OD tubing. Press the tubing into the 10-32 coned port at the front of the reservoir and secure in place with the ferrule and fitting. Make sure that the tubing is pressed into the reservoir as deep as it will go, and that the ferrule is firmly seated onto the tubing. The gapping tool may be reused from here on out.

Using the small rod, push the Teflon sphere(s) into the reservoir bore until they are stopped by the gapping tool. The gapping tool prevents the spheres from advancing into the larger diameter region at the front end of the reservoir. If the spheres have advanced into this region, then the above steps must be redone or the sample loading will fail, since the Teflon balls are now stuck and cannot be moved back into the reservoir anymore.

With the Teflon spheres loaded and pushed to the front of the reservoir, thread in a loading needle. The loading needle is assembled from a 22 gauge 1.25" syringe needle (Hamilton), and 10-32 coned port fitting with a 1/16" OD 685 micron ID Teflon adapter sleeve (IDEX F-246x). Insert the needle into the sleeve, and then the sleeve through the fitting and ferrule. Seat the ferrule with the correct amount of sleeve protruding from the front of the ferrule by tightening the fitting into the reservoir with the sleeve pressed into the port as far as it will go (see Figure 4.10).

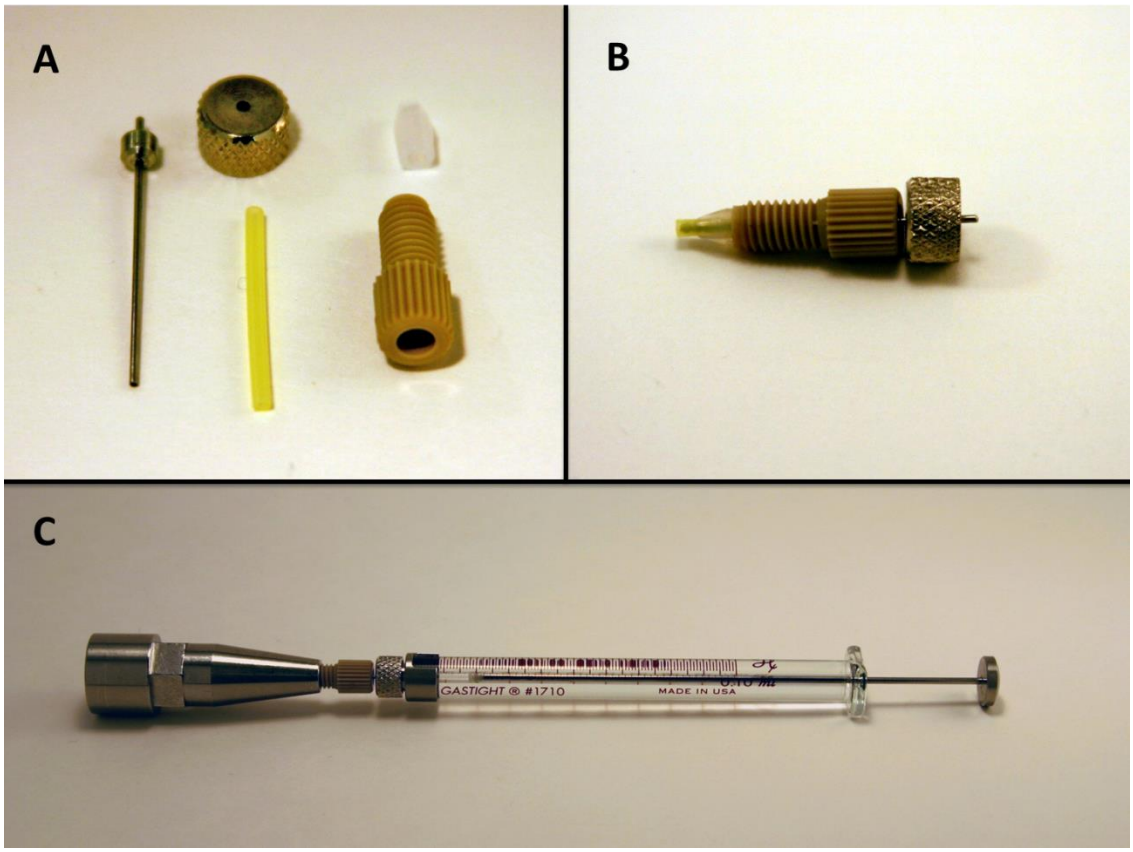

Figure 4.10: Loading Needle Assembly and Use
Figure shows the loading needle parts (A), the fully assembled needle (B), and the loading needle attached to a LCP reservoir and a Hamilton syringe (C).

With the loading needle attached to the reservoir, attach the other end of the needle to the syringe containing the sample (Hamilton). Ensure that the needle is firmly tightened in the reservoir, and onto the syringe. Press lightly on the Hamilton syringe plunger, and record the change in volume on the syringe. This represents the dead volume of the particular sample which includes any air bubbles in the LCP plus the volume of the needle, and the dead volume of the reservoir. Press firmly on the plunger to load LCP into the reservoir being careful not to overload the reservoir, and record the amount of LCP loaded.

Remove the Hamilton syringe, and set aside. Keep the loading needle in the reservoir until the nozzle is ready to be attached to the reservoir. This prevents dehydration of the sample.

4.8 Building the Nozzle

The nozzle is assembled from several parts, some of which must be made beforehand. The fabrication of the nozzle tip and the gas aperture will be briefly covered here, followed by the instructions for assembly.

4.8.1 Grinding the Tips

In the injector, the LCP is extruded through a short length of fused silica capillary tubing (Molex/Polymicro) with outer diameter 360 microns and inner diameter between 10 and 50 microns. The end of this capillary tubing is conically ground. A grinder/polisher like the Allied Multiprep or the Ultrapol fiber lensing machine is used. A capillary rotation stage may need to be fabricated to facilitate the grinding. The capillary end should be ground into a cone with an angle of 15-20 degrees. After grinding, the capillary tubing may be trimmed to 10cm in length for storage and transport.

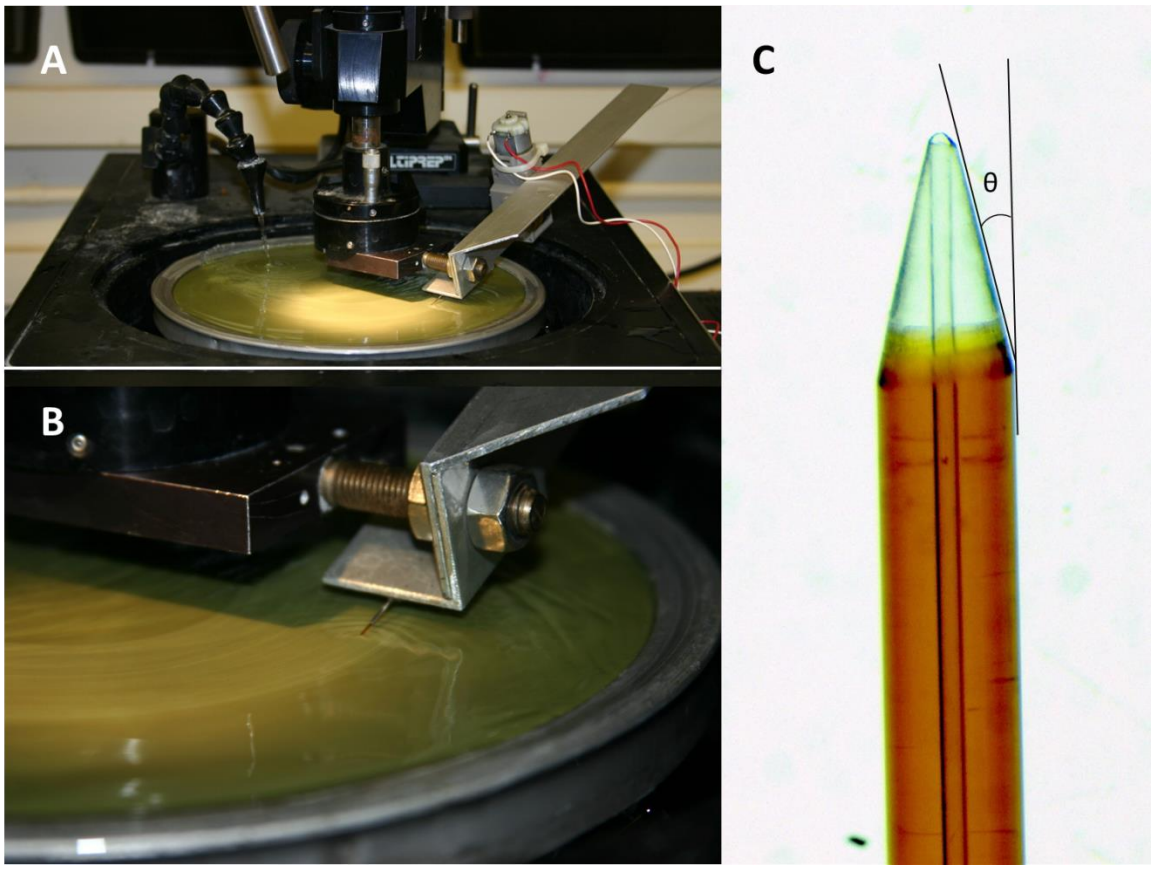

Figure 4.11: Tip Grinding
(A) Photograph of one type of grinder used in tip grinding. (B) Close up of capillary tubing on grinding surface. Capillary is clamped in a rotation stage, and oscillated across the grinding pad. (C) Microscope image of finished LCP tip angle θ should be between 15 and 20 degrees.

4.8.2 Melting the Apertures

The injector uses a sheath gas to keep the LCP stream on axis. The sheath gas leaves the nozzle through a gas aperture. The aperture is constructed from a flame polished square profiled glass tube (Friedrich & Dimmock) glued into a one inch long piece of stainless steel tubing (IDEX U-115). The square glass tubing has inside dimensions of 0.4mm wall to wall, with 0.1mm glass thickness. The stainless steel tubing has 1/16” outer diameter and 0.03” inner diameter.

Carefully cleave a 1cm piece of square glass tubing with the diamond file. Note that the end of the glass tubing must be as flat as possible to ensure correct melting. Insert the glass tubing about halfway into the stainless steel tubing. Glue in place with the quick set epoxy (Hardman).

After the epoxy has set, the glass tip can be melted. Hold the tip of the glass tubing into a small propane flame. Melting should only happen at the very end of the tube, and should still allow for a capillary tip to protrude 200-300 microns from the opening. Note that an over-melted aperture can be salvaged by grinding the aperture back until the opening is large enough. Finally, a gas aperture must be pre-seated in a 10-32 coned port fitting (IDEX F-333N) prior to use in a standard nozzle body.

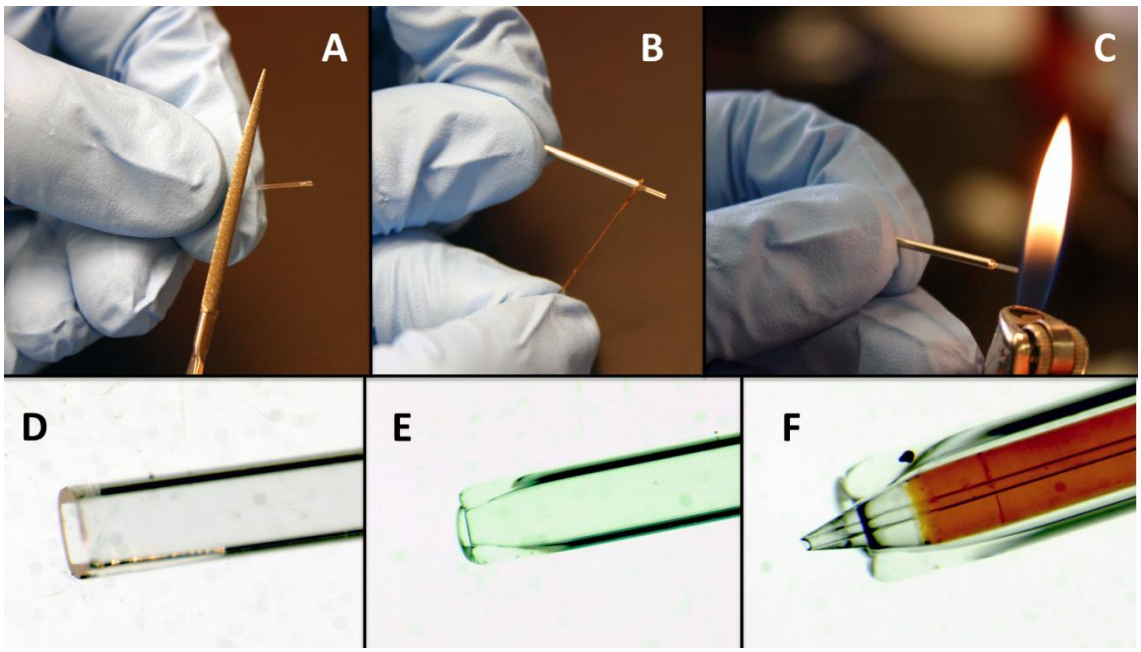

Figure 4.12: Gas Aperture Construction
Gas aperture construction begins with (A) glass cleaving with the diamond file. After a 1-2cm piece of square glass profiled tubing is cut, ensure that it has a flat side (D). Glue the glass into a 1" piece of stainless steel tubing (B). After the glue has set melt the gas aperture by placing the tip in a propane flame (C). After the tip is melted (E), a ground capillary cone should protrude 150-250 microns from the front (F).

4.8.3 Assembling the Nozzle

To assemble a complete LCP nozzle, first cut a green 360 micron to 1/16” adapter sleeve (IDEX F-242) in 13mm sections, insert sleeve into a LiteTouch SealTight ferrule (IDEX LT-135), and lightly seat ferrule onto sleeve by compressing ferrule into a 10-32 coned port (i.e. in an LCP reservoir). Note that the sleeve should protrude from the tip of the ferrule the appropriate amount (3/32”). Select coned LCP capillary of the desired inner diameter, and insert the end without the cone through the sleeve. Carefully pass the tip of the capillary through the nozzle body, and secure in place by pressing the sleeve into the hole of the nozzle body fitting. Slide the gas aperture over the tip of the capillary and thread into the 10-32 coned port on the front of the nozzle body. Adjust the position of the capillary, by pressing it forward or pulling back, until the gas aperture is tight, and the capillary tip just protrudes from the front of the gas aperture (Figure 4.13).

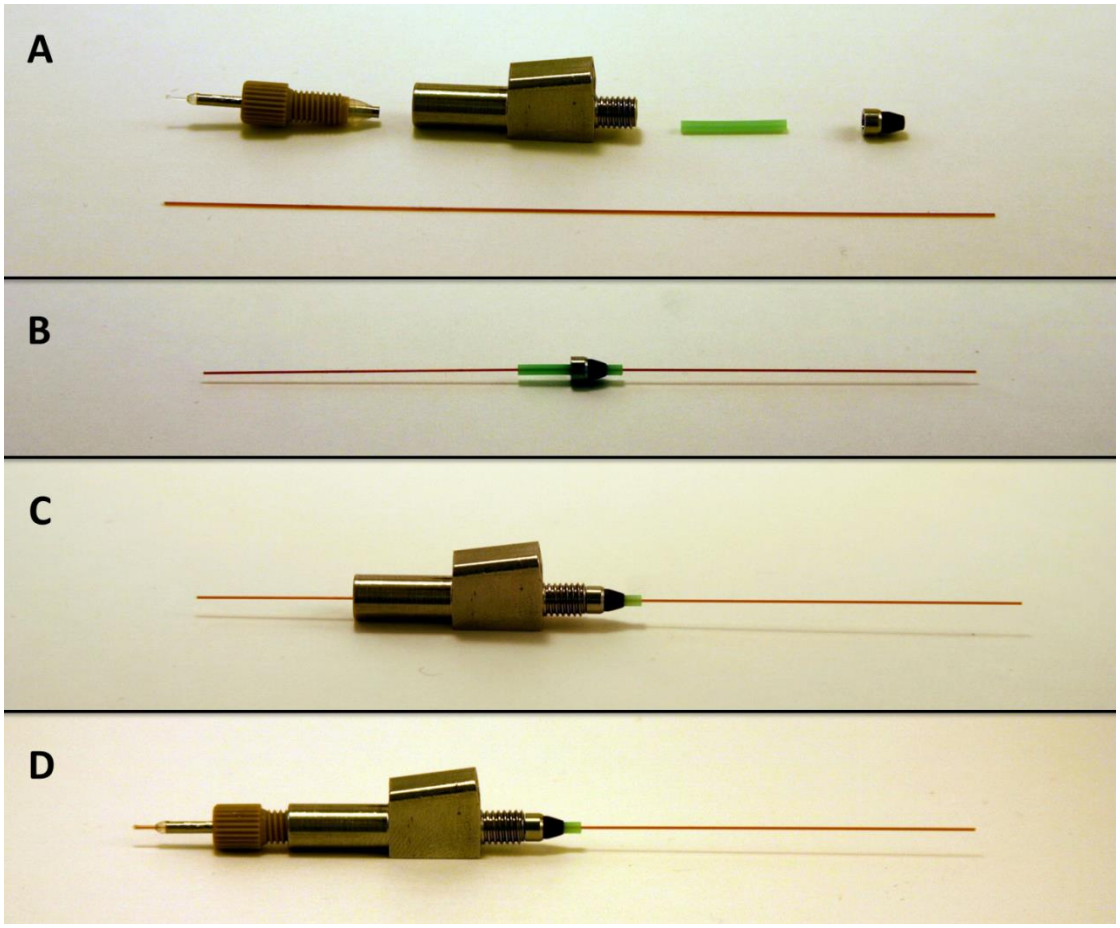

Figure 4.13: Nozzle Assembly 1
To assemble a nozzle, gather the necessary parts: (A) a gas aperture seated in a 10-23 fitting, a nozzle body, a Teflon 1/16" to 360 micron adapter sleeve, a SealTight, LiteTouch ferrule, and a conically ground capillary tube. (B) Push the unground end of the capillary through the sleeve, and ferrule. (C) Carefully pass the ground tip through the nozzle body. (D) Put the ground tip of the capillary into the gas aperture, and gently thread the 10-32 fitting into place. Adjust the capillary as needed until the conical tip protrudes from the front of the gas aperture.

With the gas aperture tightened into the nozzle body and the capillary adjusted to the proper length, trim the excess capillary with the diamond file. The capillary should be trimmed right as it exits the green Teflon sleeve. The nozzle is now ready to thread into a loaded reservoir. Unscrew the gas aperture threads a few turns to protect the gas aperture from breaking while the nozzle is tightened. Remove the loading needle, and thread the

nozzle into the reservoir. With the reservoir on a table, place a 12mm open ended wrench on the hex flats at the base of the reservoir, and hold secure. Place a ¼" or an adjustable wrench on the nozzle body, and tighten to secure the nozzle to the reservoir. Note the green Teflon sleeve and ferrule can be reused (all nozzle parts can be reused provided they are cleaned), but not after the ferrule has been over-compressed.

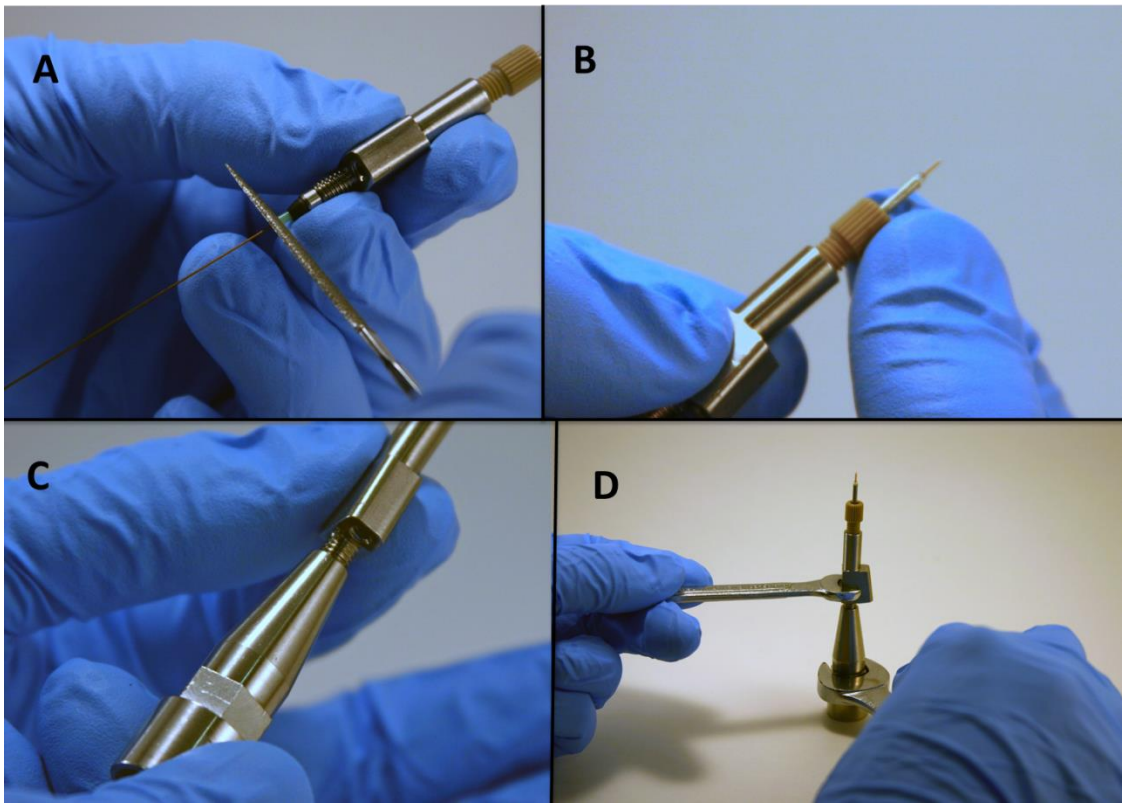

Figure 4.14: Nozzle Assembly 2
To install the nozzle onto the reservoir, first (A) cleave the capillary tube at the back of the nozzle. (B) Loosen the gas aperture a few turns to protect it during installation. (C) Screw the nozzle into the reservoir. (D) Tighten the fitting, with a 12mm wrench, and a ¼" wrench. Anchoring the reservoir on the table top protects the fragile nozzle tip during this step.

After the nozzle is connected, the gas aperture must be retightened. If a new ferrule is being used the nozzle body will have taken a few turns to tighten, and consequently the capillary will be pushed forward slightly. Carefully tighten the gas

aperture until the capillary tip protrudes 100-300 microns out of the front. If the capillary is protruding, but the aperture fitting is not gas tight then the aperture must be adjusted. To adjust the gas aperture, loosen the fitting and grip the stainless steel tubing with a pair of small needle nose pliers. Using the pliers gently twist and pull/push the gas aperture into a new position in the fitting. Try to retighten the gas aperture fitting to test for the correct protrusion. Note that the gas aperture is extremely fragile and an attempt to tighten the aperture, if the capillary tip is already protruding, will break the glass.

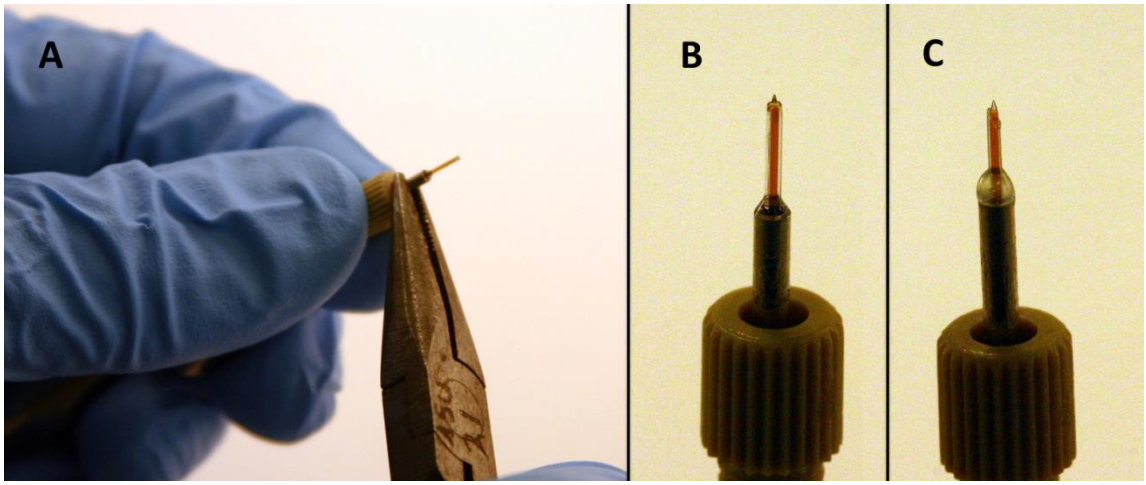

Figure 4.15: Gas Aperture Adjustment
During reservoir/nozzle assembly the capillary tip very likely moved from its ideal position. To adjust the gas aperture, loosen the 10-32 fitting a few turns, and grip the metal tube with a pair of small needle nose pliers (A). Push or pull the gas aperture into position, while gently twisting, until the gas aperture is in the new position. Attempt to retighten the gas aperture. If the gas aperture is adjusted properly the capillary tip will just protrude from the opening of the gas aperture (B). If the tip protrudes too far and the gas aperture is tightened then the glass of the aperture will break (C).

The process of adjusting the gas aperture is difficult and broken apertures are a common occurrence, especially during training. To ease this process the next generation of nozzle body will be equipped with a compression fitting instead of a 10-32 coned port. The compression fitting allows for easy adjustment to the gas aperture. To use the new compression fitting nozzle body follow the instructions as outlined above, ignoring the

section on gas aperture adjustment. When adjusting the capillary in the nozzle body, prior to trimming, simply slide a gas aperture (no fitting needed) over the tip of the capillary and into the compression fitting. Adjust the position of the capillary as above, and trim the length. Withdraw the gas aperture a few millimeters, and attach the nozzle to the reservoir. Afterward adjust the gas aperture (it should require very little pressure to move) and when the capillary tip is protruding correctly, tighten the compression fitting. Finger tight should be adequate, but the compression fitting can be wrench tightened if need be.

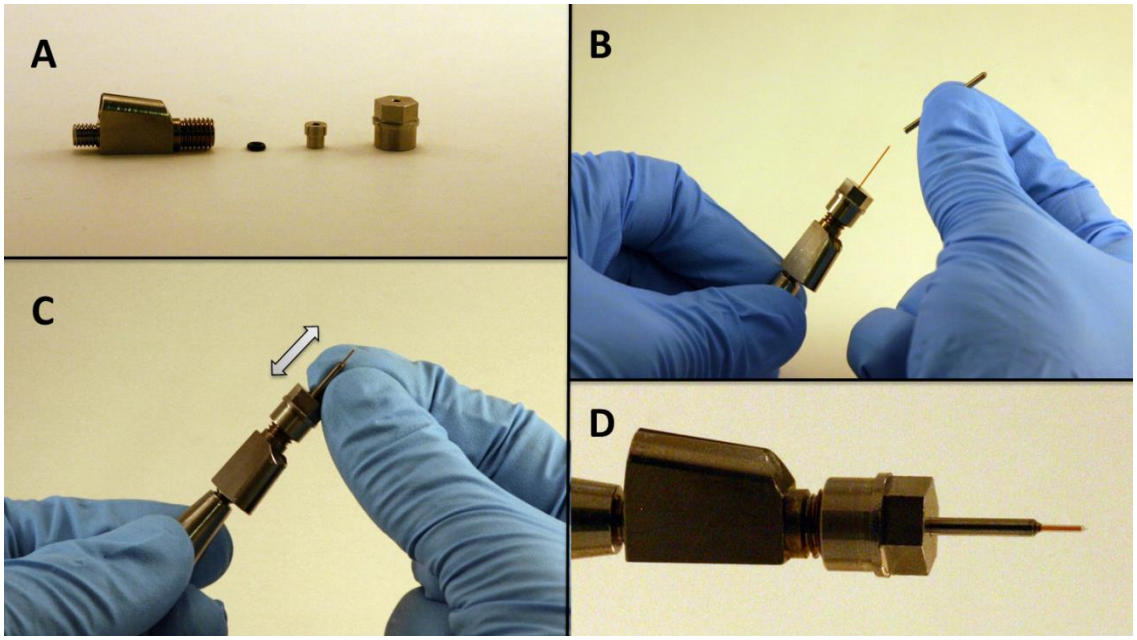

Figure 4.16: Compression Fitting Nozzle Body Assembly
The compression fitting nozzle body has four parts (A), and is assembled by placing the O-ring in the compression fitting followed by the compression ring, and then the nut. The compression fit nozzle body is used like the standard nozzle body except for the installation of the gas aperture. (B) The gas aperture is placed over the capillary tip, and pushed into the compression fitting. (C) The gas aperture is adjusted until the capillary tip protrudes from the opening. (D) Finally the nut is tightened to secure the gas aperture in place.

4.8.4 A Note about Preparation

As beamtime (especially at XFELs) can be rare, it is wise to prepare as much as possible in advance. Practically speaking this means preparing many capillary tips and gas apertures in advance. If one shift of beamtime is twelve hours, and one calculates a full sample reservoir to run for three hours that suggests only four capillary tips are required for that shift of beamtime. This allows for no error, does not account for clogs, and does not consider that some parts may break during setup. For best results, an excess of parts should be available for the injector. Additionally, samples should be tested for "injectability" well in advance of beamtime, so that jetting conditions may be established, or changes to the sample composition may be made.

4.9 Putting the Loaded Reservoir/Nozzle in the Injector

To begin data collection the reservoir/nozzle must be loaded into the injector. The nozzle/reservoir must be threaded onto the hydraulic stage, but it is critical that the piston in the hydraulic stage be matched to the reservoir. For example, a large diameter reservoir should have the large diameter piston installed in the hydraulic stage body, and likewise for the small diameter reservoir.

For the in vacuum injector the reservoir is loaded via the nozzle rod. Thread the reservoir onto the hydraulic stage (finger tight is adequate), and attach the gas line to the nozzle via the 6-32 port on the nozzle body. Tighten the fitting with the knurled pliers to ensure that the connection is secure. Insert the nozzle rod into the injector, clamp the KF flange feedthrough to the bellows, and pump down the load lock chamber. After the load lock chamber is pumped down, open the injector gate valve, and push the nozzle rod into the chamber until the nozzle tip is visible on the microscope camera. Turn on the gas, and

open the shut-off valve in the liquid line. Press on the syringe to advance the hydraulic piston into contact with the Teflon sphere at the back of the reservoir. Pressure can be applied to the syringe until sample begins to leave the nozzle, but this is not necessary. Close the shut-off valve. The nozzle is now ready for operation.

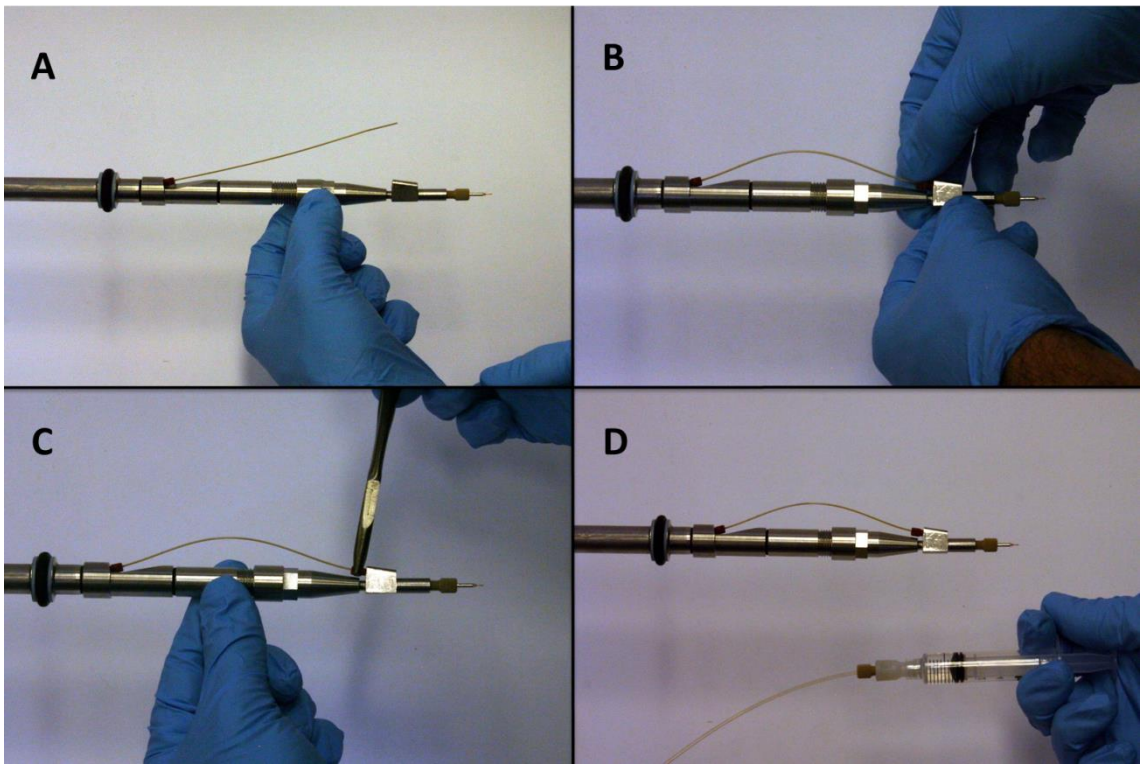

Figure 4.17: Reservoir/Nozzle Installation
The reservoir/nozzle installation is shown for the in vacuum setup, but the steps are similar for in air operation. (A) The reservoir/nozzle is attached to the hydraulic stage (resetting the piston if necessary). (B) The gas line is attached to the nozzle with a 6-32 fitting, and (C) secured in place with the knurled pliers. (D) The plunger is advanced via the inline syringe assembly. The final step pushes the piston into contact with the Teflon spheres in the bore of the reservoir.

For reservoir/nozzle installation for an in air or standalone setup, withdraw the injector away from fragile components, and thread the reservoir/nozzle onto the hydraulic stage (finger tight is adequate), and attach the gas line to the nozzle via the 6-32 port on the nozzle body. Tighten the fitting with the knurled pliers to ensure that the connection

is secure. Slide or swing the injector back into the interaction region and roughly position the nozzle with the aid of the microscope camera. Turn on the gas, and open the shut-off valve in the liquid line. Press on the syringe plunger to advance the hydraulic piston into contact with the Teflon sphere at the back of the reservoir. Pressure can be applied to the syringe until sample begins to leave the nozzle, but this is not necessary. Close the shut-off valve. The nozzle is now ready for operation.

4.10 Operating the Injector

With the nozzle installed, the gas flowing, and the hydraulic piston advanced, operation of the LCP jet can begin. First, however, a final alignment of the LCP nozzle into the X-ray beam must occur. This alignment is usually done remotely via a three axis stage. The alignment may also require that the LCP jet be running.

Calculate the desired flow rate in the sample $Q = \pi(d/2)\text{^}2\, ns$. Where n is the X-ray pulse repetition rate, the diameter of the capillary tubing is d, and the desired distance between shots is s.

The flowrate entered at the pump is the desired flow rate in the sample reservoir divided by the amplification factor. For the small reservoir the amplification factor is 34, and for the large bore reservoirs the amplification factor is 14. Note that the pressure in the reservoir is the pressure at the pump multiplied by the amplification factor. For the small bore reservoirs this means that a pump pressure of 300psi means a reservoir pressure of over 10,000psi. It is critical that, depending on the amplification factor, a maximum pressure be set at the pump. The only fitting in the injector subject to the amplified pressure is between the nozzle and reservoir. The ferrules suggested for use in

this protocol are rated to 10,000psi (690bar). That equates to a maximum pump pressure of 300 psi for the small bore reservoir, and 550psi for the large bore reservoir.

After the desired flow rate and maximum pressure are calculated and entered into the pump, turn the pump on. LCP injection starts when the pressure in the reservoir is high enough to force extrusion of LCP through the capillary tubing. As the pressure builds at the pump the LCP should begin to extrude slowly from the nozzle tip. The LCP stream will accelerate until the pressure stabilizes. Once steady state operation is reached, record the pressure. Adjust gas pressure to maximize jet stability (see figure 18). Pressure buildup during this phase of operation can be quite slow, and if there are any leaks or clogs this is the time that they will manifest. Consult the trouble shooting table for further help.

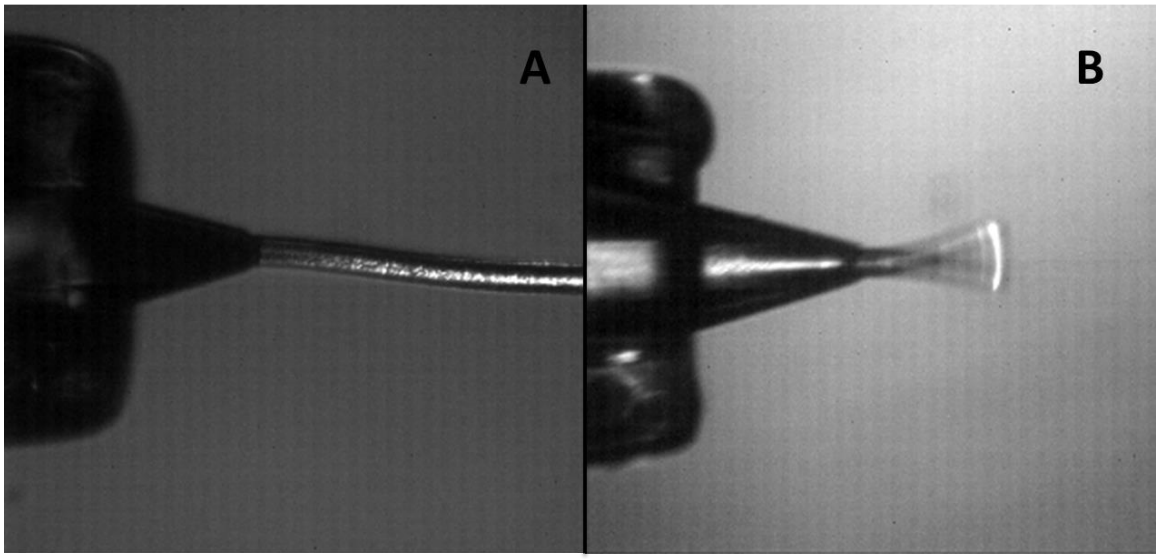

Figure 4.18: LCP Steam Stability
A) An LCP stream extruding in vacuum. Note that although the stream does not stay on axis that it remains stable. B) The LCP stream exhibits some oscillatory instability. Note that the instability pictured above may be mitigated by a change in gas pressure.

With a stable jet aligned to the X-ray beam, the injector should run until the sample is consumed. Sample run time can be estimated by dividing the volume of sample loaded by the flowrate. When the sample is exhausted the LCP extrusion will stop intermittently and the pressure will continue to rise. When it is determined that the sample has run out, remove the reservoir/nozzle and replace with the next sample.

4.10.1 Nozzle Removal for the In Vacuum Injector

Nozzle removal from the in vacuum injector is accomplished by first ensuring that both the pump and gas regulator are switched off, and the liquid line depressurized. Withdraw the nozzle rod from the injector, securing it in place when it has been pulled out the maximum distance. Close the gate valve. Vent the load lock, and unclamp the nozzle rod from the injector. Remove the rod from the injector and set the rod in a supported location near the injector. Detach the reservoir, and examine the hydraulic stage for leaks. Also note the position of the piston in the hydraulic stage body. If the sample has run out, the piston will have been pushed forward the maximum distance. If the piston has only partially advanced then there is likely still sample in the reservoir (this indicates a clogged capillary). Open the shut-off valve, and carefully press the piston back into the hydraulic stage body. Close the shut-off valve. The injector is now ready for the next nozzle/reservoir.

4.10.2 Nozzle Removal for In Air/Standalone Operation

Nozzle removal from an in air/standalone injection setup is accomplished by first ensuring that both the pump and gas regulator are switched off, and the liquid line depressurized. Extract the injector from the interaction region, carefully avoiding sensitive or fragile components. Unthread the reservoir, and examine the hydraulic stage

for leaks. Also note the position of the piston in the hydraulic stage body. If the sample has run out the piston will have been pushed forward the maximum distance. If the piston has only partially advanced then there is likely still sample in the reservoir. Open the shut-off valve, and carefully press the piston back into the hydraulic stage body. Close the shut-off valve. The injector is now ready for the next nozzle/reservoir.

4.10.3 Nozzle/Reservoir Disassembly

After removal, the nozzle/reservoir should be disassembled, cleaned, and prepped for reuse. First, remove the gas aperture, then, using wrenches, detach the nozzle body from the reservoir. The capillary, sleeve and ferrule will likely stay stuck in the 10-32 coned port on the reservoir, and can be removed by gripping the sleeve, with a small pair of needle nose pliers, and pulling firmly. Remove the Teflon balls and excess sample by pushing the Teflon spheres out the front of the reservoir with the small diameter rod. Clean the reservoir, and the ferrule/sleeve if reusing, and prepare reservoir for reloading as described above.

If the sleeve is pulled out of the ferrule and the ferrule is stuck in the reservoir, it can be removed by pushing on the Teflon balls with the small diameter rod; this should force the ferrule out.

4.11 Troubleshooting

During data collection any number of problems can occur with the injector that interfere with data collection. The LCP jet may clog or curl back, plugging part of the gas aperture. Capillary tubing may clog and liquid lines may leak. To help users deal with common LCP injection setbacks a troubleshooting guide may be found below.

One problem unique to LCP injection in vacuum is the transition from the cubic phase to lamellar crystalline phase. The problem can be mitigated by switching sheath gas from the standard helium to nitrogen. If lamellar phase rings are observed on the detector, and a remote controlled valve was installed for gas switching, try nitrogen as the sheath gas.

Table 4.4: LCP Injector Troubleshooting Guide

Problem	**Diagnostics**	**Suggested Solutions**
LCP not extruding	Ensure that shut-off valve is closed Ensure that the pump is on, pumping, and the vent valve is closed. Is there pressure building at the pump?	Open shut-off valve, press syringe to advance plunger, and close valve. Check for leaks in the liquid line. Air bubbles in the liquid lines may take a long time to compress at a small fixed flow rate. Purge lines to remove air bubbles.
	If the LCP was extruding previously. Calculate expected end time. Is there excessive pressure build up at the HPLC pump?	You may be out of sample. There may be a clog. Change the capillary tip.
Sharp rings at high Q on the detector.	This could be due to the lipid matrix transitioning from the cubic to the lamellar phase (Uwe Weierstall et al. 2014). Transition occurs in vacuum due to rapid dehydration/evaporative cooling.	Jet could be too slow. Increase flow rate. Switch sheath gas to nitrogen. LCP material stuck to the nozzle tip may have transitioned. Clean nozzle and try again. Problem may be sample dependent. Consider using a different lipid.
Sample runs out early	Is the pump running at correct calculated flow rate?	Check for improper reservoir loading. Sample may leak from loading needle during loading if it is under tightened.

Pressure too high	Is the LCP extrusion slow or stopped?	Sample may be running out. Check calculated end time. Check how far plunger has advanced to estimate remaining sample. Capillary may be partially clogged. Change capillary.
	Is the LCP jet otherwise running normally?	Check for constrictions, kinks or other resistance in the liquid line. Problem may be sample dependent.
Jet is not stable	Ensure sheath gas is on. Adjust sheath gas higher and lower. Does gas pressure max out below the expected value?	Gas cylinder may be running low. Check pressure at the tank.
	Does gas adjustment not affect LCP jet?	Gas line may not be delivering sufficient flow to nozzle. Check for kinks in line, long lengths of small diameter tubing, or other sources of resistance.
Jet is too short	Turn gas pressure down. Does the jet get longer?	Problem may be sample dependent.
	Is the capillary tip extruding from the gas aperture 200-300 microns?	Reassemble nozzle.
Capillary tip is being pushed out of the nozzle.	Ensure that you have not run out of sample. Is the Nozzle body properly tightened onto the reservoir?	Check for a crushed ferrule, and replace if necessary. Retighten.

5 ARIZONA STATE ANTI-SETTLER OPERATIONS PROTOCOL

The anti-settler is a portable device designed to be used in serial crystallography, or other X-ray scattering experiment, where a pressurized reservoir of liquid is used to supply sample to a nozzle. Depending on the sample volume, data collection can take hours, and over this period of time the sample may degrade in the reservoir.

In the serial crystallography method, samples are prepared to optimize crystal growth or quality. The variability in sample conditions often results in requirements in the sample environment to maintain crystal viability during the data collection. The most requested environmental conditions are: that the sample be maintained at a specific temperature, avoid light exposure, and be gently agitated to avoid crystal settling (Lomb et al. 2012). To facilitate these needs the injector lab at Arizona State University has constructed a temperature controlled anti-settler.

This chapter will cover the setup procedure for the anti-settler, and the filling procedure for the reservoirs. While there are many ways to configure the system, here I will explain the simplest configurations. Table 5.1 gives a small parts list for operating a liquid jet experiment with the ASU anti-settler.

Table 5.1: Anti-Settler Parts List

Part	Supplier: Part number(s)	Part	Supplier: Part number(s)
Water Supply Tubing	IDEX: 1533	Inline filters	IDEX: A-355
Sample Supply Tubing	IDEX: 1535	Filter body	IDEX: A-122
10-32 coned port fittings	IDEX: LT-110	Anti-settler control box	ASU: custom part
10-32 coned port ferrules	IDEX: LT-100	Anti-settler rotor and stand	ASU: custom part
Two position valves optional	IDEX: MXP7900-000	Hydraulic syringe reservoirs	ASU: custom parts
Multi-position valves optional	IDEX: MXP7970-000	Hydraulic seals	Trelleborg: Variseal M/Radial seal PVA000080 – T40SD

5.1 Anti-Settler Device Setup

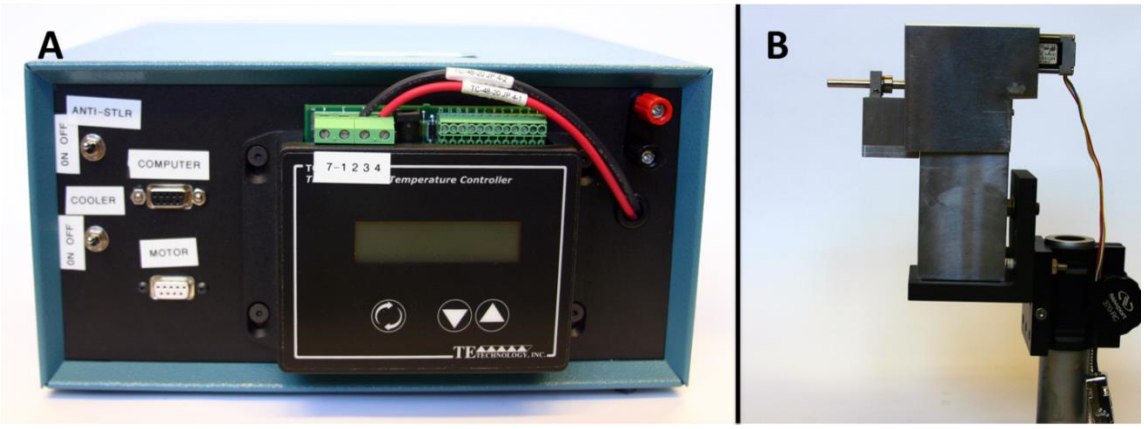

Figure 5.1: Anti-Settler Components
Figure shows the ASU designed anti-settler control box(A), and the rotor stand (B).

The anti-settler consists of a control box, and a reservoir stand (Figure 5.1). The control box needs only 120 volt AC power, and should be set on a flat surface as near the injector as possible. The reservoir stand should be bolted to the table not more than two feet (60cm) from the control box. The motor on the stand should then be plugged into the 9-pin DIN connector on the front of the control box labeled “MOTOR”. The cable of the motor is short, and a male to male 9-pin DIN cable should be used as an extension. The rotor is then affixed to the stand via a small set screw using a 1/16” hex wrench (Figure 5.2). The rotor consists of a small air cooled thermoelectric cold plate (TE Technologies) and a syringe clamp. Once the rotor is in place the thermoelectric cooler should be wired into the temperature controller on the control box (Figure 5.3).

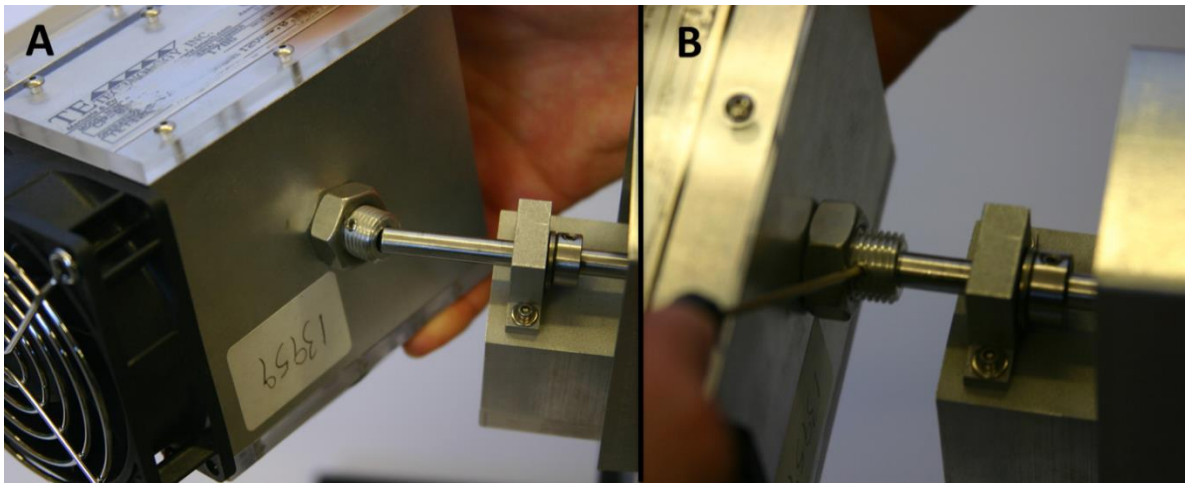

Figure 5.2: Rotor Installation
To install the rotor push the rotor onto the shaft of the motor (A), and tighten the set screw with a 1/16” hex wrench.

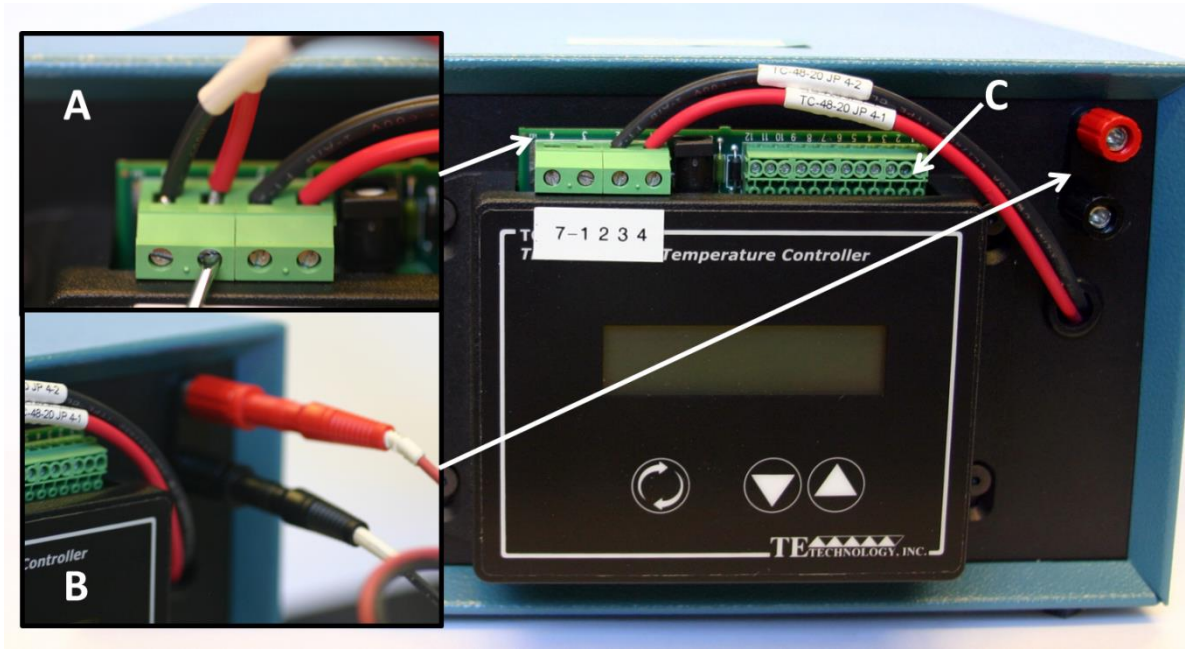

Figure 5.3: Attach Cooler Wiring
Wire the thermoelectric cooler into the terminal block on top of the temperature controller (A). Plug in the red and black power leads into their corresponding plugs (B), and attach the thermistor to the small terminal block (positions 1 and 2) (C).

As the rotor spins there is a risk of interference with the wires and tubing that are attached to the moving parts. These lines necessitate an attachment point to prevent

tangling. An optical post or other ridged fixed point located on the axis of rotation about 30cm from the rotor is ideal. Cables and tubing should be routed through a loose loop fixed to the post (Figure 5.4).

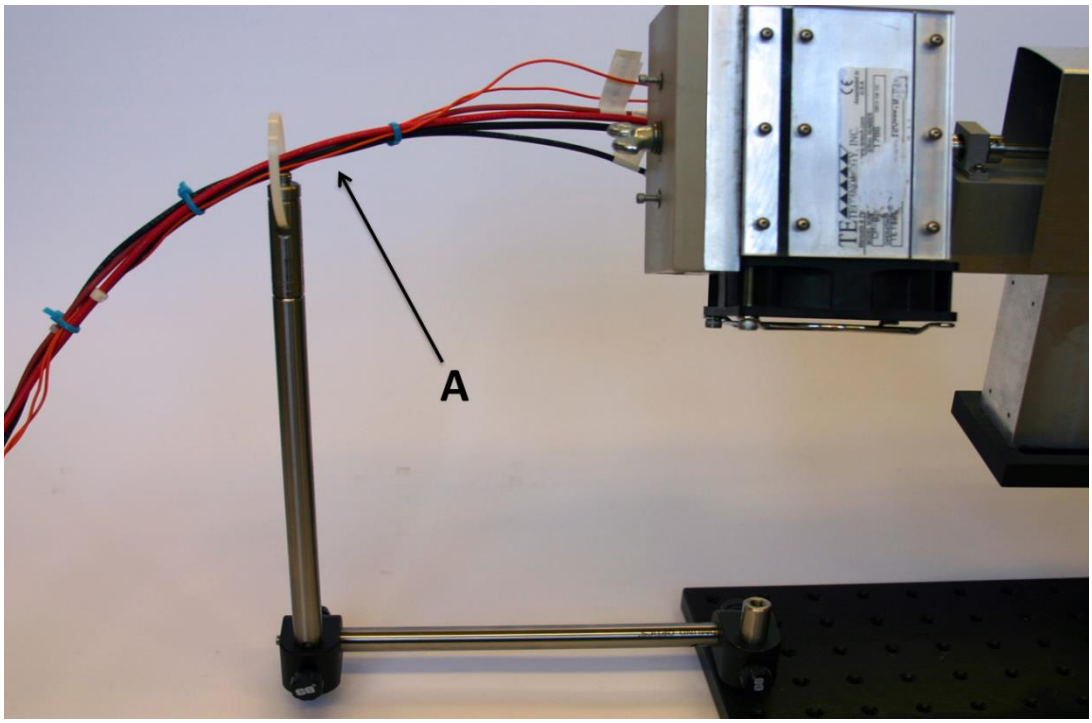

Figure 5.4: Wiring and Tubing Support Loop
All wires and tubing should be routed through a loose loop (A) located about 10” away from the rotor along the axis of rotation.

5.2 Anti-Settler Device Pretest

Flip the master power switch on the back of the control box to “ON” to power the device. Switches to power the temperature controller and motor are on the front panel. Flip the “ANTI-STLR” switch and observe the rotor. It should rotate a full 360 degrees before switching direction. If the motor does not work check power switches, and motor connections. The motor is a small stepper motor (Applied Motion Products) attached to a gear box with a four to one gear ratio. It is possible to over-torque the motor and cause it to stall, but this is intended as a safety feature to prevent wires and tubing from being

wound around the rotor. Note that the motor will begin a full 360 degree rotation starting from where the motor is resting while the switch is off. The motor contains no encoder, and the motor controller does not know if the rotor is over-rotating.

To test the cooler flip the switch labeled “COOLER”, and the screen on the temperature controller should light up. If the screen fails to light, check the fuse on the back of the control box (1 amp slow-blow). The screen should read the current temperature of the device from a thermistor attached to the cold side of the rotor. The fan on the rotor should start spinning, and the current to the cooler (represented as a percent of the maximum) should appear on the display (Figure 5.5). You may want to check that the device is cooling properly by checking the readout frequently.

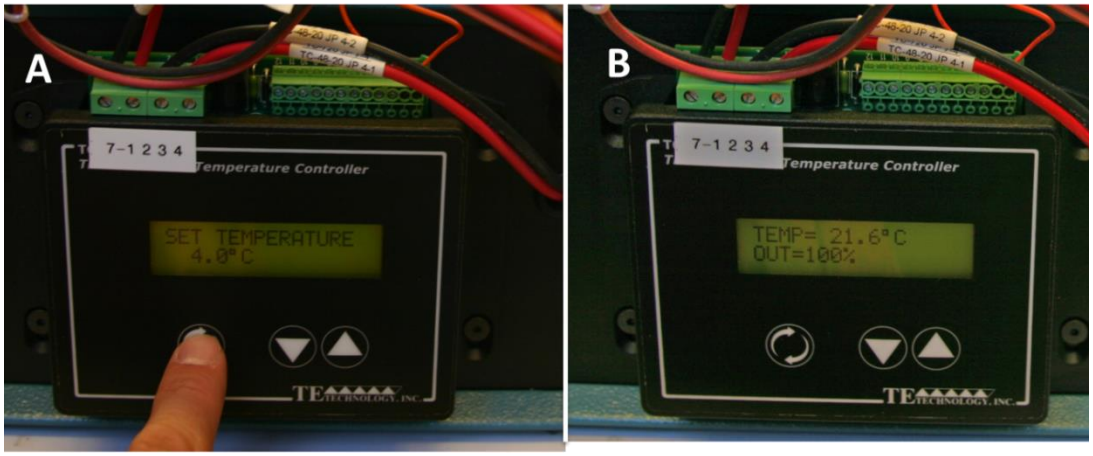

Figure 5.5: Setting the Temperature Controller
To set the temperature press the menu button until the “set temperature” option appears (A). Use the up and down arrows to select the temperature. Once the temperature is selected the display will show current output (as a percentage), and the temperature set point (B).

5.3 Sample Delivery System Setup

With the device installed and tested you are ready to begin setup of the liquid sample delivery system. This part of the installation guide is the most flexible. Sample

delivery using a pressurized syringe reservoir requires a pump (or other means of supplying pressure i.e. compressed gas), and one or more valves for switching to a wash line or between multiple reservoirs.

Typically pressure is supplied by a constant flow rate pump, of the kind commonly used in HPLC systems (Shimadzu). Unless the pump can be controlled remotely it should be installed outside the X-ray hutch where it can be accessed while the X-rays are on. This may require routing tubing through a chicane or other hutch feedthrough. This tubing should have a small inner diameter to minimize purging time, but large enough to flow water at low pressures. Tubing should also be inelastic as elasticity in the liquid lines creates significant lag in the response time of the pump. Tubing is typically made of stainless steel or PEEK (IDEX).

Once the pump is installed (with a large reserve of pure water), and the supply line is routed, purge the supply line, and connect the line to a switching valve. Proceed to connect individual water supply lines from the valve through the loop of the tubing support, and purge each line. After the reservoirs are installed (see sections 5.4 and 5.5), connect the sample line of the nozzle to the appropriate valve output. The system is now ready to receive a loaded syringe reservoir.

Note that it is possible to configure the system with one or two two-position valves or with two multi-position valves or with combinations of the two. Figure 5.6 and Figure 5.7 show examples of sample delivery schemes using different valves (one with a single two-position valve, and one with two multi position valves). The valves will have to be installed near the injector, and therefore need to be controlled remotely.

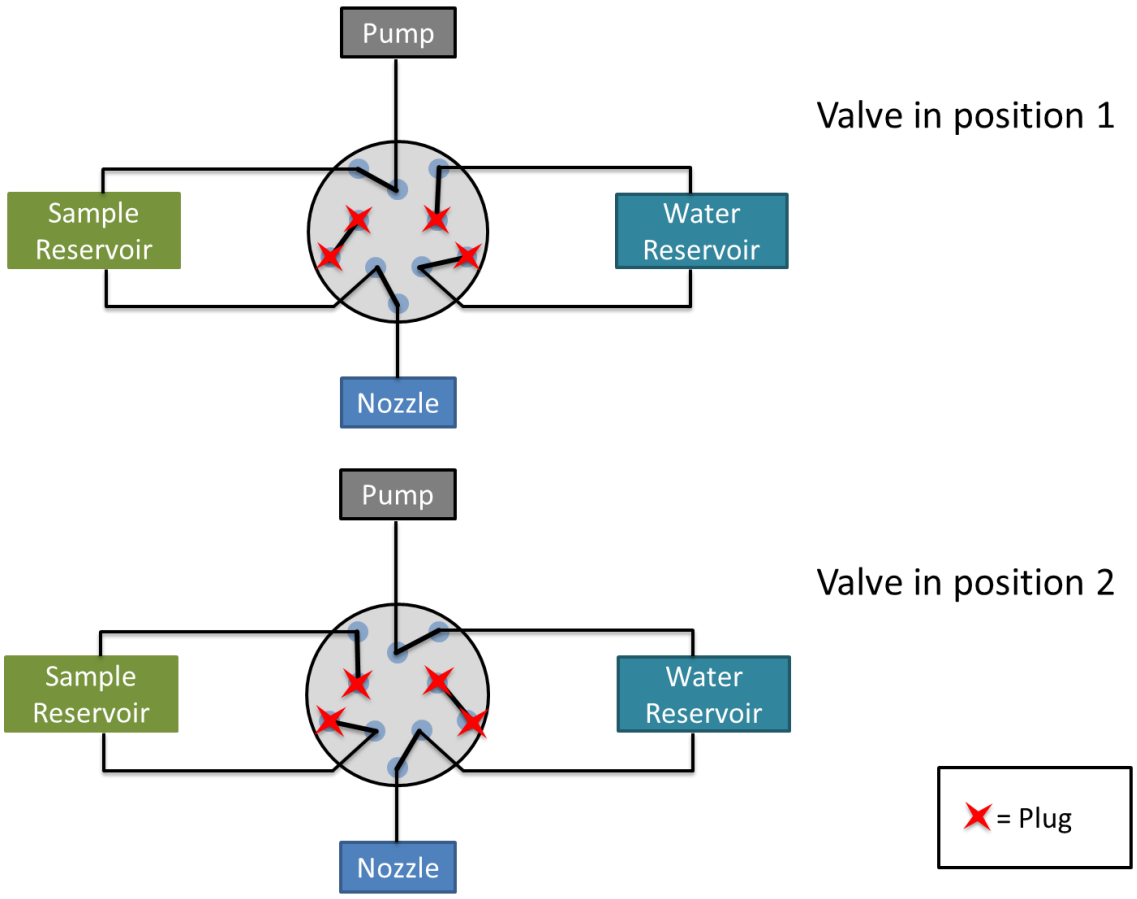

Figure 5.6: Single Valve Tubing Schematic
A sample delivery tubing diagram using a single two-position valve. Position one sends sample to the nozzle. Position two is shown attached to a water reservoir (typically water is used to wash the nozzle between samples).

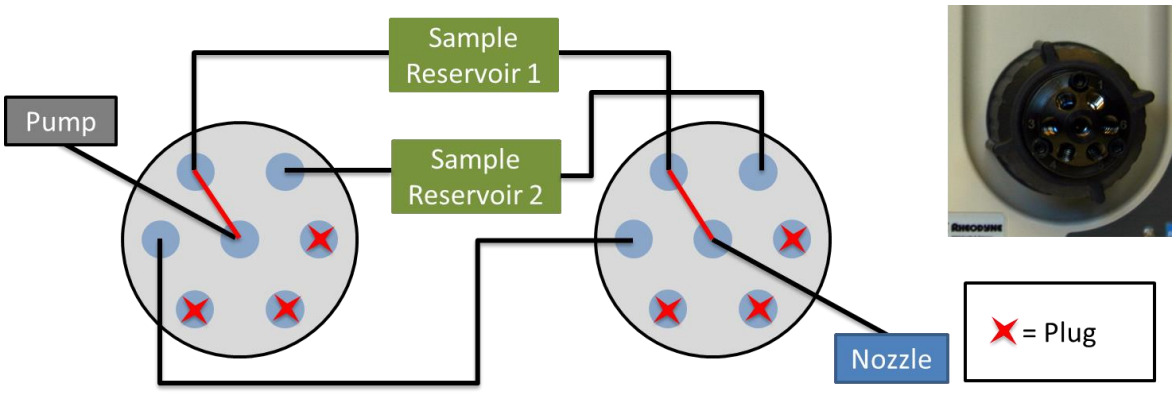

Figure 5.7: Two Multi-position Valve Tubing Schematic
A sample delivery tubing diagram using two six-position valves. The valve on the left switches the supply line to the different reservoirs, and the valve on the right sends sample to the nozzle. Two sample reservoirs are shown (because that is the number of syringes that fit in the anti-settler) and a single bypass line used to send water to the nozzle.

5.4 Reservoir Preparation and Loading

With the temperature controlled anti-settler working and the pump and valve(s) installed and purged you are prepared to load and install the sample syringes. The syringes are similar to those described in Lomb et al. (2012). The syringes consist of a stainless steel body with a smooth bore 8mm ID, and a stainless steel plunger sealed with hydraulic gaskets (Trelleborg). Syringes should be disassembled, cleaned, and clearly labeled prior to loading. Gloves should be worn to prevent contamination of the syringe parts.

First insert the plunger carefully to avoiding cutting the gasket on the edge of the bore (Figure 5.8). If the gasket is pinched or the seal otherwise compromised it should be removed and replaced. Press in the plunger until it is well seated. Using a plastic syringe or pipet, dispense a small amount of pure water on the plunger until a large meniscus is formed. Take care to remove any air bubbles. While holding the syringe upright, screw

the PEEK cap onto the syringe, and tighten with wrenches (Figure 5.9). This is done to prevent air bubbles caused by the syringe dead volume. Note that during these steps care should be taken to avoid introducing any air into the system.

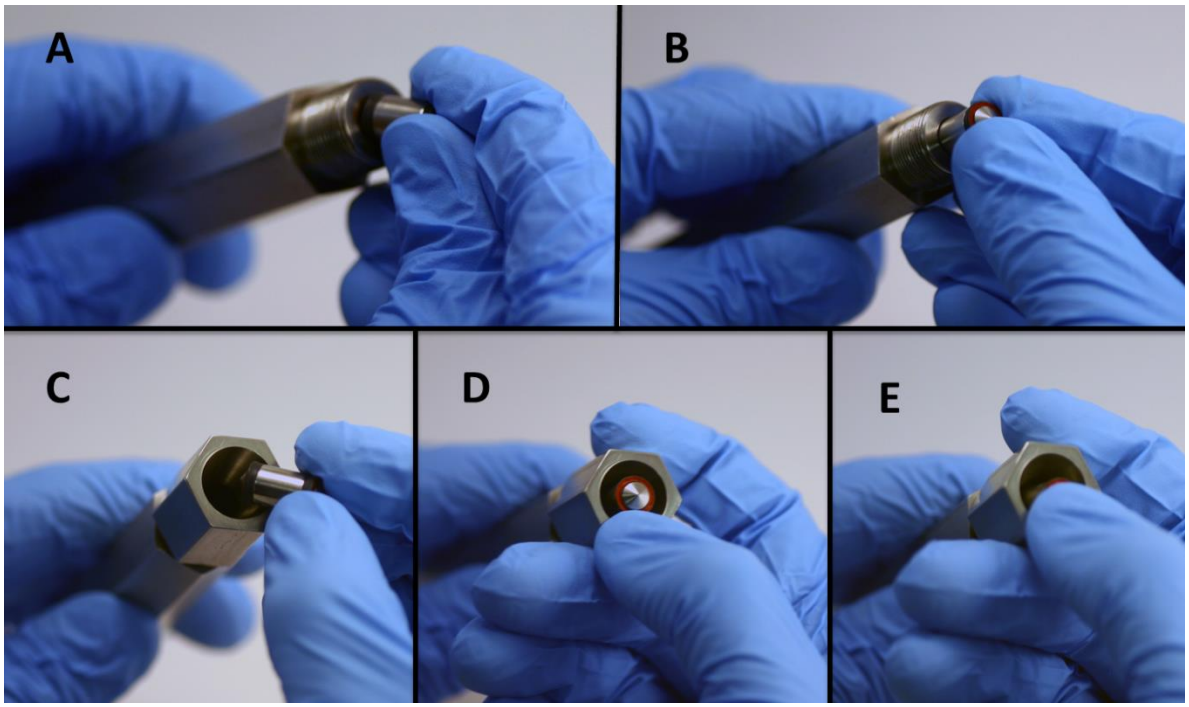

Figure 5.8: Inserting Plunger
The plunger must be inserted carefully to keep the sealing surface viable. First the gasket is compressed against the side (A), and then gently inserted (B) while avoiding pinching the seal. If plunger insertion tool is available (a tapered bore that meets the inner bore and allows the gasket to evenly compress during insertion) thread the tool onto the reservoir (C), insert the plunger (D), and press the plunger into the reservoir bore.

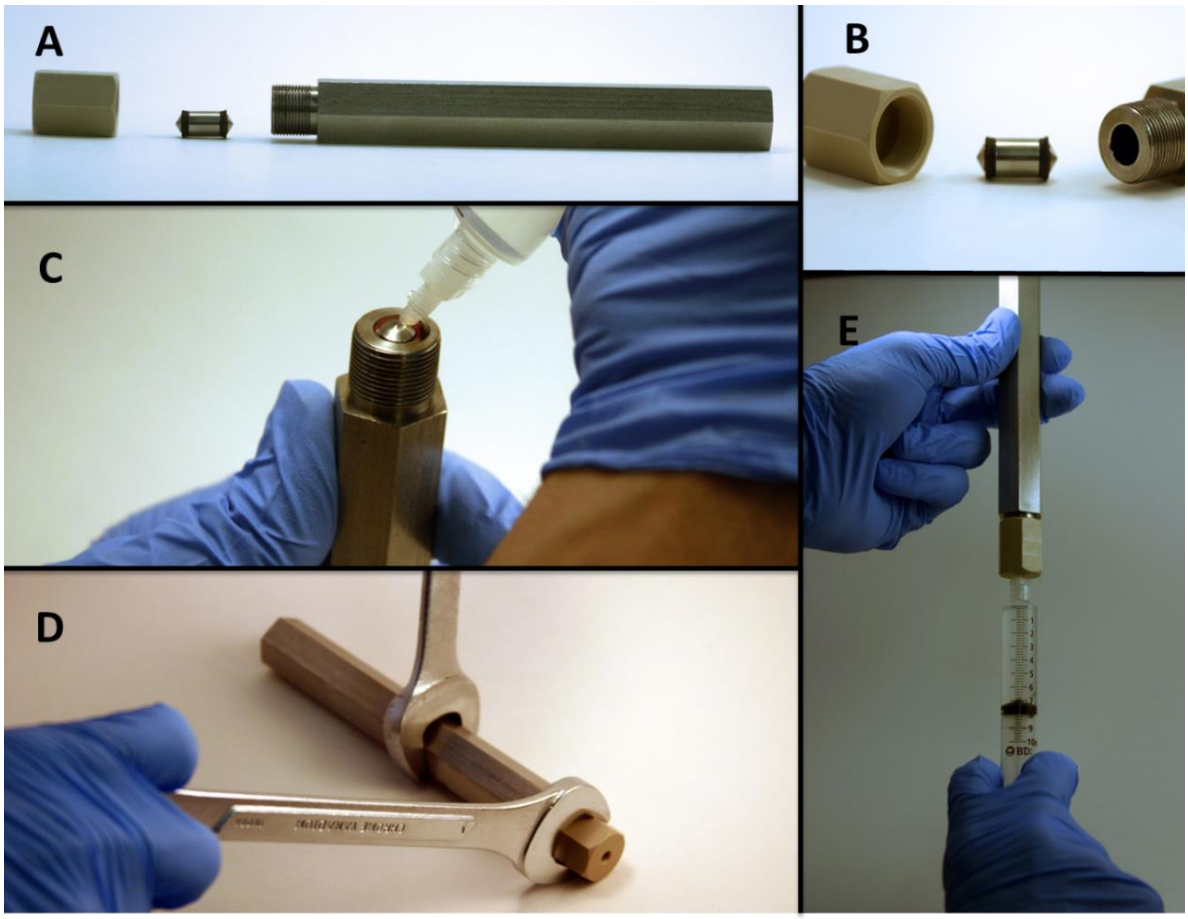

Figure 5.9: Syringe Assembly
The parts of the syringe reservoir are shown in (A) and (B). To minimize air cover the plunger with a bead of water (C) before tightening with wrenches (D). Make a wet connection and attach syringe (E) push plunger to advance plunger.

Attach a plastic 10ml syringe filled with pure water to the 10-32 coned port in the PEEK cap with a male Luer Lock to male 10-32 coned port adapter (IDEX P-642). Press the plunger on the plastic syringe to fill the reservoir with water. The stainless steel plunger should be pushed to the opposite end of the reservoir (Figure 5.9). The reservoir is now ready to be loaded with sample, however, should the sample need to be kept at a specific temperature during data collection the reservoirs should be precooled prior to loading.

To load sample, attach a plastic syringe filled with the sample liquid to the stainless steel 10-23 coned port with another Luer lock to 10-32 coned port adapter. Press down on the plunger until the desired amount of sample is loaded into the reservoir. At this point the sample is loaded, but there are probably air bubbles in the reservoir on the sample side. An attempt can be made to remove them by manual centrifugation. After centrifuging the reservoir any air bubbles should be at the outlet. Remove the plastic sample syringe, and attach a pre-assembled sample line (Figure 5.10).

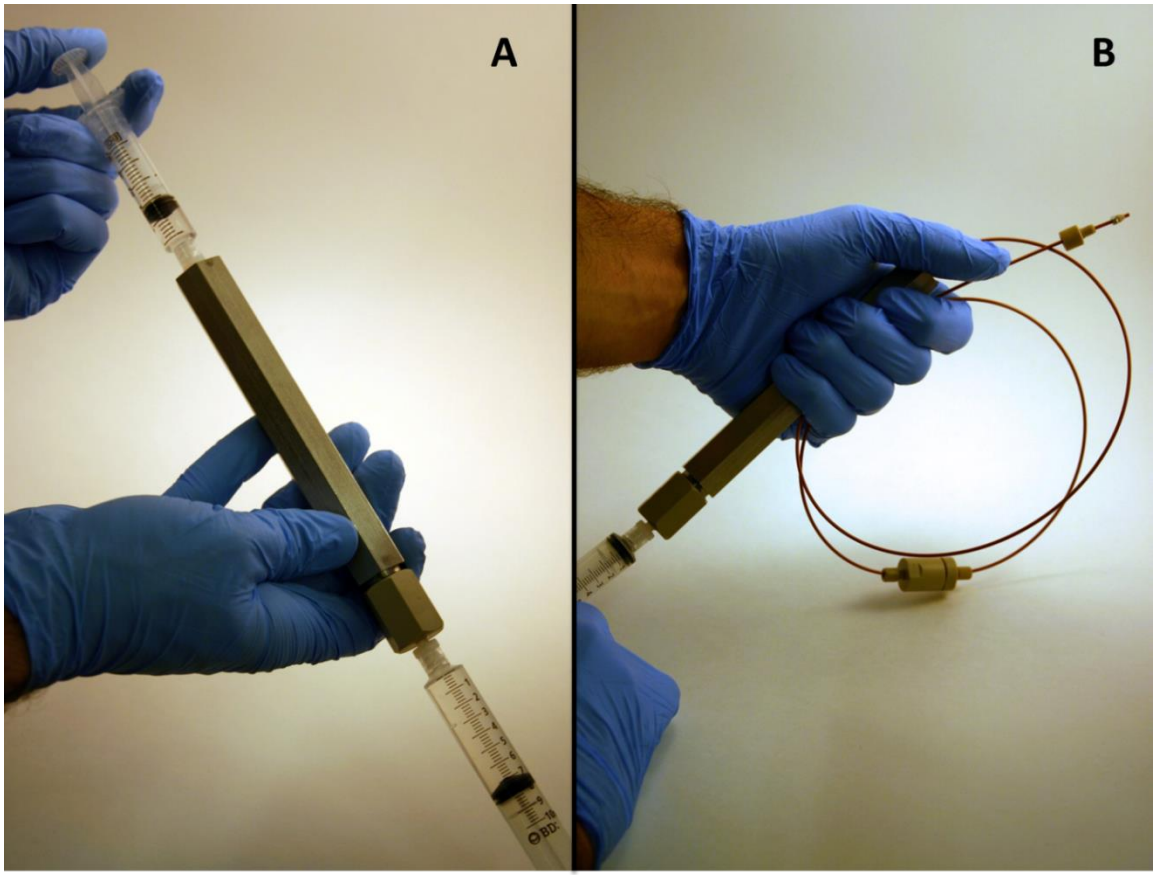

Figure 5.10: Sample Loading and Sample Line Purging
With the water syringe still attached, attach sample syringe (A). Load the desired amount of sample, and attach sample line. Press water syringe to purge sample line (B). Sample line is purged when pure sample (no bubbles) appears at the end of the sample line.

The sample line has appropriate lengths of small inner diameter PEEK tubing and an inline filter (IDEX). Tubing inner diameter should be selected to minimize dead volume, and filter size should be appropriate to prevent nozzle clogging (typically 20 microns). The sample line should be attached with a 10-32 coned port fitting that can be wrench tightened, or be rated to 6000psi when finger tightened. With the tubing and filter attached press firmly on the water syringe to purge the sample line. Continue pressing until all the air is expelled, and sample liquid is observed at the outlet (Figure 5.10).

5.5 Loading the Syringe into the Anti-Settler

With sample loaded into a precooled reservoir and the sample line purged, the reservoir is ready to be loaded into the anti-settler. Turn off the rotation motor by flipping the switch labeled “ANTI-SLTR” to the off position. The rotor will now rotate freely. Loosen the thumbscrew on the front of the rotor until the clamp is loose enough for the reservoir to slide easily into one of the two receptacles. Tighten the thumbscrew to secure the reservoir in the clamp. Route the sample line through the tubing support, and attach it to the appropriate port on the output valve. Attach the supply line to the reservoir, making sure that the line is still purged, and that the fitting is tightened appropriately (Figure 5.11).

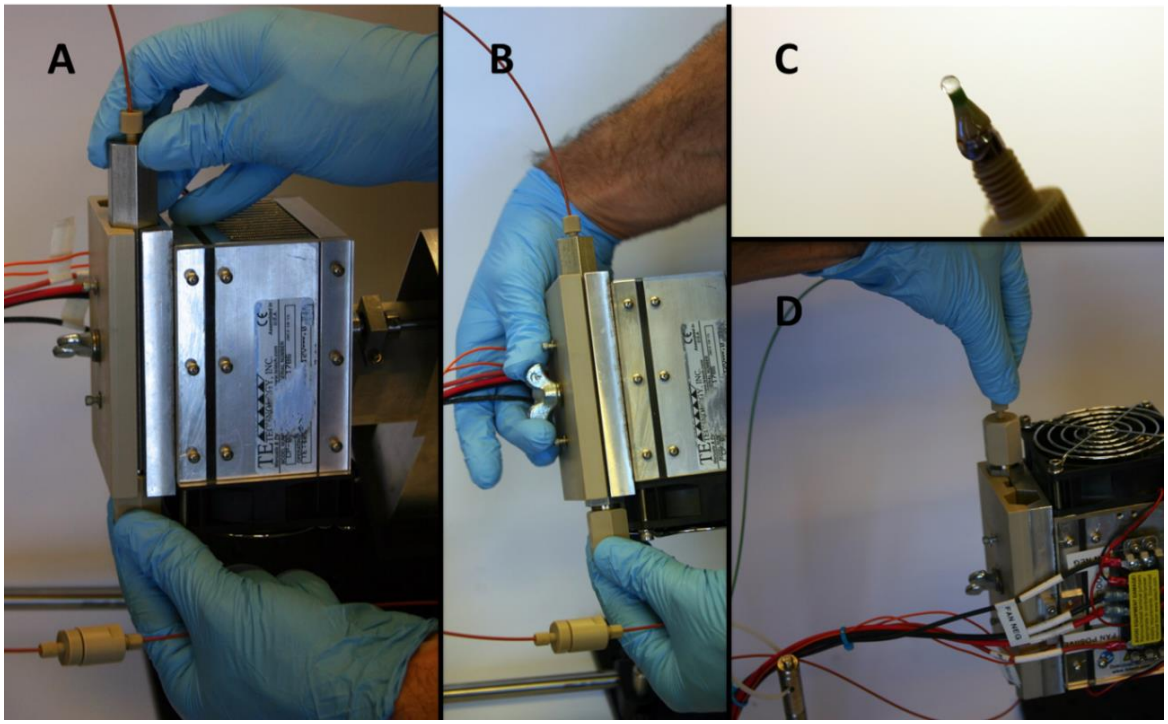

Figure 5.11: Syringe Loading
Load the syringe into the rotor by loosening the thumbscrew on the front of the rotor and sliding the rotor into one of the two receptacles (A). Secure the reservoir by tightening the thumbscrew (B), and attach sample line to valve. Purge supply line (C), and attach to the reservoir (D).

Check that the cooler is operating by reading the cold plate temperature on the display of the temperature controller. Start rotation of the rotor by flipping the switch labeled “ANTI-STLR” to the on position. Observe the rotor to ensure that the wires and tubing do not interfere with the rotation. If the motor appears to be pulling or tangling the lines in the tubing support loop ensure that the rotor started in a neutral position. Remember that the motor start position is determined by the position of the rotor when the anti-settler switch is flipped on.

5.6 Operating the Injector System

With all fittings tightened, valves in the appropriate starting positions, and the rotation and temperature control operational, the system is ready to begin operation. The detailed operation of a liquid jet is not given here, however, detailed knowledge of flow focused nozzle or GDVN (DePonte et al. 2008) is needed in order to operate the pump(s) effectively. The sheath gas for the nozzle should be flowing and set to the pressure given in individual nozzle parameters. Engage the pump that will supply water to the nozzle, and let the pressure build. It is helpful to build the pressure well above the jet onset level before opening the output valve. Once valves are opened the pressure will drop and the nozzle line will purge. Observe the nozzle and confirm jet onset. Let pressure stabilize at the pump at the desired flow rate, and record the baseline pressure.

Baseline pressure is the amount of pressure required to form a water jet taking into account all components in the system (minus the syringe reservoir, and inline filter). After jetting sample liquids, the nozzle should return to baseline pressure during a water wash. Pressures higher than baseline during water wash indicate a nozzle clog. Unions are the most common locations for clogs, especially when there is a constriction. The most common clogging happens where the sample line connects to the glass capillary tubing of the nozzle. If there is a suspected clog, before changing the nozzle, it is a good idea to trim a centimeter off of the nozzle line and attempt to reestablish a jet at baseline pressure.

Once a stable water jet is established the hutch is usually closed and all injector, and sample delivery control must be done remotely. It is critical to have a microscope

focused on the jet with adequate lighting for this purpose. There is no other reliable way to know that the nozzle is jetting without visual feedback.

If your system is using multiple pumps, start building pressure on the desired sample reservoir. When the pump pressure has exceeded baseline by a few hundred psi, switch the valve to sample. Despite best efforts there will be an air gap in the line between water and sample, there is a risk that this air gap will lead to ice events at the nozzle tip. Adjust the pump flow rate until a stable jet is formed, adjusting gas pressure as needed. Wait for pressure to stabilize and record a baseline pressure for the sample. If the pressure begins to rise consider switching to water and washing the line, then resuming data collection.

Given that most sample liquids have a higher viscosity than water and a high concentration of suspended nanocrystals the pressure required to jet sample is often much higher than baseline. If you are approaching maximum pressure and there is no jet visible try adjusting gas pressure. If there is nothing coming out of the nozzle and the pressure is rising fast there is likely a clog. If the pressure at the pump is stable, but nothing is coming out of the nozzle there is most likely a leak.

When the sample in the reservoir is exhausted the jet will sputter and the pressure will rise sharply. An estimated sample run time can be calculated by dividing the volume of sample loaded by the pump flow rate. After the sample runs out switch the valve to water and wash the nozzle line. Then, either switch to the second sample, or open the hutch and remove the reservoir.

5.7 Removing the Reservoir

To remove the reservoir stop the rotation by flipping the switch labeled “ANTI-STLR” to off. Detach the sample line at the valve and the supply line from the reservoir. Loosen the thumbscrew on the front of the rotor, and remove the reservoir. Note that once the thumbscrew is loose the reservoir will fall out of the rotor under its own weight if it is not prevented from doing so.

With the reservoir removed one can now load another as described above. If the next sample requires a new temperature setting on the cold plate, make the change and give the cooler ample time to come to the new temperature.

REFERENCES

Aherne, Margaret, Joseph a Lyons, and Martin Caffrey. 2012. “A Fast, Simple and Robust Protocol for Growing Crystals in the Lipidic Cubic Phase.” *Journal of Applied Crystallography* 45 (Pt 6): 1330–33. doi:10.1107/S0021889812037880.

Aquila, Andrew, Mark S Hunter, R Bruce Doak, Richard a Kirian, Petra Fromme, Thomas a White, Jakob Andreasson, et al. 2012. “Time-Resolved Protein Nanocrystallography Using an X-Ray Free-Electron Laser.” *Optics Express* 20 (3): 2706–16. http://www.ncbi.nlm.nih.gov/pubmed/23633593.

Arnlund, David, Linda C Johansson, Cecilia Wickstrand, Anton Barty, Garth J Williams, Erik Malmerberg, Jan Davidsson, et al. 2014. “Visualizing a Protein Quake with Time-Resolved X-Ray Scattering at a Free-Electron Laser.” *Nature Methods*, no. August (August). doi:10.1038/nmeth.3067.

Ayvazyan, V., N. Baboi, J. Bähr, V. Balandin, B. Beutner, a. Brandt, I. Bohnet, et al. 2006. “First Operation of a Free-Electron Laser Generating GW Power Radiation at 32 Nm Wavelength.” *European Physical Journal D* 37: 297–303. doi:10.1140/epjd/e2005-00308-1.

Barty, Anton, Carl Caleman, Andrew Aquila, Nicusor Timneanu, Lukas Lomb, Thomas a White, Jakob Andreasson, et al. 2012. “Self-Terminating Diffraction Gates Femtosecond X-Ray Nanocrystallography Measurements.” *Nature Photonics* 6 (December): 35–40. doi:10.1038/nphoton.2011.297.

Barty, Anton, Richard a. Kirian, Filipe R N C Maia, Max Hantke, Chun Hong Yoon, Thomas a. White, and Henry Chapman. 2014. “Cheetah: Software for High-Throughput Reduction and Analysis of Serial Femtosecond X-Ray Diffraction Data.” *Journal of Applied Crystallography* 47. International Union of Crystallography: 1118–31. doi:10.1107/S1600576714007626.

Bogan, Michael J, Dmitri Starodub, Christina Y Hampton, and Raymond G Sierra. 2010. “Single-Particle Coherent Diffractive Imaging with a Soft X-Ray Free Electron Laser: Towards Soot Aerosol Morphology.” *Journal of Physics B: Atomic, Molecular and Optical Physics* 43 (19): 194013. doi:10.1088/0953-4075/43/19/194013.

Bogan, Michael J., Sébastien Boutet, Henry N. Chapman, Stefano Marchesini, Anton Barty, W. Henry Benner, Urs Rohner, et al. 2010. “Aerosol Imaging with a Soft X-Ray Free Electron Laser.” *Aerosol Science and Technology* 44 (3): i – vi. doi:10.1080/02786820903485800.

Boutet, Sébastien, and Garth J Williams. 2010. “The Coherent X-Ray Imaging (CXI) Instrument at the Linac Coherent Light Source (LCLS).” *New Journal of Physics* 12 (3): 035024. doi:10.1088/1367-2630/12/3/035024.

Boutet, Sébastien, Lukas Lomb, Garth J Williams, Thomas R M Barends, Andrew Aquila, R Bruce Doak, Uwe Weierstall, et al. 2012. “High-Resolution Protein Structure Determination by Serial Femtosecond Crystallography.” *Science (New York, N.Y.)* 337 (6092): 362–64. doi:10.1126/science.1217737.

Breedlove, J R, and G T Trammell. 1970. “Molecular Microscopy: Fundamental Limitations.” *Science (New York, N.Y.)* 170 (3964): 1310–13. doi:10.1126/science.170.3964.1310.

Chapman, Henry N, Petra Fromme, Anton Barty, Thomas a White, Richard a Kirian, Andrew Aquila, Mark S Hunter, et al. 2011. “Femtosecond X-Ray Protein Nanocrystallography.” *Nature* 470 (7332). Nature Publishing Group, a division of Macmillan Publishers Limited. All Rights Reserved.: 73–77. doi:10.1038/nature09750.

Cherezov, Vadim. 2011. “Lipidic Cubic Phase Technologies for Membrane Protein Structural Studies.” *Current Opinion in Structural Biology* 21 (4). Elsevier Ltd: 559–66. doi:10.1016/j.sbi.2011.06.007.

Cherezov, Vadim, Daniel M Rosenbaum, Michael a Hanson, Søren G F Rasmussen, Foon Sun Thian, Tong Sun Kobilka, Hee-Jung Choi, et al. 2007. “High-Resolution Crystal Structure of an Engineered Human beta2-Adrenergic G Protein-Coupled Receptor.” *Science (New York, N.Y.)* 318 (November): 1258–65. doi:10.1126/science.1150577.

Cohen, Aina E., S. Michael Soltis, Ana González, Laura Aguila, Roberto Alonso-Mori, Christopher O. Barnes, Elizabeth L. Baxter, et al. 2014. “Goniometer-Based Femtosecond Crystallography with X-Ray Free Electron Lasers.” *Proceedings of the National Academy of Sciences* 111 (48): 17122–27. doi:10.1073/pnas.1418733111.

DePonte, D P, U Weierstall, K Schmidt, J Warner, D Starodub, J C H Spence, and R B Doak. 2008. “Gas Dynamic Virtual Nozzle for Generation of Microscopic Droplet Streams.” *Journal of Physics D: Applied Physics* 41 (19): 195505. doi:10.1088/0022-3727/41/19/195505.

Emma, P, R Akre, J Arthur, R Bionta, C Bostedt, J Bozek, A Brachmann, et al. 2010. “First Lasing and Operation of an Ångstrom-Wavelength Free-Electron Laser.” *Nature Photonics* 4 (9). Nature Publishing Group: 641–47. doi:10.1038/nphoton.2010.176.

Gañán-Calvo, Alfonso M., Daniel P. DePonte, Miguel a. Herrada, John C H Spence, Uwe Weierstall, and R. Bruce Doak. 2010. "Liquid Capillary Micro/nanojets in Free-Jet Expansion." *Small* 6 (7): 822–24. doi:10.1002/smll.200901786.

Gañán-Calvo, Alfonso M., and José M. Montanero. 2009. "Revision of Capillary Cone-Jet Physics: Electrospray and Flow Focusing." *Physical Review E - Statistical, Nonlinear, and Soft Matter Physics* 79: 1–18. doi:10.1103/PhysRevE.79.066305.

Garman, Elspeth F. 2013. "Radiation Damage in Macromolecular Crystallography: What Is It and Why Do We Care?" *NATO Science for Peace and Security Series A: Chemistry and Biology*. International Union of Crystallography, 69–77. doi:10.1007/978-94-007-6232-9-7.

Gualtieri, E. J., F. Guo, D. J. Kissick, J. Jose, R. J. Kuhn, W. Jiang, and G. J. Simpson. 2011. "Detection of Membrane Protein Two-Dimensional Crystals in Living Cells." *Biophysical Journal* 100 (1). Biophysical Society: 207–14. doi:10.1016/j.bpj.2010.10.051.

Hunter, Mark S, Brent Segelke, Marc Messerschmidt, Garth J Williams, Nadia a Zatsepin, Anton Barty, W Henry Benner, et al. 2014. "Fixed-Target Protein Serial Microcrystallography with an X-Ray Free Electron Laser." *Scientific Reports* 4 (January): 6026. doi:10.1038/srep06026.

Johansson, Linda C, David Arnlund, Thomas a White, Gergely Katona, Daniel P DePonte, Uwe Weierstall, R Bruce Doak, et al. 2012. "Lipidic Phase Membrane Protein Serial Femtosecond Crystallography." *Nature Methods* 9 (3): 263–65. doi:10.1038/nmeth.1867.

Kirian, Richard a, Xiaoyu Wang, Uwe Weierstall, Kevin E Schmidt, John C H Spence, Mark Hunter, Petra Fromme, Thomas White, Henry N Chapman, and James Holton. 2010. "Femtosecond Protein Nanocrystallography-Data Analysis Methods." *Optics Express* 18 (6): 5713–23. http://www.ncbi.nlm.nih.gov/pubmed/20389587.

Kirian, Richard A, Thomas A White, James M Holton, Henry N Chapman, Petra Fromme, Anton Barty, Lukas Lomb, et al. 2011. "Structure-Factor Analysis of Femtosecond Microdiffraction Patterns from Protein Nanocrystals." *Acta Crystallographica Section A Foundations Of Crystallography* 67: 131–40.

Kupitz, Christopher, Shibom Basu, Ingo Grotjohann, Raimund Fromme, Nadia a. Zatsepin, Kimberly N. Rendek, Mark S. Hunter, et al. 2014. "Serial Time-Resolved Crystallography of Photosystem II Using a Femtosecond X-Ray Laser." *Nature*, July. doi:10.1038/nature13453.

Kupitz, Christopher, Ingo Grotjohann, Chelsie E Conrad, Shatabdi Roy-Chowdhury, Raimund Fromme, and Petra Fromme. 2014. "Microcrystallization Techniques for Serial Femtosecond Crystallography Using Photosystem II from

Thermosynechococcus Elongatus as a Model System." *Philosophical Transactions of the Royal Society of London. Series B, Biological Sciences* 369 (1647). doi:10.1098/rstb.2013.0316.

Landau, E M, and J P Rosenbusch. 1996. "Lipidic Cubic Phases: A Novel Concept for the Crystallization of Membrane Proteins." *Proceedings of the National Academy of Sciences of the United States of America* 93 (December): 14532–35. doi:10.1073/pnas.93.25.14532.

Li, Dianfan, Joseph a Lyons, Valerie E Pye, Lutz Vogeley, David Aragão, Colin P Kenyon, Syed T a Shah, Christine Doherty, Margaret Aherne, and Martin Caffrey. 2013. "Crystal Structure of the Integral Membrane Diacylglycerol Kinase." *Nature* 497: 521–24. doi:10.1038/nature12179.

Liao, J., H. Li, W. Zeng, D. B. Sauer, R. Belmares, and Y. Jiang. 2012. "Structural Insight into the Ion-Exchange Mechanism of the Sodium/Calcium Exchanger." *Science*. doi:10.1126/science.1215759.

Liu, Wei, Andrii Ishchenko, and Vadim Cherezov. 2014. "Preparation of Microcrystals in Lipidic Cubic Phase for Serial Femtosecond Crystallography." *Nature Protocols* 9 (9): 2123–34. doi:10.1038/nprot.2014.141.

Liu, Wei, Daniel Wacker, Cornelius Gati, Gye Won Han, Daniel James, Dingjie Wang, Garrett Nelson, et al. 2013. "Serial Femtosecond Crystallography of G Protein-Coupled Receptors." *Science (New York, N.Y.)* 342 (6165): 1521–24. doi:10.1126/science.1244142.

Lomb, Lukas, Jan Steinbrener, Sadia Bari, Daniel Beisel, Daniel Berndt, Christian Kieser, Martin Lukat, Niklas Neef, and Robert L. Shoeman. 2012. "An Anti-Settling Sample Delivery Instrument for Serial Femtosecond Crystallography." *Journal of Applied Crystallography* 45 (4). International Union of Crystallography: 674–78. doi:10.1107/S0021889812024557.

Lyubimov, Artem Y., Thomas D. Murray, Antoine Koehl, Ismail Emre Araci, Monarin Uervirojnangkoorn, Oliver B. Zeldin, Aina E. Cohen, et al. 2015. "Capture and X-Ray Diffraction Studies of Protein Microcrystals in a Microfluidic Trap Array." *Acta Crystallographica Section D Biological Crystallography* 71 (4): 928–40. doi:10.1107/S1399004715002308.

Madey, John M. J. 1971. "Stimulated Emission of Bremsstrahlung in a Periodic Magnetic Field." *Journal of Applied Physics* 42 (5): 1906. doi:10.1063/1.1660466.

Mezzenga, Raffaele, Cedric Meyer, Colin Servais, Alexandre I Romoscanu, Laurent Sagalowicz, and Ryan C Hayward. 2005. "Shear Rheology of Lyotropic Liquid Crystals: A Case Study." *Langmuir : The ACS Journal of Surfaces and Colloids* 21 (8): 3322–33. doi:10.1021/la046964b.

Neutze, R, R Wouts, D van der Spoel, E Weckert, and J Hajdu. 2000. “Potential for Biomolecular Imaging with Femtosecond X-Ray Pulses.” *Nature* 406 (6797): 752–57. doi:10.1038/35021099.

Nogly, P., James, D., Wang, D., White, T. A., Zatsepin, N., Shilova, A., Nelson, G., Liu, H., Johansson, L., Heymann, M., Jaeger, K., Metz, M., Wickstrand, C., Wu, W., Bath, P., Berntsen, P., Oberthuer, D., Panneels, V., Cherezov, V., Chapman, H., Schertl, U. 2015. “Lipidic Cubic Phase Serial Millisecond Crystallography Using Synchrotron Radiation.” *IUCrJ* 2 (2): 168–76. doi:10.1107/S2052252514026487.

Pebay-Peyroula, E, G Rummel, J P Rosenbusch, and E M Landau. 1997. “X-Ray Structure of Bacteriorhodopsin at 2.5 Angstroms from Microcrystals Grown in Lipidic Cubic Phases.” *Science (New York, N.Y.)* 277 (September): 1676–81. doi:10.1126/science.277.5332.1676.

Qiu, Hong, and Martin Caffrey. 2000. “The Phase Diagram of the Monoolein/water System: Metastability and Equilibrium Aspects.” *Biomaterials* 21 (3): 223–34. doi:10.1016/S0142-9612(99)00126-X.

Rayan, Gamal, Vladimir Adrien, Myriam Reffay, Martin Picard, Arnaud Ducruix, Marc Schmutz, Wladimir Urbach, and Nicolas Taulier. 2014. “Article Surfactant Bilayers Maintain Transmembrane Protein Activity.” *Biophysj* 107 (5). Biophysical Society: 1–7. doi:10.1016/j.bpj.2014.07.016.

Redecke, Lars, Karol Nass, Daniel P DePonte, Thomas a White, Dirk Rehders, Anton Barty, Francesco Stellato, et al. 2013. “Natively Inhibited Trypanosoma Brucei Cathepsin B Structure Determined by Using an X-Ray Laser.” *Science (New York, N.Y.)* 339 (6116): 227–30. doi:10.1126/science.1229663.

Santos, Jose S., Guillermo a. Asmar-Rovira, Gye Won Han, Wei Liu, Ruhma Syeda, Vadim Cherezov, Kent a. Baker, Raymond C. Stevens, and Mauricio Montal. 2012. “Crystal Structure of a Voltage-Gated K+ Channel Pore Module in a Closed State in Lipid Membranes.” *Journal of Biological Chemistry* 287: 43063–70. doi:10.1074/jbc.M112.415091.

Sauter, Nicholas K., Johan Hattne, Ralf W. Grosse-Kunstleve, and Nathaniel Echols. 2013. “New Python-Based Methods for Data Processing.” *Acta Crystallographica Section D: Biological Crystallography* 69. International Union of Crystallography: 1274–82. doi:10.1107/S0907444913000863.

Schmidt, Marius. 2013. “Mix and Inject: Reaction Initiation by Diffusion for Time-Resolved Macromolecular Crystallography.” *Advances in Condensed Matter Physics* 2013. doi:10.1155/2013/167276.

Seibert, M Marvin, Tomas Ekeberg, Filipe R N C Maia, Martin Svenda, Jakob Andreasson, Olof Jönsson, Duško Odić, et al. 2011. “Single Mimivirus Particles

Intercepted and Imaged with an X-Ray Laser." *Nature* 470 (7332): 78–81. doi:10.1038/nature09748.

Sierra, Raymond G, Hartawan Laksmono, Jan Kern, Rosalie Tran, Johan Hattne, Roberto Alonso-Mori, Benedikt Lassalle-Kaiser, et al. 2012. "Nanoflow Electrospinning Serial Femtosecond Crystallography." *Acta Crystallographica. Section D, Biological Crystallography* 68 (Pt 11): 1584–87. doi:10.1107/S0907444912038152.

Smith, Janet L., Robert F. Fischetti, and Masaki Yamamoto. 2012. "Micro-Crystallography Comes of Age." *Current Opinion in Structural Biology* 22 (5). Elsevier Ltd: 602–12. doi:10.1016/j.sbi.2012.09.001.

Soares, Alexei S., Matthew A. Engel, Richard Stearns, Sammy Datwani, Joe Olechno, Richard Ellson, John M Skinner, Marc Allaire, and Allen M Orville. 2011. "Acoustically Mounted Microcrystals Yield High-Resolution X-Ray Structures." *Biochemistry* 50 (21): 4399–4401. doi:10.1021/bi200549x.

Spence, J C H, U Weierstall, and H N Chapman. 2012. "X-Ray Lasers for Structural and Dynamic Biology." *Reports on Progress in Physics. Physical Society (Great Britain)* 75 (10): 102601. doi:10.1088/0034-4885/75/10/102601.

Tenboer, Jason, Shibom Basu, Nadia Zatsepin, Kanupriya Pande, Despina Milathianaki, Matthias Frank, Mark Hunter, et al. 2014. "Time-Resolved Serial Crystallography Captures High-Resolution Intermediates of Photoactive Yellow Protein." *Science* 346 (6214): 1242–46. doi:10.1126/science.1259357.

Trebbin, Martin, Kilian Krüger, Daniel Deponte, Stephan V Roth, Henry N Chapman, and Stephan Förster. 2014. "Microfluidic Liquid Jet System with Compatibility for Atmospheric and High-Vacuum Conditions." *Lab on a Chip*, 1733–45. doi:10.1039/c3lc51363g.

Wang, Dingjie, Uwe Weierstall, Lois Pollack, and John C. H. Spence. 2014. "Liquid Mixing Jet for XFEL Study of Chemical Kinetics." *Journal of Synchrotron Radiation* In submiss. International Union of Crystallography: 1364–66. doi:10.1107/S160057751401858X.

Weierstall, U, J C H Spence, and R B Doak. 2012. "Injector for Scattering Measurements on Fully Solvated Biospecies." *Review of Scientific Instruments*. doi:10.1063/1.3693040.

Weierstall, Uwe, Daniel James, Chong Wang, Thomas a White, Dingjie Wang, Wei Liu, John C H Spence, et al. 2014. "Lipidic Cubic Phase Injector Facilitates Membrane Protein Serial Femtosecond Crystallography." *Nature Communications* 5 (January): 3309. doi:10.1038/ncomms4309.

White, Stephen H. 2005. “The Progress of Membrane Protein Structure Determination,” no. 2004: 1948–49. doi:10.1110/ps.04712004.Figure.

White, Thomas a., Richard a. Kirian, Andrew V. Martin, Andrew Aquila, Karol Nass, Anton Barty, and Henry N. Chapman. 2012. “CrystFEL: A Software Suite for Snapshot Serial Crystallography.” *Journal of Applied Crystallography* 45. International Union of Crystallography: 335–41. doi:10.1107/S0021889812002312.